Necroptosis in cardiac cells

Necroptosis; friend or foe during ischemia and reperfusion in cardiac cells

by Christina Mathisen Heiestad

Thesis for the Master`s degree (MSc) in
Molecular Biosciences
(60 study points)

Supervisors: Kåre-Olav Stensløkken, May-Kristin Torp and Göran Nilsson

Department of Biosciences

Division of Physiology – Institute of Basic Medical Sciences

UNIVERSITY OF OSLO

August 2016

Necroptosis in cardiac cells

Necroptosis; friend or foe during ischemia and reperfusion

Master thesis by Christina Mathisen Heiestad

2016

Necroptosis in a cardiac model

http://www.duo.uio.no/

Print: Reprosentralen, Universitetet i Oslo

Acknowledgements

First of all I would like to thank Professor Kåre-Olav Stensløkken for giving me the opportunity to do my master thesis in the Heart Physiology group. You have kept me busy from day one. Even though you have been immensely occupied with teaching, you have always taken the time to discuss progress and problems. Your guidance and advices have been highly appreciated. I would also like to thank you for bringing me along on conferences and giving me the opportunity to present my work.

I also have to thank Professor Göran Nilsson for being my internal supervisor and for never questioning the work of this group.

I am exceptionally grateful to my co-supervisor May-Kristin Torp. You have always been so helpful and patient. You kept me going when times were though and it has been great working alongside of you. I am grateful and humble for all your help.

This project required a lot of guidance and assistance from the whole group. Thank you all, for all the encouragement, insightful comments, critical questions and for always making lunch a highlight during the day. Thanks to Li for putting on the job of analyzing all the infarction photos. Also, thanks to Kristin Larsen Sand for helping me getting started with HL-1 cells and flow cytometry. Torun, it has been an enjoyment to share office with you. Thank you for always being so caring and for everything you have taught me in the laboratory.

I would also like to thank my fellow students for a great time at Blindern. Kristine, Ane and Ole, even though my desk at KB has been empty most of the time the last years, you have made my life at Blindern enjoyable and eventful.

I would also like to thank my family for the continuous support and for always showing an interest in my work. Thank you Mimmi for keeping me well-fed and for always shaking me back to reality when my emotions get out of hand.

And Nils, thank you for being endlessly patient, kind and loving.

Christina Mathisen Heiestad
August
2016

List of abbreviations

A

ADAMs - Disintegrin and metalloproteinase
AKT – Protein kinase B (PKB)
AMPK – AMP-activated protein kinase

B

Bak - Bcl-2 homologous antagonist/killer
Bax - Bcl-2-associated X protein
BDM - 2,3-butanedione monoxime
BSA - Bovine serum albumin

C

CaMKII - Ca^{2+}-calmodulin-dependent protein kinase
CCCP - Carbonyl Cyanide M-Chlorophenylhydrazone
CVD - Cardiovascular diseases

D

DAMPs – Damage associated molecular patterns
DISC/complex II - Cytosolic death-inducing signaling complex
DMSO - Dimethyl sulfoxide
Drp-1 - Dynamin-related protein-1
dsDNA – Double stranded DNA
dP/dt max - Maximal left ventricular global contractility
dP/dt min - Minimal left ventricular global contractility

E

ERK1/2 - Extracellular signal-regulated kinases

F

FADD - Fas-Associated protein with Death Domain
FCS - Fetal calf serum

H

HL-1 cells - AT-1 mouse atrial cardiomyocyte tumor lineage
HMGB-1 – High mobility group box 1 protein
HR - Heart rate
HSPs – Heat shock proteins

I

IDO - Indoleamine 2,3-dixogynease
IL-6 – Interleukin 6
IL-33 – Interleukin 33
IL-1α – Interleukin1 alpha
IL-1β – Interleukin 1 beta

J

JNK - c-JUN NH_2 terminal kinases

L

LVdevP - Left ventricular developed pressure
LVEDP - Left ventricular end-diastolic pressure
LVSP - Left ventricular systolic pressure

M

MAPK – Mitogen-activated protein kinases
MI – Acute myocardial infarction
MLKL - Mixed linage domain-like protein
MOMP - Mitochondrial outer membrane permeabilization
MPTP – Mitochondrial permeability transition pore

N

Nec-1 - Necrostatin-1/ methyl-thiohydantion-tryptophan (MTH-Trp)
Nec-1i – Necrostatin-1 Inactive
Nec-1s - Nec-1 stable (7-Cl-O-Nec1)
NFDM – Nonfat dry milk
NF-κB - Nuclear factor- κB
NOD – Nucleotide-binding oligomerization domain

P

P38 – p38 MAPK
PBS - Phosphate-buffered saline
PGAM5 - Phosphoglycerate mutase 5
PI - Propidium Iodide
PIPs - Phosphatidylinositol phosphates
P-MLKL - Phosphorylated Mixed linage domain-like protein
PRR – Pathogen recognition receptor

R

RHIM - RIP homotypic interaction motif
RIPK - Receptor interacting protein kinase
RIPK1 - Receptor interacting protein kinase 1
RIPK3 - Receptor interacting protein kinase 3
RISK – Reperfusion injury salvage kinases
RPL32 - Ribosomal Protein L32
ROS - Reactive oxygen species
RPP - Rate pressure product

T

TNF-α - Tumor necrosis factor-α
TNFR - Tumor necrosis factor receptor
TNFR1 - Tumor necrosis factor receptor 1
TLRs – Toll-like receptors
TTC - 2, 3, 5-Triphenyl-2H-tetrazolium chloride

Z

Z-VAD-FMK (Z-Vad) - Pan-Caspase Inhibitor

Abstract

Acute myocardial infarction (MI) is the most common and frequent cardiac injury and is one of the leading causes of morbidity and mortality, throughout the world. During MI, insufficient blood supply to the cardiac tissue results in cell death due to direct or indirect effects of oxygen deprivation. If the ischemic period extends for more than 20 minutes, cytotoxic spilling of necrotic debris will harm neighboring cells and trigger an inflammatory response. Cell death will continue to spread through the myocardium which eventually results in a lethally damaged heart. The most effective and convincing therapeutic therapy for treating MI is early reperfusion and restoration of blood flow. Paradoxically, reperfusion may itself cause additional damage to the myocardium, an event known as reperfusion-injury, associated with increased death of cardiomyocytes.

Death of cardiomyocytes in ischemia-reperfusion injury has for a long time been thought to be mainly caused by necrosis, an accidental and uncontrolled process, in response to excessive cellular stress. Even though little is known of the magnitude of apoptotic cell death involved in ischemia-reperfusion injury, apoptosis has for a long time been thought to be the only type of cell death in the heart that it is possible to manipulate. It is now clear that necrotic cell death can also be driven by other defined molecular pathways, and during the last decades investigation of the molecular mechanisms of cell death have increased exponentially and challenged the classical understanding and classification of cell death modes. Now, a variety of types of regulated necrosis have been identified.

Necroptosis is currently the best studied type of regulated necrosis and is defined as regulated cell necrosis whose molecular components are partially shared with apoptotic cell death. Necroptosis can be triggered by the same death signals as apoptosis and the mechanisms that decide if the cell death pathway is executed through apoptosis or necroptosis are under intensive investigation. Over the past two decades initiators and effectors have been identified in the necroptotic pathway. Similar to necrosis, necroptotic cell death provokes an inflammatory response, as a result of the lost membrane integrity and the release of cellular content. Due to the similar morphological characteristics of necroptosis and necrosis the perception is that they are both harmful and cause inflammation through damage associated molecular patterns (DAMP) release, reactive oxygen species (ROS) and cytokine production.

Identification of inhibitors, necrostatins, has made it possible to interfere and investigate the role of necroptosis in different diseases.

Our goal was to study the molecular mechanisms of necroptosis in cardiac cells, with the main goal of finding an approach to reduce necroptotic cell death after myocardial infarction and thereby limit the following sterile inflammation. We investigated the effect of necrostatins in different cardiac cell models and in Langendorff-perfused mouse hearts. We showed, for the first time, that Necrostatin-1S (Nec-1S) improved post-ischemic cardiac function, supported by reduced p38 MAPK (p38) phosphorylation, in Langendorff-perfused mouse hearts and that Necrostatin-1 (Nec-1) tended to protect primary mouse cardiomyocytes from cell death caused by mitochondrial debris exposure. We also found elevated levels of Bcl-2-associated X protein (Bax), which can be an indication of increased apoptosis, when hearts were subjected to necrostatins.

Table of contents

1 Introduction

1.1 Ischemic heart injury

Cardiovascular diseases (CVD) are today the most prominent and fastest growing epidemic in a global health perspective [1]. Acute myocardial infarction (MI) is among the most common and frequent CVD and is one of the leading worldwide causes of morbidity and mortality, for both men and women [2, 3].

To understand and improve treatment for MI, it is important to acknowledge the cellular composition of the mammalian heart. It is comprised of a number of different cell types including cardiomyocytes, cardiac fibroblasts, endothelial cells and vascular smooth muscle cells [4]. Terminally differentiated cardiomyocytes are the most predominant cell type, not by number, but by occupying about 75 % of myocardial tissue volume [5, 6]. The cardiomyocytes are large muscle cells responsible for the contractile properties of the heart [5]. Cardiac fibroblasts are the most abundant non-cardiomyocyte cell type in heart and are found throughout the cardiac tissue, often in close relation to cardiomyocytes [4, 6]. Cardiac fibroblasts hold a variety of complex properties and contribute in a range of different roles including cell signaling, cell development, and myocardial structuring [6].

The mammalian heart is an organ with little regeneration capability [7]. After embryonic development cardiomyocytes lose their ability to proliferate, DNA synthesis after birth is associated with multinucleation, and cardiac growth is a result of increased myocytes volume rather than increased cell number [5]. Due to mechanical forces like stretch and contraction, exposure to toxic metabolic byproducts and hemodynamic forces, life is hard for viable cardiac cells even under normal conditions. Because of the almost non-existing capability of the heart to renew and repair tissue after cell loss, the heart is vulnerable to disease and injury.

During MI, insufficient blood supply to the cardiac tissue may result in cell damage and cell death due to direct or indirect effects of oxygen deprivation. The harmful cellular conditions during ischemia cause cardiomyocyte death mainly through necrosis, although some apoptosis have been reported, especially in the border zone of the infarcted area [8, 9]. If the ischemic period lasts for more than 20 minutes in mammals, cytotoxic spilling of necrotic debris will harm neighboring cells and trigger an inflammatory response, and cell death will

continue to spread through the myocardium which eventually results in a lethally damaged heart [9, 10]. Despite the abundance of cardiac fibroblasts, little is known of their involvement in disease. Compared to cardiomyocytes, the cardiac fibroblasts are more resistant to ischemic death, but they may serve as inflammatory regulators and as a source of pro-inflammatory cytokines [11]. It is clear that cell death is important in the pathogenesis of MI and loss of cardiomyocytes results in scar formation and can lead to reduced heart function [10].

The most effective and convincing therapeutic therapy for treating MI is early reperfusion and restoration of blood flow [9]. Paradoxically, reperfusion may itself cause additional damage to the myocardium, an event known as reperfusion-injury [9, 12, 13]. Restoration of oxygen leads to increased death of cardiomyocytes due to reactivation of the electron transport chain and elevated reactive oxygen species (ROS) generation [9].

1.1.1 Inflammation and scar formation in ischemia-reperfusion

The cellular progression after a MI eventually ends with dead cardiomyocytes being replaced by a collagenous scar [14]. The complex process that starts with cell death during the ischemic period, leading to wound healing and scar formation, can be divided into three different phases (Fig.1); inflammatory phase, fibrotic phase and remodeling phase [14].

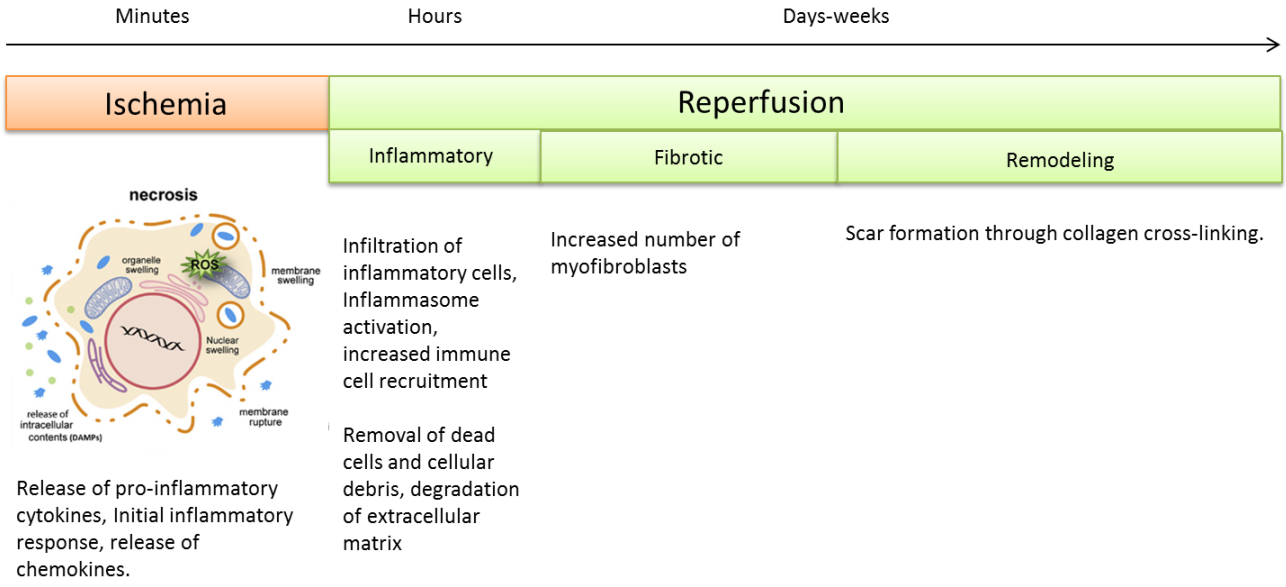

Figure 1: Illustration of events following an ischemic insult in the heart. During the ischemic period lack of oxygen causes cell damage resulting in cell death and release of cytotoxic content initiating an inflammatory response. During the inflammatory phase necrotic tissue are infiltrated by inflammatory cells (e.g. neutrophils, macrophages and lymphocytes) and more immune cells are recruited to the area for removal of dead tissue. The fibrotic phase is associated with collagen accumulation and a massive increase in the number of myofibroblasts. During the last phase the number of myofibroblasts is reduced by apoptosis, and the scar matures through stabilization of collagen cross-linking.

During the early inflammatory phase, within the first 24 hours in adult animals [15], release of damage-associated molecular patterns (DAMPs) from necrotic cells causes a local inflammation that can be harmful to the surrounding tissue and is characterized as a sterile inflammatory response [12, 14]. Inflammation is a crucial and an inevitable defense mechanism against invasive microorganisms and their pathogens. In response to such stimuli, inflammatory cells are recruited to the site where they phagocytize intruding pathogens and in addition produce cytokines and chemokines to recruit and activate lymphocytes and adaptive immune responses [16]. The inflammation that is caused by ischemia-reperfusion injury is named “sterile inflammation” due to the lack of invasive and threatening microorganisms [16].

Inflammation plays an important role in protecting and repairing tissue and is essential for cardiac repair, but in situations where damage is massive, like MI, sterile inflammation can be detrimental [10, 17]. Immune cells (e.g. neutrophils, macrophages and lymphocytes) that are recruited to the injured area, initiates remodeling of the area by activation of cell and matrix degradative proteinases and by stimulating cardiac fibroblast to differentiate into myofibroblasts [14, 18].

The fibrotic phase lasts from one to several weeks, and is characterized by collagen accumulation and a massive increase in the number of myofibroblasts [14]. After the fibrotic phase the last step of scar formation is initiated. This phase can last from several weeks to months in bigger animals, and is termed the remodeling phase. The number of myofibroblasts is reduced by apoptosis, and the scar matures through stabilization of collagen cross-linking [14].

1.1.2 Therapeutic strategies

Today the best therapeutic strategy to minimize damage and save myocardial tissue in patients with MI is early reperfusion, despite its harmful effect. However, there is a lack of strategies that prevents damage caused by reperfusion or targets on the molecules involved in the inflammatory pathway. The possibility of manipulating the so-called reperfusion injury salvage kinases (RISK) pathway has been under investigation and considered as a potential strategy for treating reperfusion injury. These kinases are associated with pro-survival properties [19]. Two kinases have been identified as participants in the RISK pathway, protein kinase B (AKT) and extracellular signal-regulated kinases (ERK1/2) [19]. c-JUN NH_2 terminal kinases (JNK), p38-MAPK (p38) and AMP-activated protein kinase (AMPK) are known as survival kinases due to their possible cardio-protective effects [20, 21].

One important therapeutic strategy in cardiology is to develop strategies to reduce the inflammation caused by necrotic cell death after MI. To make this possible, deeper understanding of the molecular details that contributes to cell death and inflammation in MI and ischemia-reperfusion is necessary.

1.2 Necrotic cell death in ischemia-reperfusion – a source of sterile inflammation

Death of cardiomyocytes in ischemia-reperfusion injury has for a long time been thought to be caused mainly by necrosis, an accidental and uncontrolled process, in response to excessive cellular stress [22].

Necrotic cell death is morphologically identified by cell swelling (oncoisis). Increased cell volume is accompanied by swelling of organelles, chromatin condensation and dilation of the nuclear membrane. All these events lead towards rupture of the plasma membrane, which is the most catastrophic and damaging part of necrosis [23].

The main underlying cause of necrotic cell death is the absence of oxidative phosphorylation and lack of ATP generation in the mitochondria. The ATP depletion during ischemia-reperfusion causes an accumulation of H^+, leading to a number of cellular events that result in necrotic cell death. To lower the levels of H^+, Na^+/H^+ exchangers activity in the plasma membrane causes elevated intracellular levels of Na^+ [24]. Henceforth, excess Na^+ is removed by Na^+/Ca^{2+} exchangers which cause cytoplasmic Ca^{2+} to accumulate [24]. Cytoplasmic Ca^{2+} is transported into the mitochondria where Ca^{2+} overload leads to ROS overproduction [24, 25]. Imbalance in ROS production and detoxification, by antioxidant enzymes, are harmful to DNA, proteins and lipids [25]. High mitochondrial Ca^{2+} levels lead to mitochondrial permeability transition pore (MPTP) opening [26], a critical event in ischemia-reperfusion injury, which results in permanent loss of ATP production, due to uncoupling, and mitochondrial swelling and rupture [27].

An important mechanism following tissue injury is alerting the immune system [16]. Acute necrotic cell death of cardiomyocytes leads to activation of the immune system through release of endogenous alarm signals, DAMPs (e.g. high mobility group box 1 protein (HMGB-1), double stranded DNA (dsDNA), interleukin 1 alpha (IL-1α), heat shock proteins (HSPs), uric acid, interleukin 33 (Il-33), interleukin-6 (IL-6)) (Fig. 2) [16, 28]. The release of DAMPs into the extracellular environment signals through Pathogen Recognition Receptor (PRR), such as Toll-like receptors (TLRs) and nucleotide-binding oligomerization domain (NOD)-like receptors on neighboring cells and stimulates secretion of pro-inflammatory cytokines and chemokines, such as interleukin 1beta (IL-1β) [16, 28].

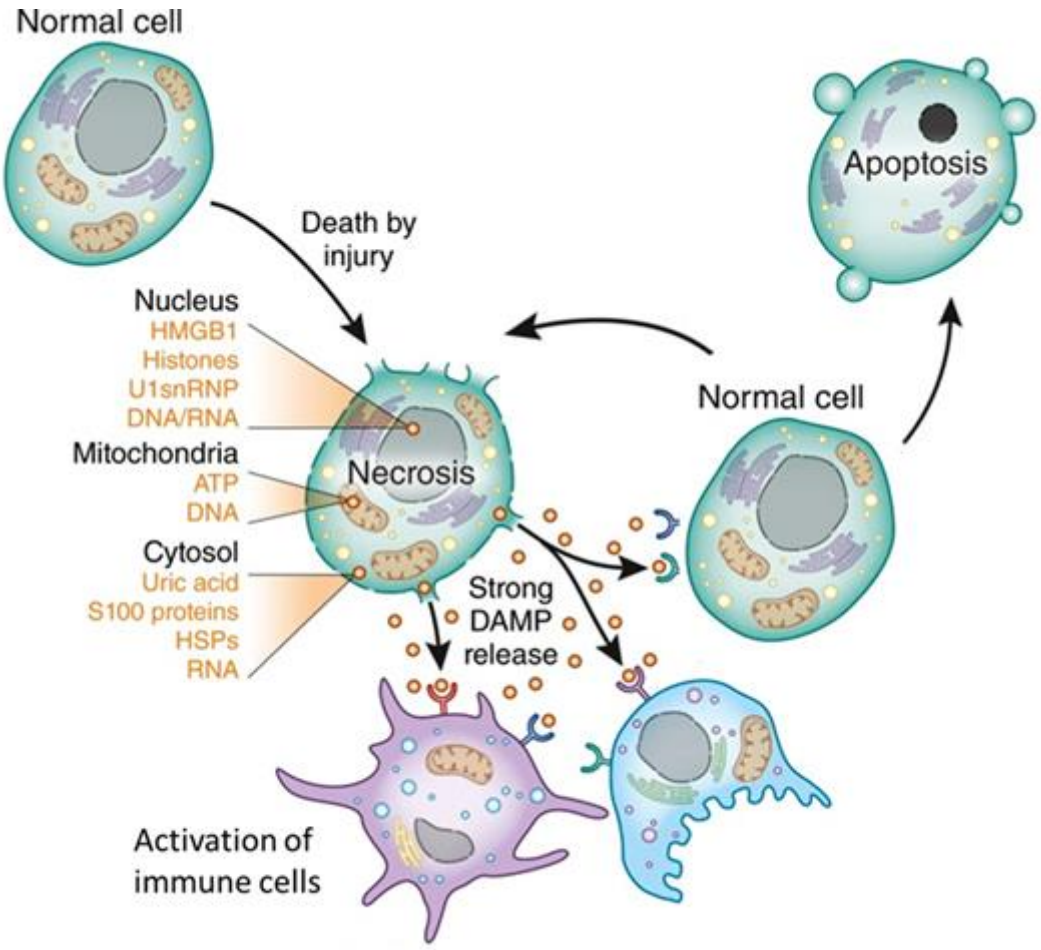

Figure 2: Release of damage associated molecular patterns (DAMPs) from necrotic cells causes a local inflammation that can be harmful to the surrounding tissue and is characterized as sterile inflammatory response. Picture modified from **[29].**

Nuclear factor- κB (NF-κB) is one of the most influential regulators of proinflammatory gene expression and is known to have a crucial role in MI and other diseases [2, 30]. Release of cytokines and ROS from necrotic cells can lead to NF-kB activation in adjacent cells and induce transcription and upregulation of proinflammatory cytokines and chemokines [30].

1.3 The involvement and possible advantage of apoptotic cell death in ischemic heart disease

At this date little is known of the amount of apoptotic contribution in cell death during MI. Involvement of apoptotic cell death in heart failure, especially in cardiomyocytes, has been under debate and investigation for many years. Even though cardiomyocyte death during MI is known to be mainly caused by necrosis, there have been reports claiming that huge amounts of cells are lost through apoptosis [14, 23]. There is however little evidence of cardiomyocytes showing the typical apoptotic morphological characteristics in heart failure studies [23].

Apoptosis is an important mechanism during embryonic development and cell homeostasis. Throughout life, apoptosis is a crucial mechanism for eliminating cells with abnormalities, misplaced, non-functional or potentially dangerous cells. Apoptotic cell death is also an important defense mechanism against viruses and other intracellular pathogens [31]. Metabolic disturbances caused by pathogens or virus infections can activate the apoptotic signaling pathway leading to cell death [31]. Evolution of functional specialization has made the apoptotic machinery in complex multicellular organisms able to respond with high specificity to different stimuli [32].

Apoptosis occurs through an activation of a molecular pathway that results in a controlled and clean breakdown of the cell. After apoptosis is initiated, the cell is programmed to dismantle itself without immediate disruption of the cellular membrane. Many different subtypes of apoptosis with different signaling pathways are identified. It is important to state that the term apoptosis defines specific features that takes place during apoptotic cell death and result in the unique morphological characteristic, first described by Kerr et.al in 1974 [33], and should not be mistaken as a synonym for programmed cell death and the involvement of caspases [23, 34].

Apoptotic cell death can be triggered by both external and internal stimuli, the extrinsic pathway, activated through death receptors located on the plasma membrane, or the intrinsic pathway, mediated by the mitochondria [23]. The extrinsic apoptotic pathway is initiated through death receptors with binding of death ligands (e.g. Tumor necrosis factor-α (TNF-α)) that leads to recruitment and complex formation of cytosolic adaptor proteins that activates downstream apoptotic effector proteins [23]. The intrinsic pathway of apoptosis is highly

dependent on loss of mitochondrial membrane potential and cytochrome c release through the pro-apoptotic Bcl-2-associated X protein (Bax)/Bcl-2 homologous antagonist killer (Bak) channel in the outer mitochondrial membrane [23, 35]. The Bax/Bak channel is regulated by members of the Bcl-2 family [23, 35].

Caspases are known to play important roles as regulators in apoptosis [23]. In mammals, caspases have specific functions in the regulation of the cell death pathway. Caspases that function as initiators of apoptosis are known as activator caspases, this includes caspase -2,-4,-8, -9 -10 and 12 [32]. Other caspases, caspase-3, -6 and -7, operate after initiation and are important in the apoptotic execution [32].

Execution of apoptotic cell death is morphologically characterized by cell shrinkage (pykniosis), nuclear and chromatin fragmentation and blebbling of the membrane into apoptotic bodies [34]. Maintenance of membrane integrity prevents leakage of cell content, thereby limiting the DAMP release (Fig.3), and makes apoptotic cell death a weak inducer of inflammation [36]. Even though apoptosis is not normally associated with inflammation it can be a potential trigger of an inflammatory response if there is a delay in the clearance of the apoptotic bodies which can then go into necrosis [16] .

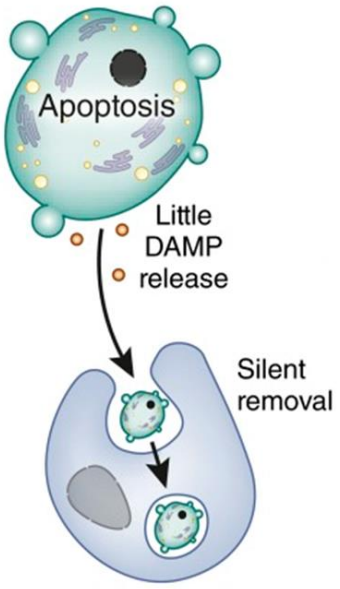

Figure 3: Apoptotic cell death is considered a weak inducer of inflammation, as the plasma membrane stays intact and prevents leakage of potentially damaging content. Picture is modified from **[29].**

1.4 Regulated necrosis

Necrotic cell death has classically been described as a passive form of cell death caused by external factors. Necrosis has been assumed to be very distinct from apoptosis because it was believed that necrosis could not be programmed by molecular events [37]. Because of the discovery of chemical inhibitors of necrosis, this view has changed. It is now clear that necrotic cell death can be driven by defined molecular pathways [37, 38]. During the last decades, investigation of the molecular mechanisms of cell death has increased exponentially and challenged the classical understanding and classification of cell death modes.

Today "regulated necrosis" is a broad term that provides great confusion. Many types of regulated necrosis have been identified (e.g. necroptosis, ferroptosis, parthanatos, pyroptosis, NETosis/ETosis) [39]. They all have unique cellular signaling mechanisms, but share the same morphological endpoint of swelling and membrane rupture, also seen in passive necrosis [39].

1.5 Necroptosis

Necroptosis is currently the best studied type of regulated necrosis and is defined as regulated cell necrosis whose molecular contributors are partially shared with apoptosis [40]. Necroptosis can be triggered by the same death signals as apoptosis and the mechanisms that decide if the cell death pathway is executed through apoptosis or necroptosis is under intensive investigation [41].

By this definition necroptosis is a regulated form of "uncontrolled" cell death, a kind if contradiction. The functional purposes of necroptotic cell death are not yet fully understood and it seems paradoxical that cells have a death program that causes extensive damage. However, viruses have been found to produce proteins that inhibit caspase activity, thereby blocking the apoptotic molecular pathway [42]. Necroptosis could be a cell protecting mechanism, with an important role in regulation of an innate immune response against bacterial and viral infections that possess such an apoptosis-inhibiting trait [42, 43].

1.5.1 Initiation of necroptosis

Many death signals are now known to initiate both apoptosis and necroptosis (e.g. death ligands, interferons, DNA, viruses and bacterial products) [44]. The best studied process of necroptosis is induced by TNF-α, a member of the tumor necrosis factor receptor (TNFR). TNF-α is important in many different actions, such as proliferation, inflammation, differentiation and death initiation [31]. Binding of TNF-α to tumor necrosis factor receptor 1 (TNFR1), initiates the assembly of a membrane associated complex (complex I) that includes receptor interacting protein kinase 1 (RIPK1) (Fig.4) [45]. After complex I formation, activation of different signaling cascades can be initiated leading towards cell survival through the NF-κB pathway, or cell death through the apoptotic or necroptotic pathways (Fig.4) [46].

As a member of the receptor interacting protein kinase (RIPK) family, RIPK1 has an important role in determining cell fate [47].While RIPK1 serves as a decision maker and regulator of multiple outcomes, receptor interacting protein kinase 3 (RIPK3) can specifically direct a cell to the necroptotic machinery. RIPK1 and RIPK3 have been shown to be essential regulators of TNFα-induced necroptosis [46].

In the cytosol RIPK1 and RIPK3 interact through a RIP homotypic interaction motif (RHIM) domain to form a pro-necroptotic complex (Fig.4) [46, 48]. This complex is often referred to as the necrosome and serves as a crucial controller of the downstream events. Deletion of either RIPK1, RIPK3 or mutation of the sequence encoding the RHIM domain prevents necroptosis [49]. After the necrosome formation the necroptotic machinery is activated through a series of auto-cross-phosphorylation events between RIPK1 and RIPK3, which are important for further recruitment of necroptotic end-effectors [44].

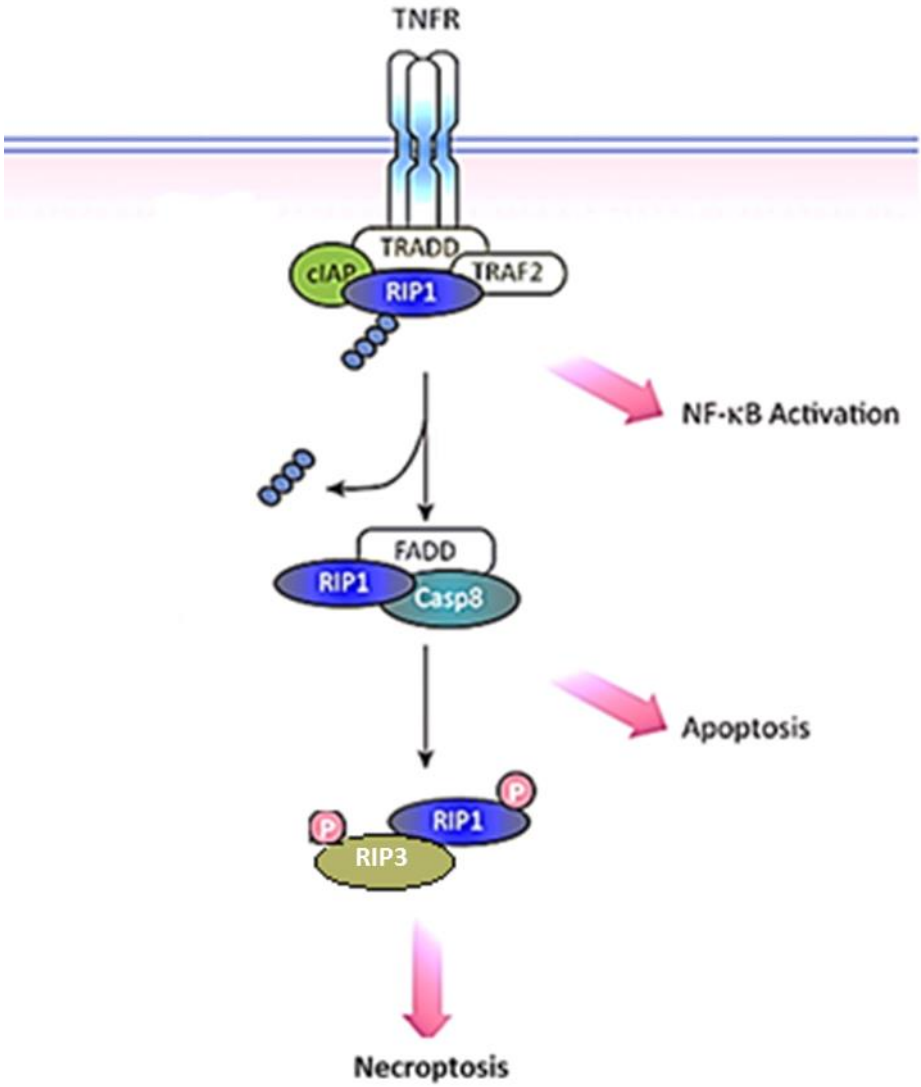

Figure 4:.TNF-α initiated necroptosis requires formation of a cytosolic complex formed by RIPK1 and RIPK3, often referred to as the necrosome. This serves as a crucial controller of the downstream events. Picture modified from [50].

RIPK1 – a crucial decision maker

Even though RIPK1 is strongly associated with necroptosis, the kinase has a more complex role due to its involvement in both cell survival and death. In response to stress signals, different RIPK1-containing complexes can be formed that result in various events that strongly influence the fate of the cell. Besides being involved in initiation of necroptosis or apoptosis, RIPK1 can also influence activation of different signaling cascades, leading towards cell survival through the NF-κB pathway (Fig.5) [46]. In response to TNF-α stimulus, activation of NF-κB leads to an upregulation of different genes important for survival and with a proinflammatory effect [51].

Another possible consequence of death receptor signaling is activation of mitogen-activated protein kinases (MAPKs) [47]. MAPKs are a family of well-studied proteins that are involved in a variety of signaling events governing and regulating cardiac development, pathological changes and physiological adaptation [52]. These kinases functions as signal transducers by converting extracellular signals into intracellular responses [53]. Their role in determining cardiomyocyte viability in myocardial ischemia-reperfusion has been frequently addressed.

Among the best studied MAPKs we find ERK 1 and 2, JNK and p38, [52, 53]. ERK1 and ERK2 are often referred to as ERK1/2 because of their similarities in both structure and function [52]. ERK1/2 has been reported to have cardio-protective effects with pro-survival and anti-apoptotic properties [52]. JNK and p38 are both stress-activated kinases that respond to many of the same events [52]. As many of the MAPKs, they have divergent properties, such as being important in both apoptosis and cell survival through cytokine production [52]. It has been suggested that p38 is the MAPK pathway that is most sensitive to ischemia [54], and by promoting expression of pro-inflammatory cytokines (e.g. IL-1β, TNF-α, IL-6) increases the immune response [52].

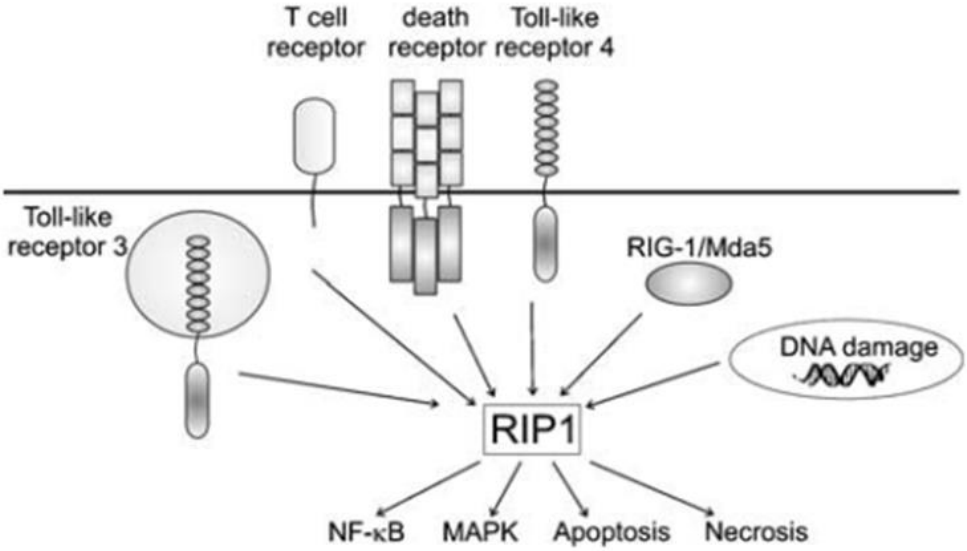

Figure 5: Illustration of the complexity of RIPK1 (RIP1) signaling. RIPK1 is capable of activating a variety of different signaling cascades, including the NF-κB pathway, different MAPKs and cell death. Picture modified from [47].

1.5.2 End-effector of necroptosis

In 2012, mixed linage domain-like protein (MLKL), a pseudo kinase, was identified as a component of the necrosome and the main effector following RIPK3 activation [44, 55]. MLKL-knockout mice were reported to be healthy without showing any abnormalities during development or in other aspects of life. MLKL deficiency did however inhibit necroptosis, without affecting necrosome assembly [56, 57].

After interaction and formation of the necrosome, MLKL is recruited and activated by RIPK3-mediated phosphorylation (Fig.6) [58]. MLKL is phosphorylated at the activation loop by RIPK3 at residues T357 and S358 [59]. Phosphorylation causes a shift in equilibrium, from the monomer to oligomer state (Fig.6) [59].

Phosphorylated MLKL (p-MLKL) oligomer has been confirmed as the true necroptotic end-effector through different mechanisms. Oligomerization of p-MLKL causes translocation from cytosol to the plasma membrane and intracellular membrane-bound organelles (Fig.6) [59]. Membrane targeting happens through a four-helical bundle domain in the N-terminal region of p-MLKL, an area rich in positively charged amino-acids [58]. The positively charged amino-acids in this area promotes binding to phospholipids [60], with a special affinity for areas rich in phosphatidylinositol phosphates (PIPs) [58].

Necrosomal signaling and execution have been thought to be highly dependent on the mitochondria and ROS generation caused by disruption of mitochondrial respiration [61]. However, little is known about the exact molecular details leading towards the mitochondrial collapse in necroptosis. It has been suggested that Bax and Bak, which are normally associated with apoptosis, could be important for causing mitochondrial dysfunction in necroptosis [62]. Translocation of p-MLKL to the mitochondria has been shown to activate phosphoglycerate mutase 5 (PGAM5) and dynamin-related protein-1 (Drp-1), leading to mitochondria fragmentation [58]. The indispensable role of the mitochondrial mechanism has later been questioned because of evidence of necroptotic cell death in mitochondria depleted cells [63]. Additional roles of p-MLKL have been documented after observations of translocation of the oligomer to the plasma membrane, where it directly caused membrane permeabilization through formations and recruitment of transmembrane cation channels (Fig.6) [57, 58].

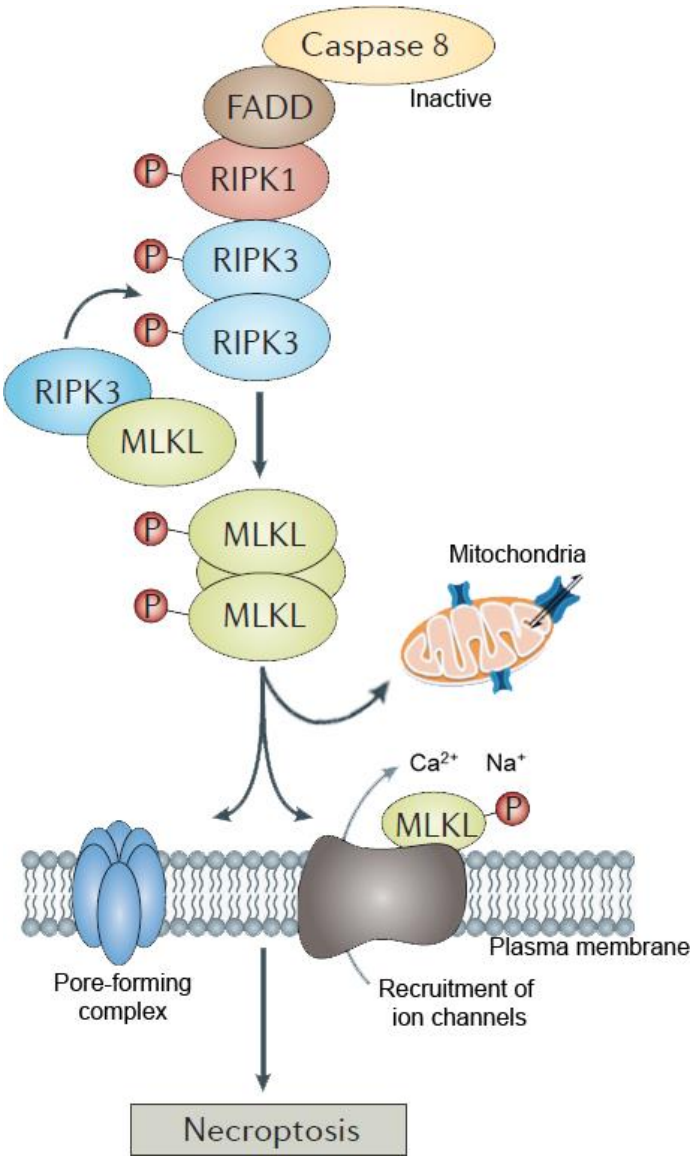

Figure 6: RIPK3-mediated phosphorylation of MLKL is a crucial step in necroptosis. p-MLKL oligomers translocate to the plasma membrane or intracellular membrane bound organelles, causing membrane permeabilization and organelle dysfunction. Picture modified from [50, 64].

Even though p- MLKL is now accepted as an important end-effector in the execution of necroptosis more investigation in the field has revealed more cell specific mechanisms. Emerging evidence has showed that RIPK3 is capable of necroptotic initiation and execution without being dependent on the necrosome. Ca^{2+}-calmodulin-dependent protein kinase (CaMKII) has been identified as a RIPK3 substrate involved in mitochondria permeabilization during necroptosis [65]. In addition to these findings, RIPK3 has been reported to translocate to the nucleus which may indicate that the kinase also has other executive functions in necroptosis [66].

1.5.3 Necroptosis and inflammation

Similar to necrosis, necroptotic cell death initiates an inflammatory response due to lost membrane integrity and release of cellular content. The similar morphological characteristics of necroptosis and necrosis indicate that both are harmful and cause inflammation through DAMP release, ROS and cytokine production. Not surprisingly, many DAMPs that are normally associated with classical necrosis have now been identified in necroptotic cell death [67].

An inflammatory response caused by necroptotic cell death has mainly been thought to be mediated through the same passive process taking place in the classical form of necrotic cell death, through release of DAMPs. New findings suggest that DAMP release is a late event in necroptosis, and that activation of a disintegrin and metalloproteinase (ADAMs) mediates release of intracellular membrane-associated proteins prior to membrane permeabilization [68].

1.5.4 Apoptosis and necroptosis share molecular mechanisms, but have distinct cellular outcome

Necroptosis can be initiated by many of the same signals that activate the apoptotic pathway. Under certain conditions the pathway can switch from apoptosis to necroptosis. When cell death is induced through activation of TNFR1, RIPK1 dissociates from the receptor associated complex, complex I, that was formed during initiation [39]. RIPK1 interacts with pro-caspase 8, Fas-Associated protein with Death Domain (FADD) and RIPK3 and forms a cytosolic death-inducing signaling complex (DISC/complex II) [39, 69]. DISC formation can result in both apoptosis and necroptosis and the outcome strongly depends on caspase 8 activity (Fig.7). As early as 1998 it was suggested that caspase activity protects cells from necrotic cell death [70], and caspase inhibition has later been shown to be a crucial part of necroptotic initiation [69]. Activation of caspase 8 is not only an important step for initiation of the pro-apoptotic signaling cascade that leads towards apoptotic execution, but also prevents necroptotic initiation by inactivating RIPK1 and RIPK3 by proteolytic cleavage [69, 71]. Under conditions where caspase 8 fails to activate or has been deleted, necroptosis is initiated [46, 69, 71]. Necroptosis is therefore often referred to as caspase-independent cell death.

The mitochondria serve as important initiators and mediators of both apoptosis and necroptosis with involvement of several downstream regulators and effectors. Mitochondrial outer membrane permeabilization (MOMP) is important in the apoptotic pathway and is strictly regulated by proteins in the Bcl-2 family [72]. Bax and Bak directly initiates MOMP during apoptosis by generating large pores in the outer mitochondrial membrane, resulting in cytochrome c release [72]. Mitochondrial permeabilization plays a crucial part in necrotic execution, carried out by MPTP opening, leading to depolarization of the inner mitochondrial membrane, loss of ATP production and generation of ROS. Little is known of the details that causes mitochondrial dysfunction during necroptosis. New findings have indicated that there could be an important role for Bax and Bak also in necroptosis as well as in apoptosis [73].

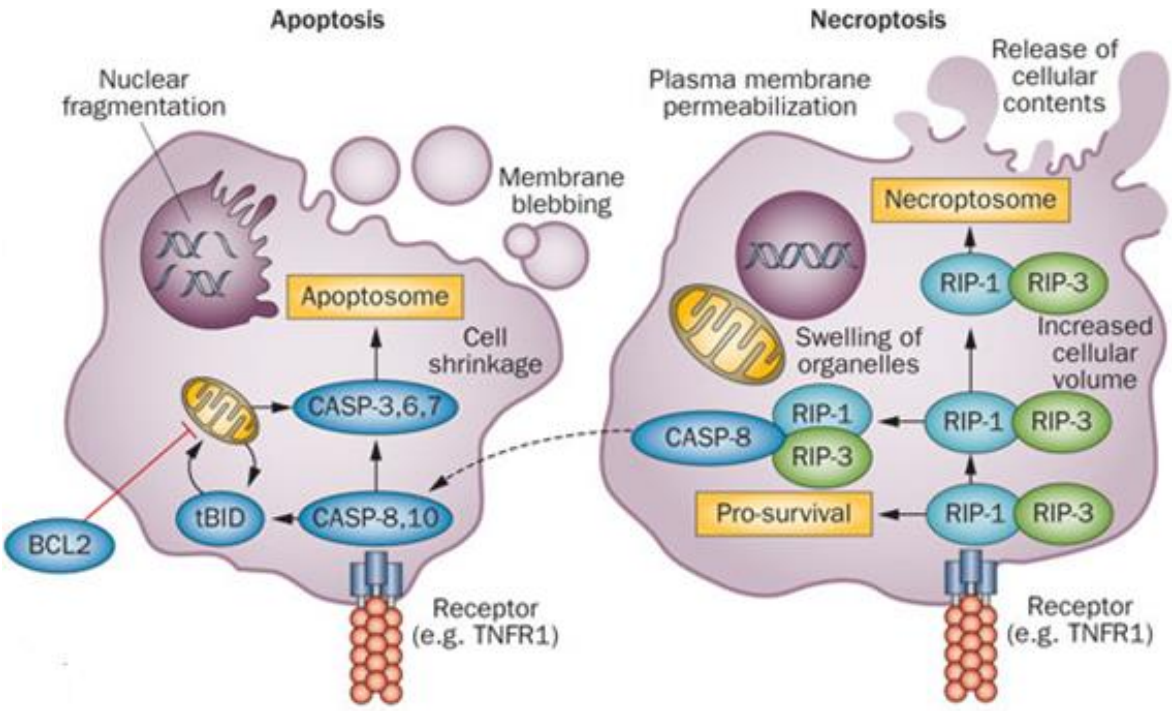

Figure 7: Illustration of the pathways of apoptosis and necroptosis, with involvement of similar molecular players, and distinct morphological characteristics. Picture is modified from [74].

Even though many of the molecular players are shared between apoptosis and necroptosis, necroptosis is different due to its proinflammatory effects. Like classical necrotic cell death, necroptosis causes cell swelling and loss of membrane integrity (Fig.7) [17]. Apoptotic cell death, on the other hand is, characterized by cell shrinkage and maintenance of plasma integrity (Fig. 7) [17]. Sensed from the immune system, handling of the two different cell death types therefore elicits distinct immune responses [69].

1.5.5 Prevention of necroptotic cell death

In 2005, Necrostatin-1 (Nec-1), a member of the necrostatin family known for their ability to block necrotic cell death, was identified by Degterev et.al [75, 76]. Nec-1 is an allosteric inhibitor that prevents the necessary phosphorylation of RIPK1 by preserving the inactive conformation [77]. Even though 33 % of the amino acids in the kinase domains of RIPK1 and RIPK3 are identical, Nec-1 is only capable of inhibiting RIPK1, and not RIPK3 [78].

After the discovery, Nec-1 has been widely used as a tool during investigation of necroptosis, and today many different necrostatins are commercially available. Even though they share a common competency they have diverse chemical structures [75].

There are some concerns about the use of these inhibitors that have been proposed and may be taken into consideration [75]. The specificity of Nec-1 has been questioned after it was shown that it also affected the activity of other kinases, and therefore could potentially influence cell viability through other mechanisms [79]. Some studies are now using Nec-1 together with its inactive derivative Nec-1i to show the effect of the inhibitor (Fig.8). The inactive form is however only inactive in some models, but highly active in others [80]. Studies have shown that different doses may have different effects [80]. Nec-1 has also been described as an indoleamine 2,3-dixogynease (IDO) inhibitor, used to interfere with inflammation-associated tumorigenesis [80], but none of the other necrostatins share the same property [81].

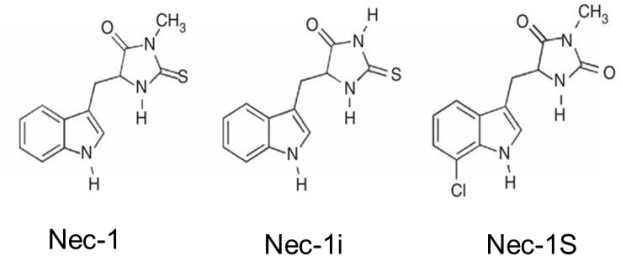

Figure 8: Illustration of the chemical structure of Nec-1, Nec-1i and Nec-1S. Picture modified from [80].

Nec-1 stable, 7-Cl-O-Nec1 (Nec-1S) is an improved version of Nec-1 (Fig.8). Like Nec-1, Nec-1S has the same ability to inhibit phosphorylation of RIPK1, although with a greater potential [80]. Nec-1S has been reported to be more specific in its binding to RIPK1 compared to Nec-1 [80].

1.5.6 Myocardial necroptosis and ischemia-reperfusion injury

Identification of inhibitors has made it possible to interfere and determine the role of necroptosis in different diseases. Already during the identification of the necrostatins, Nec-1 proved to have a protective effect in a cerebral ischemia-reperfusion model [76]. This finding led to increased interest in the field and Nec-1 has been shown to have a protective effect on ischemia-reperfusion injuries in a variety of models and in different tissue (e.g. kidney, heart and brain) [13, 82, 83].

The effect of Nec-1 has been investigated in some cardiac models and Nec-1 reduced infarct size, given at reperfusion, in isolated perfused mouse hearts [84]. Different *in vivo* models (e.g. mouse, guinea pig and pig), where Nec-1 treatment was given 5 and 10 minutes prior to reperfusion, resulted in reduced infarction size and preserved heart function [13, 22, 85]. Even though these studies show a promising trend, there are uncertainties of doses and timing of the blockers. It is therefore still unclear whether this small molecule can be used as a therapeutic strategy. Interestingly, a more prominent role for RIPK3 has been suggested in myocardial cells [48]. RIPK3 is expressed and activated in cardiomyocytes during MI and a possible co-localization between RIPK3 and the mitochondria has been suggested [48]. RIPK3 has been shown to initiate necroptosis, independent of RIPK1 and MLKL, and cause cell death through mitochondrial deficiency [65].

1.6 Aim of study

Our goal was to study the molecular mechanisms of necroptosis in cardiac cells, with the main aim to reduce necroptotic cell death after MI, by reducing infarct size and improve cardiac function. The overall aim for the research group is to understand and reduce detrimental effects of sterile inflammation following MI. Based on the knowledge of similarities and shared molecular signaling pathways between apoptosis and necroptosis, we also hypothesized that by inhibiting necroptosis, the apoptotic pathway might be activated, leading to less sterile inflammation.

2 Materials and methods

All experiments in the thesis were performed by me, except excision and mounting of mouse hearts used in the Langendorff series and primary cell isolation. From the Langendorff experiments I retrieved and analyzed the data. For the primary cell isolation experiments I prepared the cells after the cannulation. Mounting an isolated mouse heart requires months of training and we prioritized focusing on learning other methods. In addition, the pilot experiment performed on NF-κB reporter mice was conducted by another group member.

2.1 Animal model

Experiments were approved and performed in adherence with the Norwegian Animal Health Authority and the animals received humane care in compliance with the European Parliament on the protection of animals used for scientific purposes (2010/63/EU). C57BL6 male mice (Scanbur BK AS, Norway) and NF-κB luciferase reporter mice (Department of Nutrition, Institute of Basic Medical Sciences, University of Oslo, Norway) had free access to food (RM3 from Scanbur BK AS, Norway) and water and were kept in a 12:12h light/dark cycle in rooms where the temperature was set to 23°C and humidity to 55–60 %. All animals were acclimatized for at least seven days prior to the experiments.

2.1.1 Animal anesthesia

Mice (27.3 ± 1.8 g) were injected intraperitoneally (i.p) with 50 mg/kg pentobarbital (Ås Produksjonslab AS, Ås, Norway), and 500 IU of Heparin (Leo Pharma A/S, Denmark) and sacrificed by neck dislocation.

2.2 Langendorff-perfused mouse hearts

Hearts were quickly excised, with lungs and thymus, and washed in ice-cold Krebs-Henseleit buffer (in mM; NaCl 118.5, $NaHCO_3$ 25, KCl 4.7, KH_2PO_4 1.2, $MgSO_4$-$7H_2$01.2, Glucose-$1H_2O$ 11.5, $CaCl_2$ 1.33, $CaCl_2$- $2H_2O$ 1.76) before being separated from the other organs. The hearts were cannulated through the aorta (Fig.9) and mounted on a Langendorff system (Fig.10) (ADInstruments, Castle Hill, NSW, Australia).

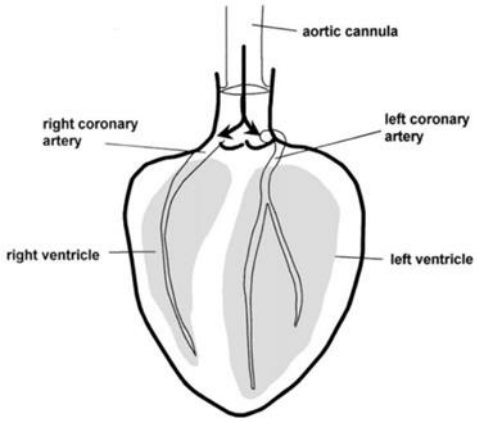

Figure 9: Isolated hearts were cannulated through aorta, which allows retrogradely perfusion. Picture from [86].

In the Langendorff system, hearts were retrogradely perfused with oxygenated (95 % O_2 and 5 % $CO_{2)}$ Krebs-Henseleit buffer preheated to a constant temperature at 37^0C and with a constant perfusion pressure of 70 mmHg (Fig.10). The temperature and perfusion pressure was monitored and kept constant throughout the experiment. To register heart rate and measure ventricular pressure a fluid filled latex balloon (volume; 80µl) was inserted in the left ventricle via the left atrium (Fig.10). Left ventricular end-diastolic pressure (LVEDP) was set to 5-10 mmHg during stabilization. Throughout the experiment recorded changes in LVEDP and measured left ventricular systolic pressure (LVSP) were used to calculate left ventricular developed pressure (LVdevP). The measurements were recorded with a Power lab system (ADInstruments, Dunedin New Zealand). Coronary flow was also measured.

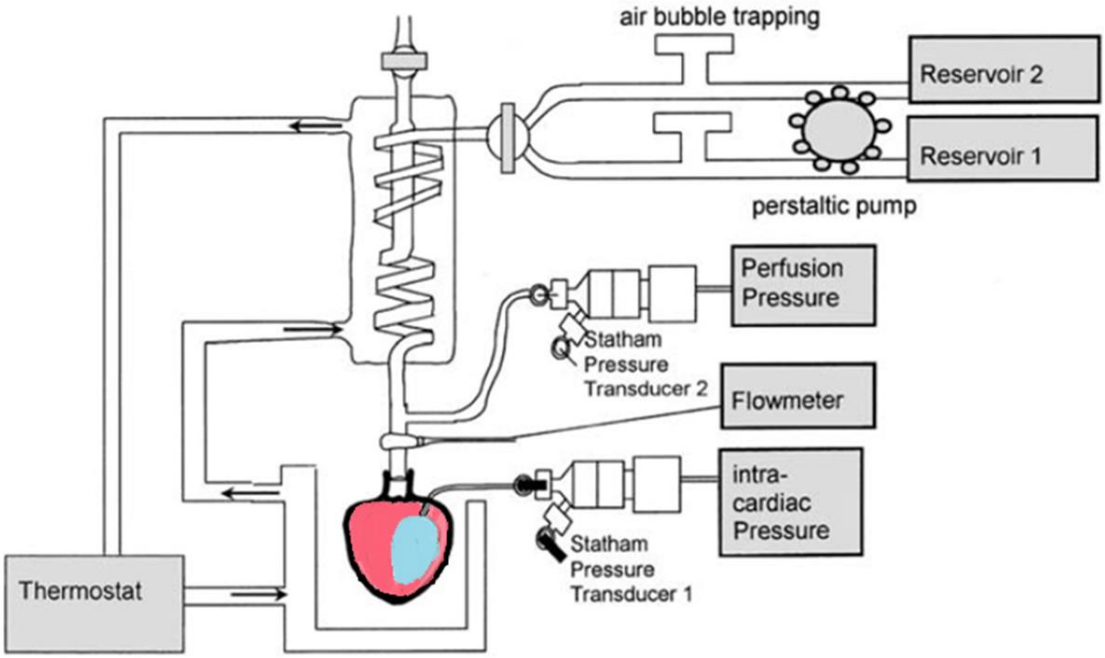

Figure 10: Langendorff system with cannulated heart and fluid filled balloon inserted in the left ventricle. Scheme modified from [86].

To be included in the study the hearts had to fulfill the following requirements; aortic cannulation time < 3minutes, coronary flow 1-4 mL/min, LVSP < 60 mmHg, heart rate < 220 beats per minute during the stabilization period. The hearts that did not fulfill these requirements were excluded from the study (7 of 36 hearts were excluded). After 20 minutes of a pre-ischemic stabilization period the hearts went through 30 minutes of global ischemia followed by 60 minutes of reperfusion (Fig.11).

During reperfusion hearts were exposed to one of three different chemical treatments, Dimethyl sulfoxide (DMSO) (Sigma-Aldrich, Missouri, US) (used as a vehicle control), Nec-1 (Sigma-Aldrich, Missouri, US) and Nec-1S (Bio-Vision, California, US), in two different series. What treatment the hearts were exposed to was randomized in each series before experiments were performed.

Experimental design

Series 1: DMSO, equivalent with the volume of DMSO in Nec-1/Nec-1S, (vehicle control) (N=5), 10 µM Nec-1 (N=4) and 10 µM Nec-1S (N=5). The necrostatins were delivered to the hearts during the first minutes of the reperfusion period. The drugs did not reach the hearts from the beginning of the reperfusion period due the distance of the tube and the container with blockers (Fig.11).

Series 2: DMSO (vehicle control) (N=7), 10 µM Nec-1 (N=7), 30 µM Nec-1 (N=2) and 1 µM Nec-1S (N=6). To assure treatment was delivered to the hearts from the first second of reperfusion, the distance through the tube delivering the drug was used to calculate the exact time to do the switch from the container with only Krebs-Henseleit buffer to the buffer containing the treatment. When this switch was done during the last period of stabilization, treatment was delivered to the hearts from the very first seconds of reperfusion (Fig.11).

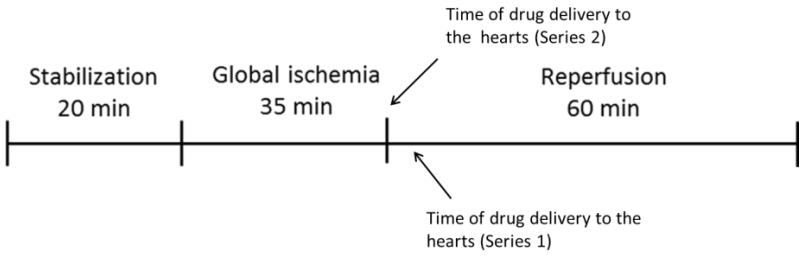

Figure 11: Representation of the different periods the hearts were exposed to in the langendorff perfusion system. Hearts were stabilized for 20 minutes before they were exposed to 35 minutes of global ischemia followed by 60 minutes of reperfusion. Arrows shows approximately when treatment was delivered to the hearts in the two different series described above.

After the 60 minutes of reperfusion period, the hearts were cut in 1 mm slices. The four central slices were transferred to a plastic petri dish, incubated at 37^0C for 15 minutes in 1 % solution of 2, 3, 5-Triphenyl-2H-tetrazolium chloride (TTC). After incubation, the heart slices were scanned in a V700 Photo scanner (EPSON, Suwa, Japan). The infarct area was calculated based on the percentage of TTC positive areas and TTC negative areas. TTC detects lactate dehydrogenase activity in viable tissue. The viable tissue will therefore appear red while the dead tissue will remain unstained and therefore white (see images in Fig.14). The experiment was blinded upon analysis.

Remaining heart tissue was snap frozen in liquid nitrogen and stored in -80^0C prior to protein and RNA isolation.

2.3 Cell cultures

2.3.1 Isolation of primary adult mouse cardiomyocytes and cardiac fibroblasts

Isolation of primary adult mouse cardiomyocytes and cardiac fibroblasts was based on the protocol described by O`Connell [87].

In short, hearts were excised and cannulated as described for the Langendorff procedure (paragraph 2.2) and initially retrogradely perfused with perfusion buffer (in mM; NaCl 120.4, KCl 14.7, KH_2PO_4 0.6, Na_2HPO_4-2 H_2O 0.6, $MgSO_4$-7 H_2O 1.2, Na-Hepes liquid 10.0, Glucose 5.5, $NaHCO_3$ 4.6, Taurine, 30.0, BDM 10.0) at flow rate 4 mL/min for 4 minutes, followed by 11 minutes of digestion buffer, containing 1.2 mg/mL Collagenase 2 (Worthington Biochemical, Lakewood, NJ) diluted in perfusion buffer. The last 8 minutes of the perfusion, 40 µM of $CaCl_2$ was added to the digestion buffer. After digestion the hearts were gently cut down into a petri dish containing digestion buffer. Buffer containing 10% fetal calf serum (FCS) (HyClone; GE Healthcare Life Sciences, Utah, US) was added to the dish to inhibit collagenase activity. The digested hearts were then brought into a sterile hood for Ca^{2+} reintroduction and cell isolation. To collect cells, tissue was suspended in perfusion buffer containing 10 % FCS by gently pipetting cell suspension up and down. To separate and isolate cardiomyocytes from non-cardiomyocytes (mainly cardiac fibroblasts) cell suspension was centrifuged at 20 x g (Heraeus Megafuge 16 centrifuge, Thermo Scientific, Massachusetts, US), for 3 minutes at room temperature and gradually reintroduced to Ca^{2+}.

Cardiomyocytes were resuspended in plating medium (Minimum essential medium eagle w/ Hanks salt (MEM w Hanks BSS), supplemented with 10 % FCS, 10 mM BDM, 100 U/mL Penicillin and 2 mM Glutamine) and seeded in 8-wells chamber slides (Nunc® Lab-Tek® chamber slide system, Sigma-Aldrich, Missouri, US) pre-coated with 1µg/cm^3 laminin (BD, Biosciences) and incubated in 37°C, 2 % CO_2. After 1-2 hours plating medium was replaced by short term medium (Minimum essential medium eagle w/ Hanks salt (MEM w Hanks BSS) supplemented with1 mM BDM, 100 U/mL Penicillin, 2 mM Glutamine and 0.10 % BSA (10 Fa-free)).

After separation from cardiomyocytes, the non-cardiomyocyte suspension was centrifuged twice at 700 x g for 5 minutes in room temperature, before being resuspended in fibroblast

medium (Minimum essential medium eagle w/Hanks salt (MEM w Hanks BSS) supplemented with 10 % FCS, 100 U/mL Penicillin and 2 mM Glutamine,) and cultured in T75-cell growth flasks (Sigma-Aldrich, Missouri, US). Cells were grown to confluency in 37°C, 5 % CO_2. Medium was changed after two-three days. Confluent cells were detached from the flask by trypsination and counted in Countess automated cell counter (Thermo Scientific, Rockford, US). ~30 000 cells were plated in each well in 8-wells chamber slides (Nunc® Lab-Tek® chamber slide system, Sigma-Aldrich, Missouri, US), whereas ~ 70 000 cells were plated in each well in 48-wells plates (Sigma-Aldrich, Missouri, US).

2.3.2 HL-1 cells

All HL-1 work was performed based on the protocol provided by Multi Channel Systems and guidelines from Dr. Claycomb [88]. HL-1 cells, a cardiac muscle cell line derived from mouse atrial cardiomyocyte tumor lineage, were received as a kind gift from Dr. Claycomb and were stored in a cryo container until usage.

Cells were quickly thawed in a 37^{0}C water bath before resuspended in pre-warmed wash medium (Claycomb medium (Sigma-Aldrich, Missouri, US) supplemented with 5 % fetal bovine serum (FBS) (Sigma-Aldrich, Missouri, US)), and 100 U/mL penicillin/streptomycin (Sigma-Aldrich, Missouri, US)), and centrifuged for 5 minutes at 500x g. After centrifugation the wash medium was gently aspirated and the cells were resuspended in pre-warmed supplemented Claycomb medium (Claycomb medium supplemented with 10 % FBS, 100 U/mL penicillin/streptomycin, 0.1 mM Norepinephrine (Sigma-Aldrich, Missouri, US) and 2 mM L-Glutamine (Sigma-Aldrich, Missouri, US)). Cell suspension was cultured in a T75-flask (Sigma-Aldrich, Missouri, US) pre-coated overnight with Gelatin/fibronectin (Fibronectin (Sigma-Aldrich, Missouri, US) diluted 1:200 in autoclaved 0.02 % Gelatin solution (Sigma-Aldrich, Missouri, US)). Cells were incubated at 37^{0}C, 5 % CO_2. Medium was changed daily. Upon confluency, cells were passaged by trypsination (Sigma-Aldrich, Missouri, US), until they detached from the bottle. Equal amount of soybean/Trypsin Inhibitor Sigma-Aldrich, Missouri, US) was added to the cell solution. Cells were dispersed between two or three pre-coated T75 flasks. Medium was changed after the cells had attached to the flask.

2.4 Cardiomyocyte and cardiac fibroblast viability assessment

Both cardiomyocytes and cardiac fibroblasts were treated over night with 1 µM, 10 µM and 100 µM Nec-1, 0.1ng/ml, 1ng/ml and 10 ng/ml TNF-α (RnD Systems, Minneapolis, US) and 10 µM Z-VAD-FMK (BioVision, Miltpas, California, United States). In line with manufacturer's protocol (BioVision, Miltpas, California, United States), Z-VAD-FMK was added 1 hour prior to the other treatments. DMSO was used as a vehicle control. Cardiomyocytes were also treated with 50µg mitochondrial debris (discarded mitochondria), isolated from mice in the lab, and mitochondrial debris in combination with 10 µM Nec-1.

After overnight incubation the cells were stained with 1 µM Hoechst (Invitrogen, California, US), 10nM Mitrotracker® Deep Red (Invitrogen, California, US) and 40 µM Propidium Iodide (PI) (Sigma-Aldrich, Missouri, US) diluted in short term/fibroblast medium. Cardiomyocytes or cardiac fibroblasts were washed twice after 30 minutes with 1X Phosphate-buffered saline (PBS) (Sigma-Aldrich, Missouri, US) and fixed with 2 % Paraformaldehyde in PBS, at 37°C, 2 or 5 % CO_2 respectively. The chamber slides were sealed with pre-heated, 55^0C, mounting medium over the fixed cells. The slides were kept in the dark at -20^0C until analysis.

Quantification of cell death was analyzed with an Olympus ScanR high-throughput microscope (Olympus life science, Olympus Corporation, Tokyo, Japan). The fixed slides were automatically scanned by the microscope based screening system and images were taken at 25 fixed positions in each well. Analysis of the images was done with the Scan^R analysis software, which was set to automatically analyze intensity and count the number of nuclei, PI-positive nuclei and number of cells.

2.5 NF-κB activity in adult mouse cardiac fibroblasts

The experiment was conducted based on previous work by Carlsen, H. [89]. Cardiac fibroblasts from NF-κB reporter mice, isolated as described earlier (paragraph 2.3.1), were treated overnight with 10 µM Nec-1, 10 ng/mL TNF-α and 10 µM Z-VAD-FMK. DMSO was used as a vehicle control. After adding D-Luciferin (Biotherma, Dalarö, Sweden) pictures were taken with an IVIS Spectrum camera (PerkinElmer, Massachusetts, US). NF-κB activity was measured as photons per second.

2.6 Flow cytometry

2.6.1 Detection of necroptosis in HL-1 cells

HL-1 cells that were utilized in the experiment were counted in a hemocytometer, and 200.000 cells were plated per well in 24-well plates (Sigma-Aldrich, Missouri, US). The HL-1 cells were treated with 100 nM, 1 µM and 10 µM of Carbonyl Cyanide M-Chlorophenylhydrazone (CCCP) (Sigma-Aldrich, Missouri, US) and in combination with 10 µM Nec-1 and 10 µM Z-VAD-FMK for 4 hours in 37^0C, 5 % CO_2. DMSO was used as a vehicle control.

Medium was harvested and cells were trypsinated until they detached from the plate. All samples were centrifuged for 5 minutes at 500 x g in room temperature, resuspended in 250 uL Annexin V Binding Buffer (BioVision, Miltpas, US) and transferred to 96-well plates (Sigma-Aldrich, Missouri, US). Cells were incubated with both Annexin V-FITC (BioVision, Miltpas, US) and PI (BioVision, Miltpas, US), and subsequently analyzed in a BD FACSCanto™ II flow cytometer (BD Biosciences, California, US).

2.7 Western blotting

2.7.1 Protein extraction and quantification of total protein

Tissue was crushed in liquid nitrogen and extracted in ice cold 1X RIPA Lysis buffer (Merck-Millipore Massachusetts, US), containing 1X Halt Protease and Phosphatase Inhibitor Cocktail (Thermo Scientific, Rockford, USA). All samples were homogenized on ice for 15 seconds with a T8-knife homogenizer (IKA-Works, Breisgau, Germany).

Total protein concentration was measured using the Micro BCA Protein Assay Kit (Thermo Scientific, Rockford, USA). 10 µL of protein sample was added to 100 µL of the BCA protein assay kit and incubated for 30 minutes at 37^{0}C. Absorbance was measured at 562 nm with an Emax Precision Microplate Reader (Molecular Devices, California, US). Protein concentration was calculated by comparison to a standard curve.

2.7.2 Western blotting

Proteins were separated by size in Criterion TGX - Long shelf life precast gels, 4-20 % (BioRad, Hercules, CA), at 200 V for approximately 45 minutes, or to the ladder was properly separated, in Tris/glycine buffer at room temperature. After separation, proteins were transferred to a nitrocellulose criterion blotter membrane (BioRad, Hercules, CA) at 100 V for 30 minutes, in ice cold Tris/glycine buffer containing methanol. Total protein load was stained in 0.1 % ponceau solution (Merck-Millipore Massachusetts, US) and scanned with a V700 Photo scanner (EPSON, Suwa, Japan).

To inhibit unspecific binding of the antibodies, membranes were blocked in 5 % Non-fat dry milk (NFDM) (BioRad, Hercules, CA) in TBSt, TBS with 5 % TWEEN (Sigma-Aldrich, Missouri, US), for 1 hour at room temperature (overnight, 4^{o}C Anti-MLKL (phospho S345) antibody (Abcam, Cambridge, UK)). Incubation with primary antibody (in 5 % NFDM in TBSt) was done overnight at 4^{0}C (except for Anti-MLKL (phospho S345) antibody where 1 hour in room temperature was used). The following day membranes were washed in TBSt three times for 15 minutes before 1 hour incubation (2 hours for Anti-MLKL (phospho S345) antibody) with secondary antibody in 5 % NFDM in TBSt, for 1 hour at room temperature. The membrane was incubated for 1minute with Pierce® ECL Western Blotting Substrate (Thermo Scientific, Rockford, US).

ChemiDoc Touch Imaging System and Image Lab Software (BioRad, Hercules, CA) was utilized to analyze the western blots.

2.8 Total RNA isolation, cDNA synthesis and qPCR

Total RNA isolation, cDNA synthesis and qPCR were performed on tissue from Langendorff-perfused hearts (paragraph 2.2) and isolated cardiac fibroblast treated similarly to cells used in the viability assessment (paragraph 2.4).

2.8.1 Total RNA isolation

Total RNA was isolated with RNeasy Mini KIT (Qiagen, Hilden, Germany) according to the manufacturer's protocol. In brief, cardiac fibroblasts utilized for total RNA isolation were washed with PBS before RLT lysis buffer (Qiagen, Hilden, Germany) was added, containing 0.1 % β-mercaptoethanol (Sigma-Aldrich, Missouri, US). Heart tissue was crushed in liquid nitrogen before it was suspended in RLT buffer, containing 0.1 % β-mercaptoethanol, and crushed with lysing matrix tubes (MP Biomedicals, California, US) in a Fast Prep™ FP120 (Thermo Savant, Thermo Fisher scientific, Rockford, US). All samples were centrifuged (Heraus fresco 21, Thermo Fisher scientific, Rockford, US) at 12.000x g for 5 minutes. The water phase was instantly blended with equal volume of 70 % ethanol. Samples were centrifuged repeatedly, washed and treated with DNase before RNA was eluted with Rnase-free water by centrifugation at 10.000 x g for 1 minute. A Nano Drop 1000 Spectrophometer (Thermo Fisher Scientific, Rockland, US) was used to measure the total RNA concentration.

2.8.2 cDNA synthesis

cDNA synthesis was performed with a qScript cDNA Synthesis Kit (Quanta Biosciences, Chicago, US) according to the manufacture`s protocol. cDNA was made from the lowest concentration of isolated RNA. RNA (150 ng for cardiac fibroblast and 200 ng from heart tissue) and Nuclease free water in a total volume of 15 µL and mixed with 4 µL qScript Reaction Mix (containing optimized buffer, magnesium, oligo (dT), and dNTPs) and 1 µL qScript Reverse Transcriptase. cDNA was synthesized in a T3 Thermocycler (Biometra, Gottingen, Germany) under the following temperature regime; 5 minutes at 22^0C, 30 minutes at 42^0C and 5 minutes at 85^0C. Samples were stored at -20^0C.

2.8.3 Quantitative Real-Time polymerase chain reaction (qPCR)

All qPCR measurements were conducted in a 7900HT Fast Real-Time PCR system, SDS2.3 (Applied Biosystems, Thermo Fisher Scientific, Massachusetts, US). Power SYBR Green PCR Master Mix (Applied Biosystems, Thermo Scientific, Rockford, USA) was used in all reactions. Reaction volume of all samples was 10µL, containing gene specific primers, F/R (RIPK1, RIPK3 and MLKL (Eurofins genomics, Edersberg, Germany), Rpl32, IL-1b, IL-6, IL-18 and TNF-α (Thermo Scientific, Massachusetts, US)), cDNA and 6 µL Power SYBR Green PCR Master Mix. Samples were loaded in 96-well plates and sealed with transparent foil. The following qPCR program was applied; 1) 50°C for 2 minutes 2) 95°C for 10 minutes 3) 95°C for 15 seconds 4) 60°C for 1 minute. Step 3 and 4 was repeated for 40 cycles. Primer design was carried out using Primer3 program (http://bioinfo.ut.ee/primer3-0.4.0/).

Table 1: List of all primers utilized in the project. F=forward primer, R=reverse primer.

Gene	Direction	Primer sequence
RIPK1	F	CCTGCTGGAGAAGACAGACC
	R	CATCATCTTCCCCTCTTCCA
RIPK3	F	ACACGGCACTCCTTGGTATC
	R	CCGAACTGTGCTTGGTCATA
MLKL	F	AGTGAAGCCCCCTGAGTTCT
	R	GCTGCTGATGTTTCTGTGGA
IL-1b	F	TGAAATGCCACCTTTTGACA
	R	TGTCCTCATCCTGGAAGGTC
IL-6	F	CTGATGCTGGTGACAACCAC
	R	CAGAATTGCCATTGCACAAC
IL-18	F	GGCTGCCATGTCAGAAGACT
	R	GGGTTCACTGGCACTTTGAT
TNF-α	F	GAACTGGCAGAAGAGGCACT
	R	GGTCTGGGCCATAGAACTGA
Rpl32	F	TCGTCAAAAAGAGGACCAAGAAG
	R	CCGCCAGTTTCGCTTAATTT

All samples were run in duplicates. Data are shown as relative expression ($2^{-\Delta\Delta ct}$), normalized to the endogenous control (Rpl32).

2.9 Statistical analysis

Values are presented as mean ± SD, unless otherwise stated. GraphPad Prism 6 (GraphPad Software, California, US) has been utilized to make all graphs and perform all statistical analysis. All data were tested for normal distribution using Kolmogorov-Smirnov test and equal standard deviation using Bartlett's- and Brow-Forsythe test. If not normal distribution or difference in standard deviation, a non-parametric ANOVA (Kruskal Wallis) was used. Otherwise, one- or two way ANOVA was used followed by Dunnett`s multiple comparison test. In the figures, the p-value of the ANOVA is shown top left and the post-tests indicated with asterisks (*<0.05, **<0.001, ***<0.0001).

2.10 Methodological considerations

2.10.1 Detection of cellular necroptosis

Stimuli that normally trigger cell apoptosis can also activate the necroptotic pathway. Because of the distinct morphological characteristic it is possible to distinguish between the two different death types with the use of dye. The necroptotic demise causes an early loss of plasma membrane integrity, therefore dual staining with Annexin V and Propidium Iodide (PI) has been used to discriminate between apoptosis and necrosis. When performing flow cytometry, Annexin V-positive/PI-negative cells are considered to be apoptotic, and PI-positive cells are necrotic.

Apoptotic regulators like caspases, Bcl-2 family members (like Bax), and mitochondrial cytochrome c release are not involved in necroptosis [90] and could therefore be used to discriminate necroptosis from cell death executed by the apoptotic machinery.

The serine/threonine kinase activity of RIPK1 and RIPK3 has been shown to be an important step in initiation of the necroptotic pathway [90]. These kinases are however both involved in other cell death modes and prosurvival pathways, and their activity is therefore not a proof of necroptosis. Phosphorylation of MLKL is the crucial step in necroptotic execution and is therefore an important target in detection of necroptosis [44].

2.10.2 P-MLKL antibody

The central role of p-MLKL in necroptosis makes it a natural target in investigation of the cell death type. An important part of this project was to look for differences in p-MLKL/total MLKL in perfused mouse hearts after treatment with necrostatins. This turned out to be challenging. Without succeeding, many attempts were performed trying to optimize Anti-MLKL (phospho S345) antibody (Abcam, Cambridge, UK), resulting in inverted blots. Different concentrations of primary and secondary antibody, proteins and blocking (both NFDM and BSA) were tested on nitrocellulose- and PVDF membranes. Multiple versions of incubation time and temperature were also tried. Other western blots that were performed simultaneously, also the non-phosphorylated version of MLKL (Anti-MLKL antibody-N-terminal (Abcam, Cambridge, UK)), gave good results, indicating that there was nothing wrong with the general protocol. After troubleshooting with the provider, a new batch was delivered with similar results. The best blots with p-MLKL, those presented in this thesis, were achieved with 40µg protein, blocked with 5 % NFDM overnight, 1hour with primary antibody (1:2500) in room temperature followed by secondary antibody (1:5000), for 1 hour, in room temperature.

Even though we managed to get some blots that were possible to analyze, the quality was very bad, with a lot of unspecific binding of the antibody and considerable background. The credibility of the results are under question, and this should be considered when reading the results.

2.10.3 Infarction size in the isolated heart preparation

Although the two series of Langendorff-perfused hearts had the same ischemic time, the infarct size in the control group in series 2 is significantly larger than the control group in series 1. This is a known phenomenon and often observed in isolated hearts, although the reason is still unknown. Tolerance to ischemia show seasonal variation and it is therefore a necessity to perform complete series within a time frame as short as possible. The absolute infarct size is not comparable between series 1 and 2, as they were performed at different times. The intra-series comparison is still valid.

2.10.4 The use of immortalized cell lines

Immortalized cell lines are cancer cells that in many respects are very different from the primary cardiac cells. The choice of utilizing HL-1 cells (an immortalized cardiomyocyte cell line) in these experiments was made because they are easily transfected and can therefore be used to reveal molecular pathways not easily manipulated in primary cells. Unfortunately, time restrictions did not allow us to complete these experiments. I chose to include these preliminary results as they show that these cells also respond to Nec-1.

3 Results

3.1 Dose response of Nec-1 in primary adult mouse cardiomyocytes and cardiac fibroblasts

3.1.1 Nec-1 has a dose dependent effect on cell death in primary adult mouse cardiomyocytes

No effect was found on the number of remaining cells after exposing cardiomyocytes to either 1 µM or 10 µM Nec-1, compared to control (Fig.12A). In contrast, 100 µM Nec-1 reduced the number by 36 % ± 18, compared to control ($p<0.001$) (Fig.12A). No morphological differences could be detected on the remaining cells (Fig.12B), but the highest dose of Nec-1 increased the number of PI-positive cells ($p<0.05$), indicating increased necrotic cell death (Fig.12C). Total and mean intensity of PI did not vary between groups (supplemental data Fig.S1).

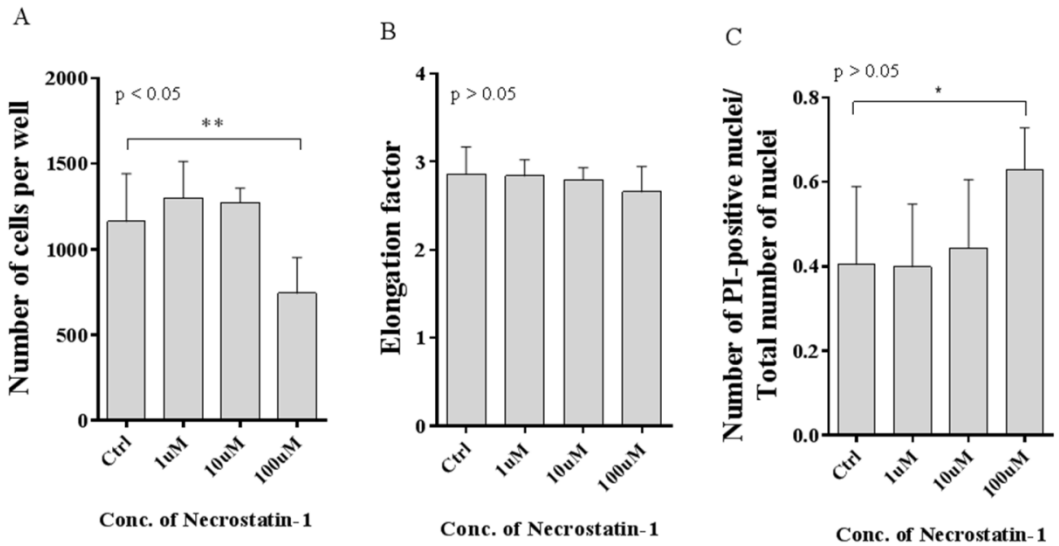

Figure 12: Dose dependent effect of Nec-1 in adult mouse primary cardiomyocytes. Cardiomyocytes were isolated from WT mice (N=6) and treated with different concentrations of Nec-1 (dissolved in DMSO). Quantification and visualization of the cells was done on an Olympus Scan^R imaging station. **A)** Number of cells present after overnight treatment. **B)** Elongation factor (length of cells/width of cells) of cells counted after treatment. **C)** Ratio of the amount of PI-positive nuclei and the total amount of nuclei. Values are presented as mean ± SD. Effects of treatment were evaluated with one-way ANOVA, followed by a Dunnett`s multiple comparison test.

3.1.2 Nec-1 has no dose dependent effect on viability in primary adult mouse cardiac fibroblasts

Different concentrations of Nec-1 were tested on cardiac fibroblasts, and did not affect cell death at any concentrations. No difference was detected in number of remaining cells (Fig.13A) or in the amount of PI-positive cells (Fig.13B), between the groups. Because fibroblasts do not show any specific morphological features that are detectable with the software used, elongation factor was not investigated. Total and mean intensity of PI did not vary between groups (supplemental data Fig.S2).

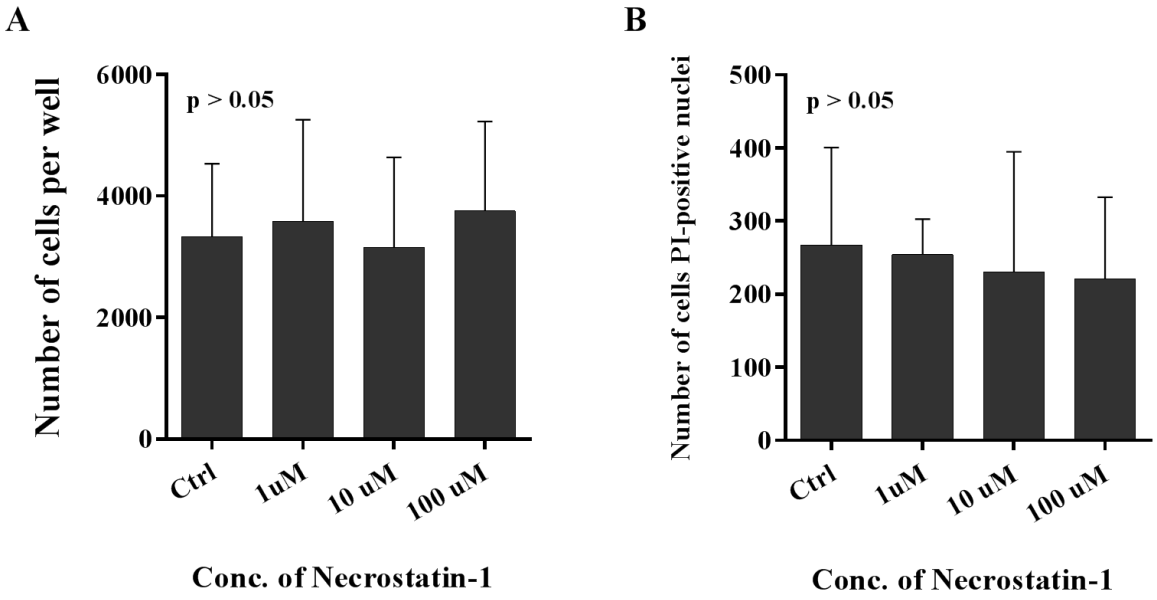

Figure 13: Effect of Nec-1 on adult mouse primary cardiac fibroblasts. Cardiac fibroblasts were isolated from WT mice (N=6) and treated with different concentrations of Nec-1 (dissolved in DMSO). Quantification and visualization of the cells was done on an Olympus Scan^R imaging station. **A)** Number of cells present after treatment. **B)** Number of PI-positive nuclei. Values are presented as mean ± SD. Effects of treatment were evaluated with one-way ANOVA, followed by Dunnett`s multiple comparison test.

3.1.3 mRNA expression of necroptotic contributors in cardiac fibroblasts in response to Nec-1.

mRNA expressions of RIPK1, RIPK3 and MLKL in cardiac fibroblast exposed to different concentrations of Nec-1 were investigated. mRNA expression of RIPK1 (Fig.14A) was not effected by any of the Nec-1 doses. Due to large variation and a non-normal distribution, the increase in RIPK3 and MLKL were not significant (Fig.14B and C). However, a tendency of increase was observed at 10 µM Nec-1 (Welch corrected t-test p=0.05 and p=0.08 for RIPK1 and MLKL respectively).

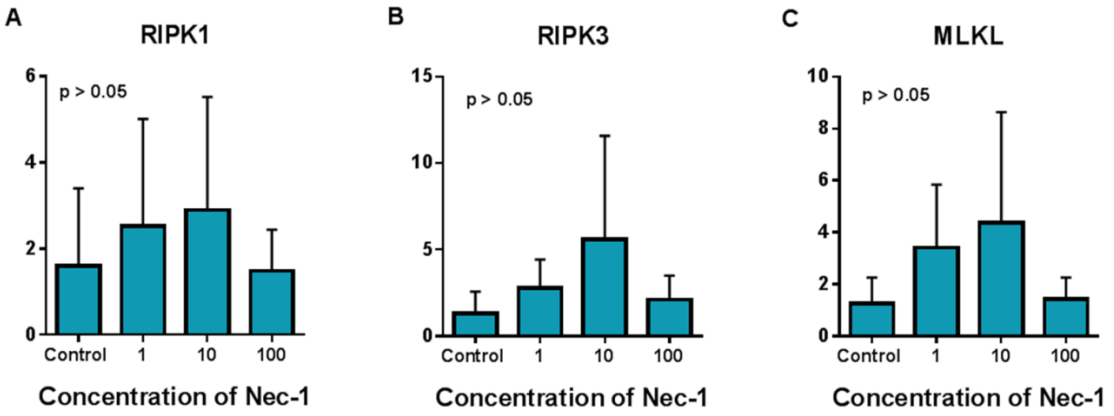

Figure 14: qPCR result of RIPK1, RIPK3 and MLKL in cardiac fibroblast treated with different doses of Nec-1: Cardiac fibroblasts were isolated from WT mice (N=6) and treated with different concentrations of Nec-1 (N=6). **A)** mRNA expression of RIPK1. **B)** mRNA expression of RIPK3. **C)** mRNA expression of MLKL. Values are presented as mean ± SD. Effect of treatment was evaluated with non-parametric ANOVA (Kruskal Wallis).

3.2 Necrostatins have a dose dependent beneficial effect on *ex-vivo* perfused heart function, but is detrimental at higher doses

In series 1, the necrostatin inhibitors were delivered to the hearts during the first minutes of reperfusion. 10 µM Nec-1S increased infarct size ($p<0.05$) (Fig.15A), indicating detrimental effect on heart tissue after ischemia-reperfusion. No difference was detected in infarct size after treatment with 10 µM Nec-1. No difference in heart function could be found between the groups (Fig.15C).

In series 2, the necrostatin inhibitors were delivered to the heart from the first second of reperfusion. No difference in infarct size was found between the groups (Fig.15D). 1 µM of Nec-1S did however improve heart function ($p<0.001$) (Fig15F). After 5 minutes of reperfusion there was a significant decrease of LVEDP between the 1 µM Nec-1S treated group and the control, indicating increased post-ischemic function.

Functional data of left ventricular systolic pressure (LVSP), left ventricular developed pressure (LVdevP), heart rate (HR) maximal left ventricular global contractility (dP/dt max), minimal left ventricular global contractility (dP/dt min), temperature (Temperature) and rate pressure product (RPP) showed no significant difference between any of the treated groups (both series 1 and 2, supplemental Fig.S3 and Fig.S4).

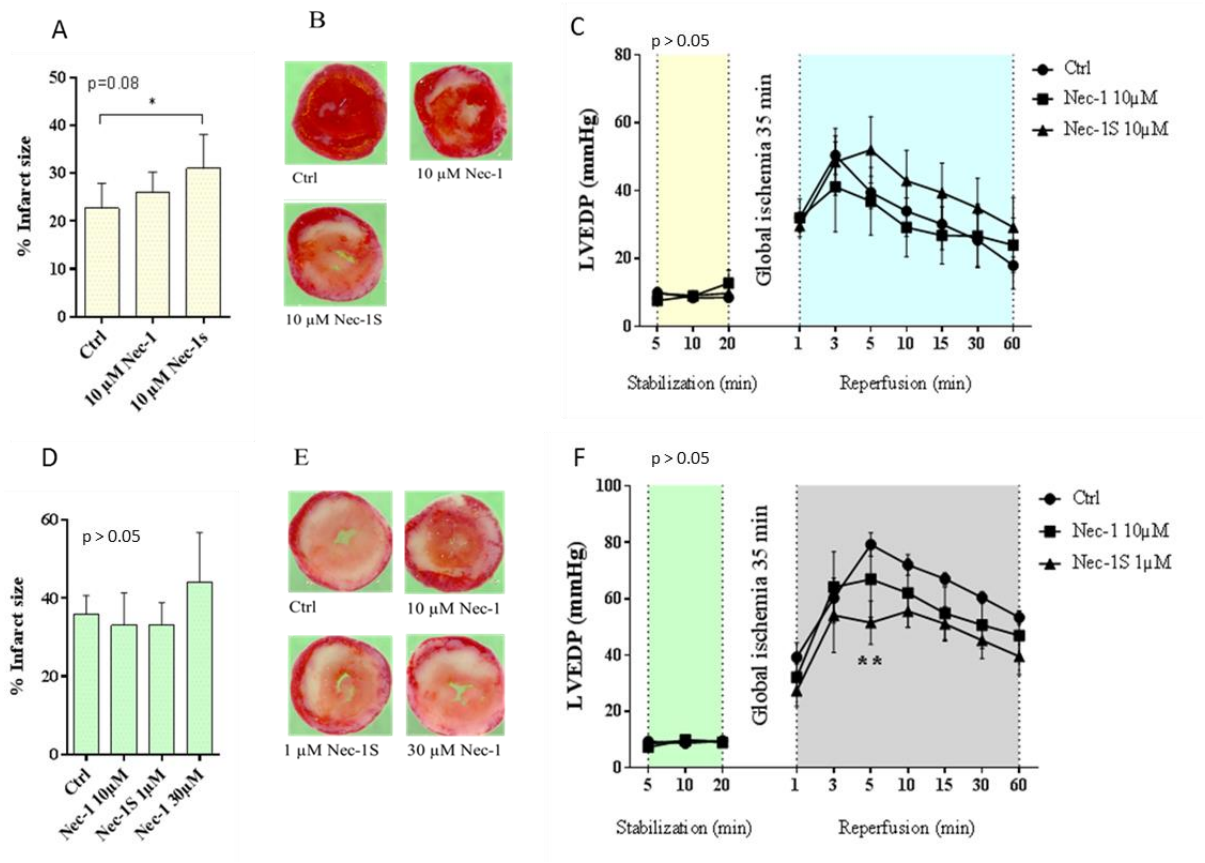

Figure 15: A, B and C: Langendorff- perfused mouse hearts in Series 1 (DMSO (Ctrl, circles N=5), 10 µM Nec-1 (squares N=4) and 10 µM Nec-1S (triangles N=5). The blockers were delivered to the hearts during the first minutes of the reperfusion period. **A)** Infarct size, calculated as a percentage of total area after it was stained with TTC. Values are presented as mean ± SD. Effect of treatment was evaluated with a one-way ANOVA, followed by a Dunnett`s multiple comparison test. **B)** Representative pictures after TTC staining. Red tissue represents healthy tissue, white tissue is dead. **C)** Recordings of LVEDP during stabilization and reperfusion. Values are presented as mean ± SEM. Effect of treatment was evaluated with a two-way ANOVA, followed by a Dunnett`s multiple comparison test.

D, E and F: Langendorff- perfused mouse hearts Series 2: (DMSO (Ctrl, circles N=7), 10 µM Nec-1 (squares N=7), 30 µM Nec-1 (N=2) and 1 µM Nec-1S (triangles N=6). Blockers were delivered to the hearts from the first second of the reperfusion period. **D)** Infarct size, calculated as a percentage of total area after it was stained with TTC. Values are presented as mean ± SD. Effect of treatment was evaluated with a one-way ANOVA, followed by a Dunnett`s multiple comparison test. **E)** Pictures after TTC staining. Red tissue represents healthy tissue, white tissue is dead. **F)** LVEDP during stabilization and reperfusion. Values are presented as mean ± SEM. Effect of treatment was evaluated with a two-way ANOVA, followed by a Dunnett`s multiple comparison test.

3.3 Western blot analysis

3.3.1 MLKL phosphorylation in necrostatin treated Langendorff-perfused hearts

No significant difference in MLKL phosphorylation could be detected between the control group and necrostatin treated groups after ischemia-reperfusion (Fig.16B). The single band detected with total MLKL antibody is clearly visible, while a very faint band with a lot of background was detected using p-MLKL (Fig.16A). (In supplemental Fig.S5; a representation of absolute intensity for both p-MLKL and total MLKL calculated from all groups).

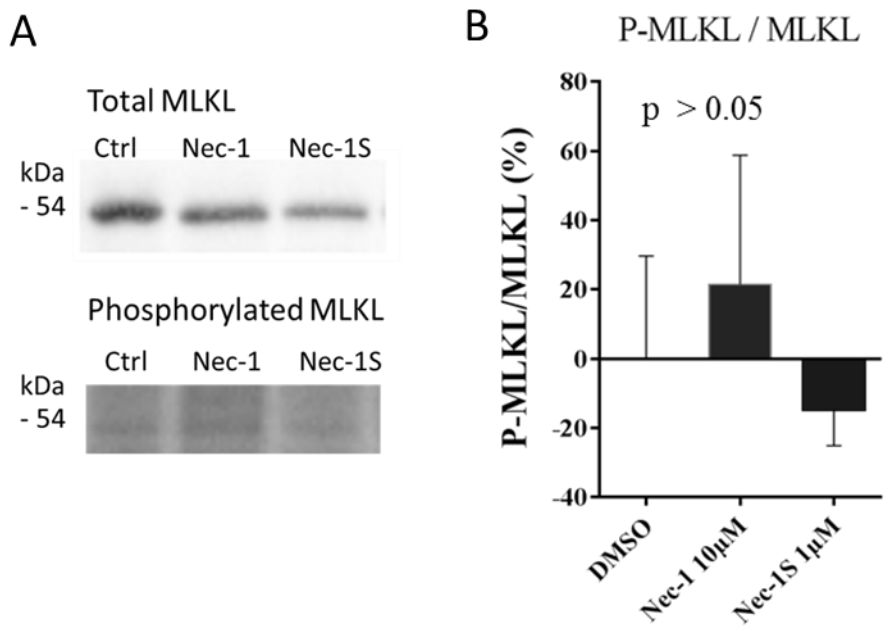

Figure 16: Western Blotting results of total MLKL and phosphorylated MLKL: Western blots were done with both phosphospecific and total protein antibodies of MLKL in the different groups from the Langendorff-perfused hearts, series 2, **(**Ctrl (N=6), 10 µM Nec-1 (N=6), 1 µM Nec-1S (N=5)). **A)** A representation of the 54 kDa band. **B)** Changes are expressed as a ratio between phospho/total. Results are normalized to control group. All values are presented as mean ± SD. Effect of treatment was evaluated with non-parametric ANOVA (Kruskal Wallis).

3.3.2 MAPK- and RISK pathway phosphorylation in necrostatin treated Langendorff-perfused hearts

Protein extracts from all three groups of Langendorff-perfused hearts in series 2 were tested for changes in phosphorylation of MAPK and proteins involved in the RISK-pathway.

P38:

We found a 78 % ± 19 ($p<0.05$) decrease in phosphorylation of p38 in hearts treated with 1 µM Nec-1S (Fig.17B). We also observed a reduction in p38 phosphorylation in the group that was treated with Nec-1 10 µM, but this was not significant (Fig.17B). (In supplemental Fig.S6; a representation of absolute intensity for both p-p38 and total p38 calculated from all groups).

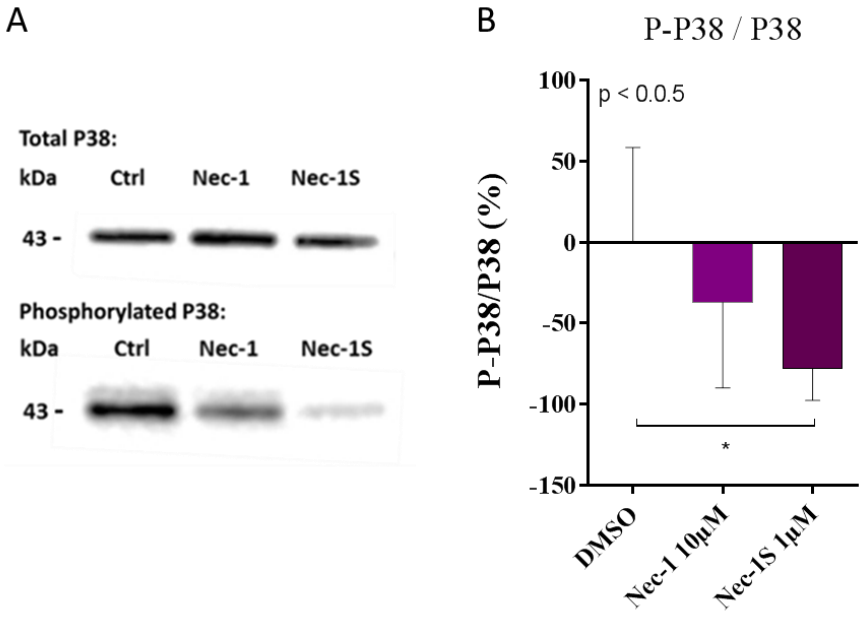

Figure 17: Western Blotting results of total P38 and phosphorylated P38: Western blots were done with both phosphospecific- and total protein antibodies of p38 in the different groups from the Langendorff-perfused hearts, series 2, **(**Ctrl (N=6), 10 µM Nec-1 (N=6), 1 µM Nec-1S (N=5)). **A)** A representation of the 43 kDa band. **B)** Changes are expressed as a ratio between phospho/total. Results are normalized to control group. All values are presented as mean ± SD. Effect of treatment was evaluated with non-parametric ANOVA (Kruskal Wallis).

No significant differences were found between the groups in either total protein or phosphorylation of AKT, AMPK, ERK, JNK (supplemental Fig.S7-Fig.S10).

3.3.3 Elevated level of Bax in Langendorff-perfused mouse hearts in presence of necrostatins

To investigate if necrostatin treatment could cause changes in the apoptotic pathway, the abundance of Bax and Bcl-2 were tested. Bax (Fig.18) increased in the hearts treated with 10 µM Nec-1, compared to the control group ($p<0.05$). Due to big variation in the results from hearts that were exposed to 1 µM Nec-1S, no significant difference was in levels of Bax. No significant differences could be detected between the groups of Bcl-2 (supplemental Fig.S11).

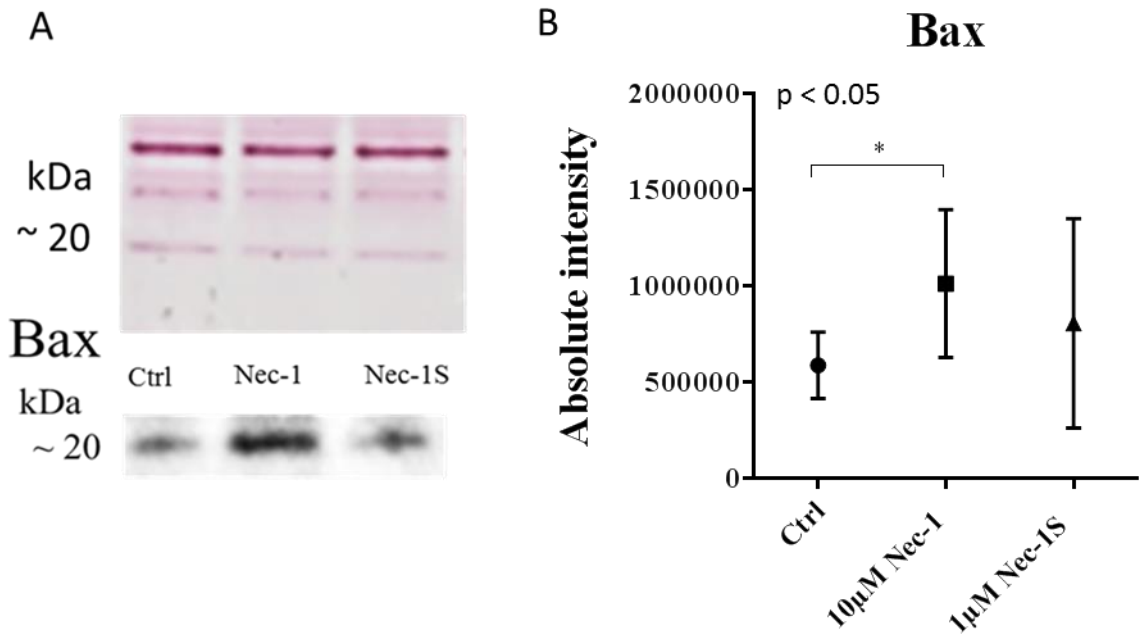

Figure 18: Western blot results of Bax: Western blots were done on the different groups of the Langendorff-perfused hearts, series 2, (Ctrl (N=6), 10 µM Nec-1 (N=6), 1 µM Nec-1S (N=5)). **A)** Above; Ponceau staining confirms equal loading, below; abundance of the 20 kDa protein in the different exposure groups. **B)** Bax protein expression after the different treatments presented as mean ± SD and evaluated with non-parametric ANOVA (Kruskal Wallis), followed by a Dunnett's multiple comparison test.

3.4 Quantitative real time PCR

3.4.1 mRNA expression of necroptotic contributors in Langendorff-perfused hearts in presence of necrostatins

To investigate transcriptional regulation of RIPK1, RIPK3 and MLKL, mRNA expression from the Langendorff-perfused hearts in series 2, were quantified by qPCR. No significant difference could be detected between the necrostatin treated groups (Fig19A, B and C).

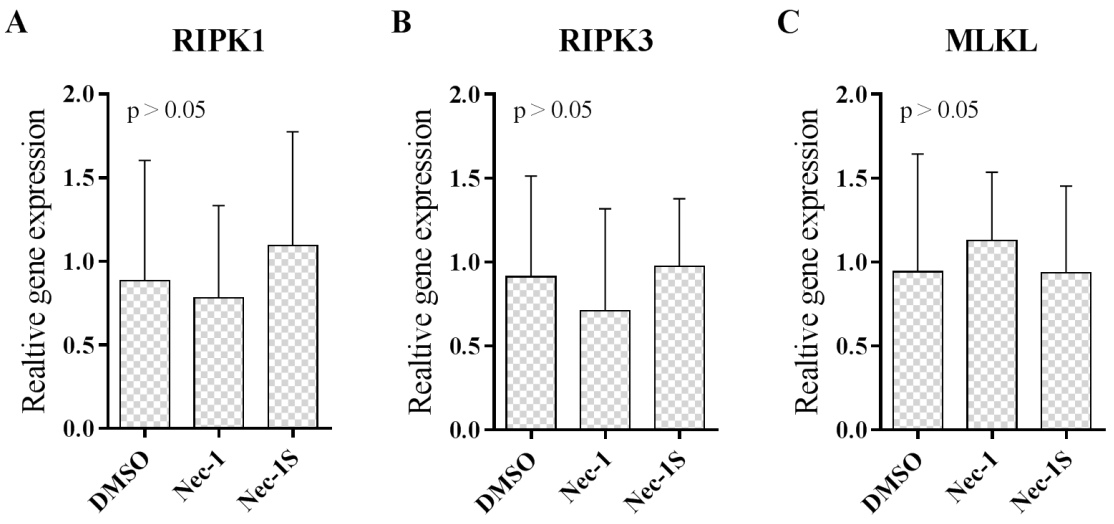

Figure 19: qPCR results of RIPK1, RIPK3 and MLKL from Langendorff-perfused mouse hearts, series 2, in presence of necrostatins: (Ctrl (N=6), 10 µM Nec-1 (N=6), 1 µM Nec-1S (N=5)) **A)** Relative mRNA expression of RIPK1. **B)** Relative mRNA expression of RIPK3 **C)** Relative mRNA expression of MLKL. The results are presented as mean ± SD and evaluated with one-way ANOVA, followed by Dunnett`s multiple comparison test.

3.4.2 mRNA expression of inflammatory cytokines in Langendorff-perfused mouse hearts treated with necrostatins

The expression of IL-1β (Fig. 20A) was increased (p=0.05) in hearts treated with 10 µM Nec-1, compared to the control group. No significant difference could be detected between the necrostatin treated groups or between the control group in mRNA expression of the three other inflammatory cytokines (IL-6, IL-18 and TNF-α) (Fig.20B, C and D).

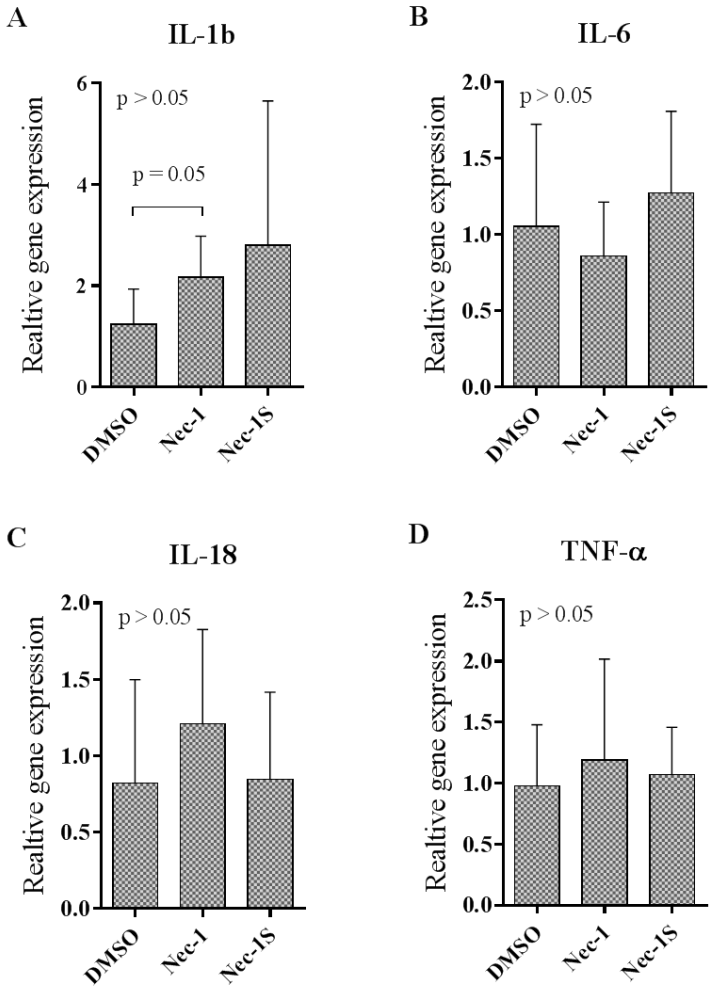

Figure 20: qPCR results of inflammatory cytokines in langendorff-perfused hearts, series 2, treated with necrostatins: (Ctrl (N=6), 10 µM Nec-1 (N=6), 1 µM Nec-1S (N=5)) **A)** Relative mRNA expression of IL-1β (IL-1b). **B)** Relative mRNA expression of IL-6 **C)** Relative mRNA expression of IL-18. **D)** Relative mRNA expression of TNF-α. The results are presented as mean ± SD. Effect of treatment was evaluated with non-parametric ANOVA (Kruskal Wallis), followed by Dunnett's multiple comparison test.

3.5 Nec-1 causes alterations in NF-κB signaling activity in primary adult mouse cardiac fibroblast

NF-κB signaling pathway activity was investigated after treatment with necroptosis inhibitor, Nec-1, in combination with the apoptosis inhibitor, Z-VAD-FMK (Z-Vad), and TNF-α. Compared to the control group, NF-κB signaling activity was significantly upregulated when cardiac fibroblasts were exposed to Nec-1 in combination with Z-VAD-FMK (Fig.21). When TNF-α was present with the two cell death inhibitors, NF-κB activity increased even further (Fig.21). Neither Nec-1 nor TNF-α alone increased NF-κB activity compared to the control (Fig.21).

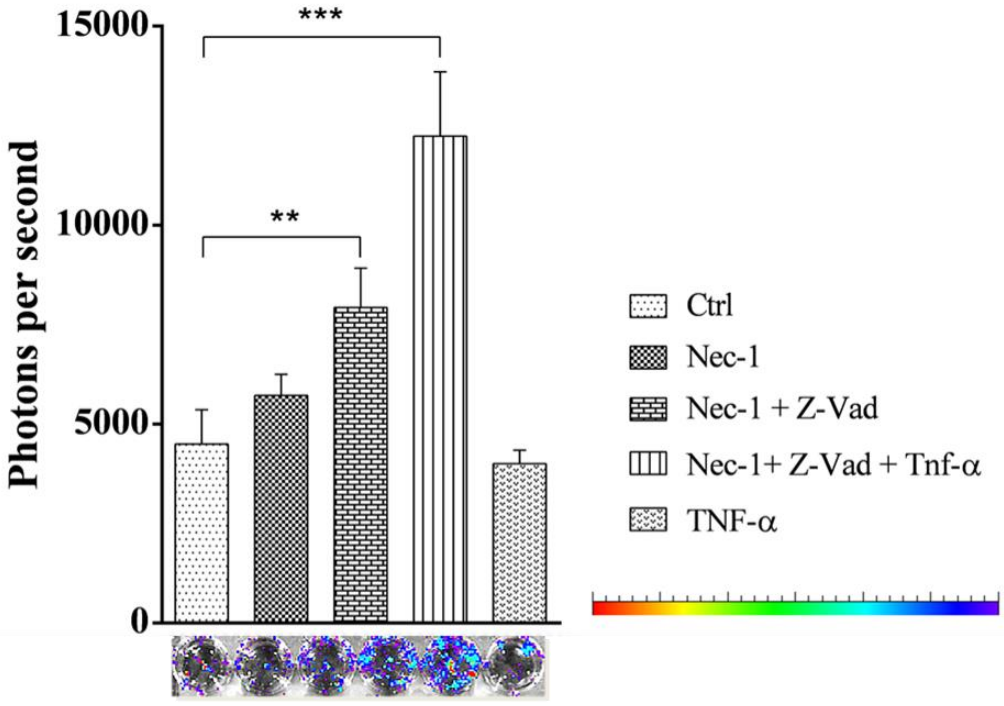

Figure 21: NF-kB Luciferase reporter activity in cultured cardiofibroblasts: Cardiac fibroblasts were isolated from NF-κB reporter mice (N=3) and treated with different combinations of Nec-1 10 µM, Z-Vad 10 µM and TNF-α 10ng/ml. The results are presented as mean ± SD. Effect of the different treatment were evaluated with one-way ANOVA, followed by Dunnett`s multiple comparison test.

3.6 TNF-α do not affect viability in primary adult mouse cardiomyocytes nor cardiac fibroblasts

3.6.1 TNF-α do not cause cell death in primary mouse cardiomyocytes

In order to manipulate necroptosis in primary mouse cardiomyocytes, a dose-response test was performed with the known cell death inducer TNF-α. No difference was found in either the number of remaining cells (Fig.22A), in morphology (Fig.20B) or in the amount of PI-positive nuclei (Fig.22C). Total- and mean intensity of PI did not show any differences between groups (supplemental data Fig.S12).

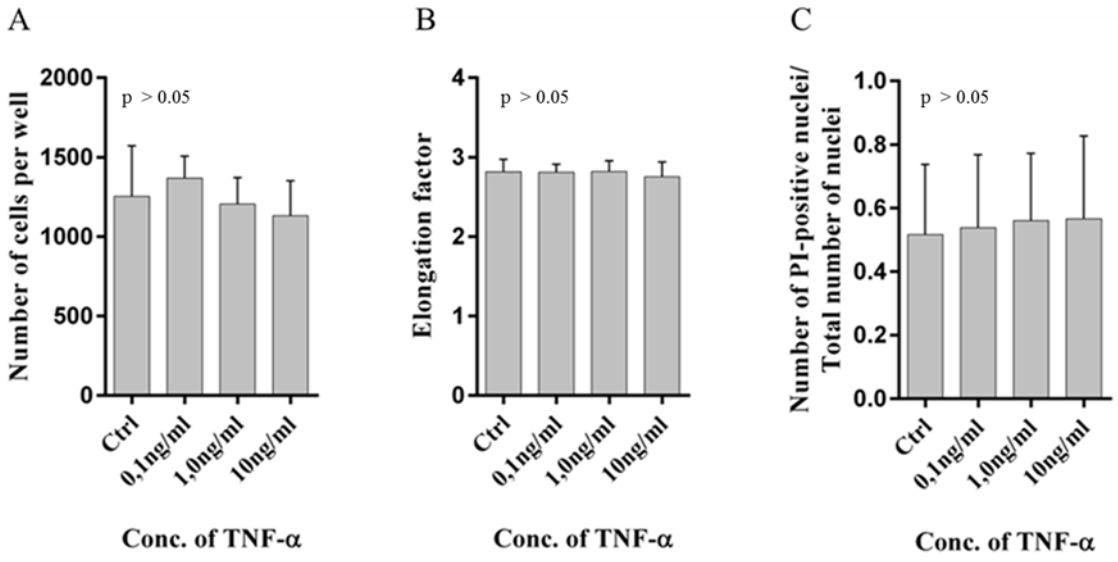

Figure 22: Induction of cell death with TNF-α in primary mouse cardiomyocytes: Adult cardiomyocytes were isolated from WT mice (N=6) and treated with different concentration of TNF-α to initiate cell death. Quantification and visualization of the cells were done on an Olympus Scan^R imaging station. **A)** Number of cells present after treatment. **B)** Elongation factor (length of cells/width of cells) of cells after treatment. **C)** Ratio of the amount of PI-positive nuclei and the total amount of nuclei. All values are presented as mean ± SD and evaluated with one-way ANOVA followed by Dunnett's multiple comparison test.

3.6.2 TNF-α have no effect on viability in primary adult mouse cardiac fibroblast

A dose-response test was also performed on cardiac fibroblasts with TNF-α to initiate cell death. No difference was detected, in number of remaining cells (Fig.23A) or in the amount of PI-positive cells (Fig.23B), between the groups. Because fibroblasts do not show any specific morphological features that are detectible with the software used, elongation factor was therefore not investigated. (Total- and mean intensity of PI did not show any differences between groups (supplemental data Fig.S13)).

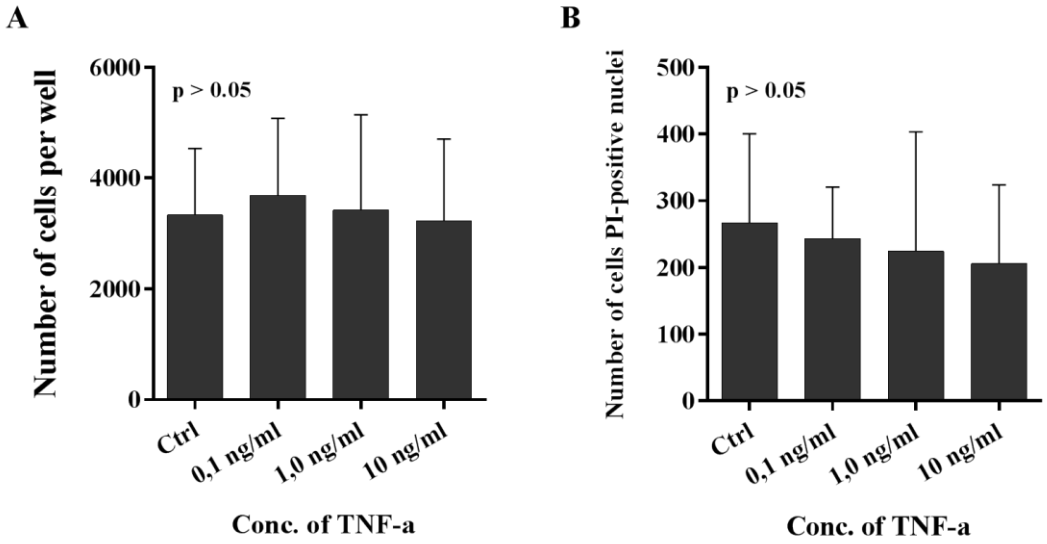

Figure 23: Effect of TNF-α on viability in cardiofibroblasts: Cardiac fibroblasts were isolated from WT mice (N=6) and treated with different concentrations of TNF-α. Quantification and visualization of the cells was done on an Olympus Scan^R imaging station. **A)** Number of cells present after treatment. **B)** Number of PI-positive nuclei. All values are presented as mean ± SD. Effects of treatment were evaluated with one-way ANOVA followed by Dunnett's multiple comparison test.

3.6.3 Viability of primary mouse cardiomyocytes is not affected when exposed to cell death stimuli in combination with cell death inhibitors

Induction of cell death with TNF-α and suppression of cell death with Nec-1, inhibitor of necroptosis, and Z-VAD-FMK (Z-Vad), inhibitor of apoptosis, in primary mouse cardiomyocytes

To identify the different cell death types, TNF-α was combined with inhibitors of necroptosis and apoptosis. No difference was found in either the number of remaining cells (Fig.24A), in morphological changes (Fig.24B) or in the amount of PI-positive nuclei (Fig.24C).

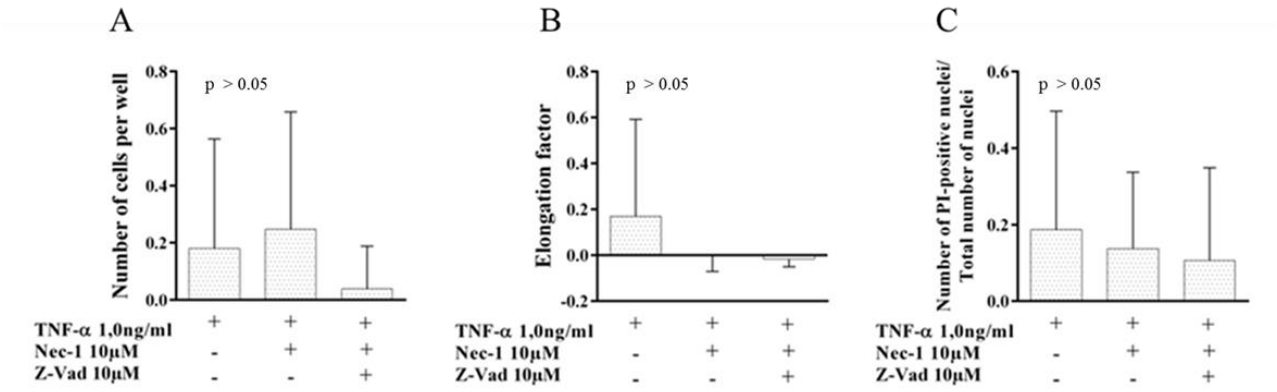

Figure 24: The effect of TNF-α combined with cell death inhibitors, Nec-1 and Z-VAD-FMK (Z-Vad): Cardiomyocytes were isolated from WT mice and treated with different combinations of TNF-α and the two cell death inhibitors Nec-1 and Z-Vad. 1.0ng/ml TNF-α (N=6), 1.0ng/ml TNF-α + 10 µM Nec-1 (N=4), 1.0ng/ml TNF-α + 10 µM Nec-1 + 10 µM Z-Vad (N=4). Quantification and visualization of the cells was done on an Olympus Scan R imaging station. All data is normalized to their respective control. **A)** Number of cells present after treatment. **B)** Elongation factor (length of cells/width of cells) of cells after treatment. **C)** Ratio of the amount of PI-positive nuclei and the total amount of nuclei. All values are presented as mean ± SD. Effects of treatment were evaluated with one-way ANOVA followed by Dunnett's multiple comparison test.

3.7 Effects of Nec-1 in the immortalized cardiac cell line HL-1

3.7.1 Determination of Nec-1 concentration in HL-1 cells

Nec-1 has a dose dependent effect on cell death in HL-1 cells

Figure 25A and B show the results of a Nec-1 dose-response test performed on HL-1 cells. Even though the number of experiments performed is low, it shows a tendency of a dose-dependent response. The amount of viable cells was slightly increased in the presence of Nec-1 in the two smallest doses, 1 µM and 10 µM, compared to the control group. The highest dose of Nec-1, 100 µM, significantly reduced cell viability. Cell death, mainly necrotic cell death was reduced when cells were exposed to Nec-1 1 µM. This indicates that necroptosis occurred in the culture.

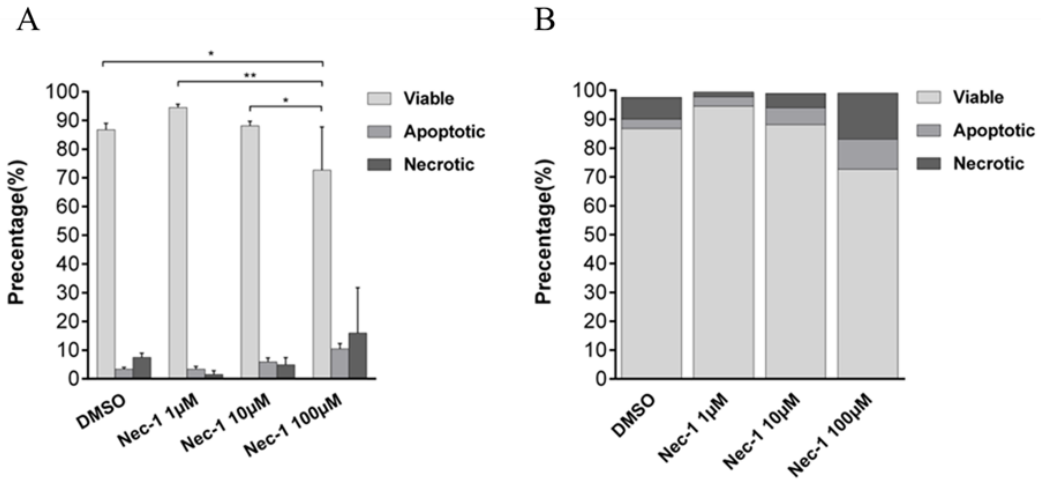

Figure 25: Effect of Nec-1 on HL-1 cells: HL-1 cells were treated with different concentrations of Nec-1 (dissolved in DMSO). Flow cytometry was used to analyze and calculate the effect of the treatment. DMSO was used as vehicle control. (Replicates: DMSO=7, Nec-1 1 µM=2, Nec-1 10 µM=3, Nec-1 100 µM=2). **A and B)** Presentation of the distribution between viable, apoptotic and necroptotic/necrotic cells in percentage after treatment with different concentrations of Nec-1. **A)** Values are presented as mean ± SEM. Effects of treatment was evaluated with two-way ANOVA, followed by Dunnett`s multiple comparisons test. **B)** For better visualization the same data are represented as ratios. Values are presented as mean.

3.7.2 Nec-1 tended to reduce the amount of both apoptotic and necroptotic cell death in HL-1 cells when exposed to CCCP

The protective effect of Nec-1, in the presence of CCCP in HL-1 cells

Figure 26A and B shows the result of a dose-response test performed with mitochondrial proton uncoupler CCCP on HL-1 cells to induce cell death. To investigate if inhibition of necroptosis could influence the amount of apoptotic cell death, 10 µM Nec-1 was combined with CCCP. The results show no significant difference between the groups. All the three different doses of CCCP show a tendency to reduce viability compared to the control. The percentage of apoptotic and necrotic cell death are higher in all of the CCCP stimulated groups compared to the control group. Nec-1 appears to have a slight protective effect when combined with CCCP. Although only a pilot, Nec-1 seems to be protective by reducing the amount of both apoptotic and necrotic cell death caused by CCCP exposure.

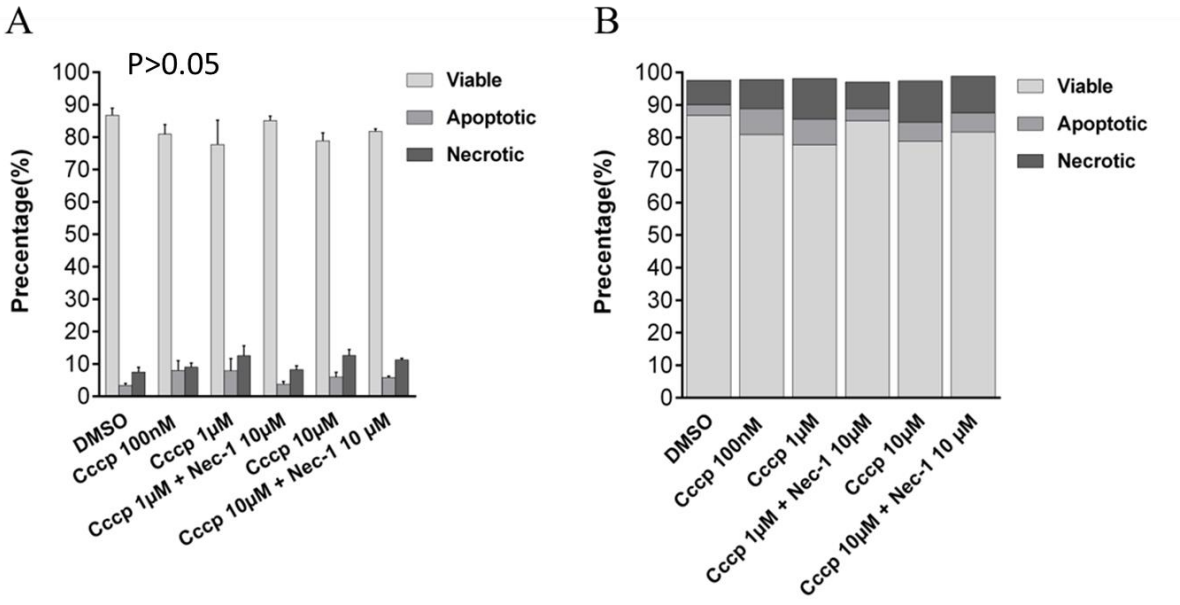

Figure 26: HL-1cells exposed to CCCP and Nec-1: HL-1 cells were treated with different concentrations of CCCP and 10 µM Nec-1 (dissolved DMSO). Flow cytometry was used to analyze and calculate the effect of the treatment. DMSO was used as vehicle control. (Replicates: DMSO=7, CCCP 100nM=8, CCCP 1 µM=9, CCCP 1 µM + Nec-1 10 µM=5, CCCP 10 µM=8, CCCP 10 µM+ Nec-1 10 µM=3). **A, B)** Presentation of the distribution between viable, apoptotic and necroptotic/necrotic cells in percentage after treatment with CCCP and Nec-1. **A)** Values are presented as mean ± SEM. Effects of treatment was evaluated with two-way ANOVA. **B)** For better visualization the same data are represented as ratios. Values are presented as mean.

3.8 Nec-1 in primary mouse cardiomyocytes exposed to mitochondrial debris

Our group has previously shown that mitochondrial debris increases cardiomyocyte cell death in comparison with mitochondrial-poor cardiac debris (Torp et al unpublished). In a proof of concept pilot we assessed viability in primary mouse cardiomyocytes after stimulation with 50 µg mitochondrial debris and 10 µM Nec-1. Compared to the control group, 50 µg mitochondrial-debris tended to reduce the amount of cells (Fig.26A), which was reversed when the cells were treated with 10 µM Nec-1. No significantly difference was found in the morphology or in amount of PI-positive cells between the groups (Fig.26B and C).

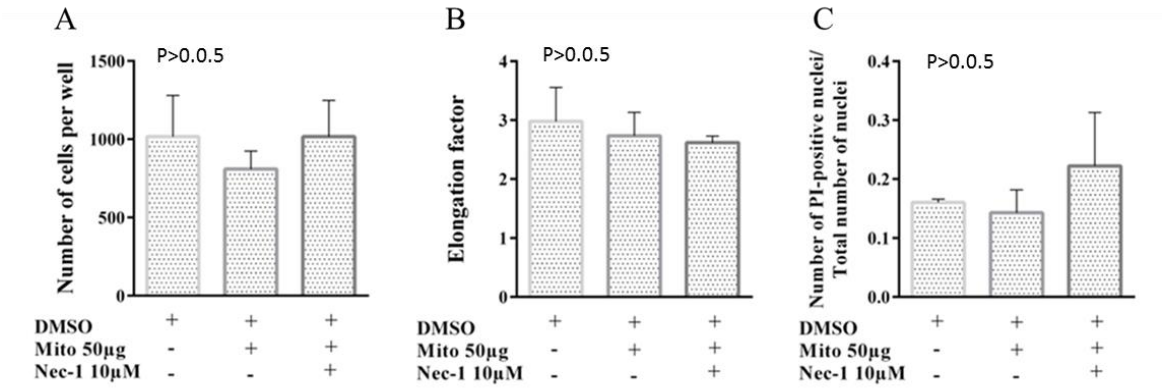

Figure 27: The effect of Nec-1 and mitochondrial debris in cardiomyocytes: Adult cardiomyocytes were isolated from WT mice (N=3) and treated with mitochondrial debris, 50 µg, and 10 µM Nec-1. DMSO was used as vehicle control. Quantification and visualization of the cells was done on an Olympus Scan^R imaging station. All data is normalized to their own controls **A)** Graph showing number of cells counted after treatment. **B)** Presentation of calculated elongation factor (length of cells/width of cells) of present cells. **C)** Presentation of the ratio between the amount of detected PI-positive nuclei and the total amount of nuclei. All values are presented as mean ± SD. Effects of treatment were evaluated with one-way ANOVA followed by a Dunnett's multiple comparison test.

4 Discussion

This study is one of only five investigations on the effect of necrostatins in cardiac models. The goal was to investigate the molecular mechanisms of necroptosis in cardiac cells and to find an approach to reduce necrotic cell death and inflammation after MI. We hypothesized that inhibition of necroptosis could lead to activation of the apoptotic pathway and thereby reducing sterile inflammation.

For the first time Nec-1S was tested in a cardiac model, and we show that Nec-1S improved post-ischemic cardiac function, supported by reduced p38 phosphorylation, in the Langendorff-perfused mouse hearts. We also found indications of increased apoptosis when hearts were subjected to necrostatins.

4.1 Necrostatins in cardiac cells and *ex vivo* perfused mouse hearts

Nec-1 has been used in different models for investigation of necroptosis and has been shown to be an effective inhibitor of RIPK1 [77, 80, 91]. In this project we found that Nec-1 has a clear dose- and cell-dependent effect on cardiac cell viability and *ex vivo* perfused mouse hearts. In addition, we show that Nec-1S has cardio-protective effects by improving heart function, and that Nec-1S has the same dose-dependent effect as Nec-1.

In support of previous observations in other cell systems, our results show that the highest dose of Nec-1, 100 µM, had a detrimental effect on isolated adult primary mouse cardiomyocytes. The immortalized cardiomyocyte cell line, HL-1, also showed increased cell death when exposed to 100 µM Nec-1. For both cardiomyocytes and HL-1 cells, the increased cell death was mainly caused by necrosis. Primary adult mouse cardiac fibroblasts, on the other hand, were not affected by the high dose of Nec-1. The two lower doses of Nec-1, 1 µM and 10 µM, did not affect viability of primary adult mouse cardiomyocytes, cardiac fibroblasts or Hl-1 cells.

The dose dependent effect of Nec-1 was also evident in our *ex-vivo* perfusion experiments. Although the experiment was only performed on two individuals, 30 µM Nec-1 extensively increased infarct size, while 10 µM did not. In a previous study of Langendorff-perfused mouse hearts, 30 µM Nec-1 was found to be protective, while 100 µM Nec-1 was detrimental

[84]. High concentrations of Nec-1 have been observed to have a cytotoxic effect, decreasing cell viability through unknown mechanisms [84, 92, 93]. Our observations are in agreement with these studies and show a strikingly dose-dependent effect of Nec-1. In addition to high dose toxicity, off-target effects of Nec-1 have been observed [80, 94, 95]. Lack of evidence of the exact mechanisms for these observations has led to speculations regarding the specificity of Nec-1. Besides being an effective RIPK1 inhibitor, Nec-1 could interfere with other signaling proteins [79, 80, 94, 95].

To prevent unspecific targeting, an optimized version of Nec-1 was made, called Nec-1S [96]. Due to its chemical structure, Nec-1S should be more selective in RIPK1 inhibition [80, 81]. We tested the effect of Nec-1S on Langendorff-perfused mouse hearts and found that infarction size was increased when hearts were exposed to 10 µM, while 1 µM did not affect infarction size. This indicates that Nec-1S has similar effect as Nec-1, but at lower doses. However, higher concentrations of Nec-1S, 200 µM, 50 µM and 25 µM, have been utilized in studies with different cell models [91, 97], but to our knowledge, this is the first observation of a cytotoxic dose-dependent effect of Nec-1S.

Previous studies have demonstrated that Nec-1, given at the right concentration, has a cardio-protective effect in ischemia-reperfusion. In this project, Nec-1 failed to protect Langendorff perfused mouse hearts from ischemia-reperfusion injury. In 2007, Smith et al [84] showed that Nec-1 given at reperfusion in an *in* vivo mouse ischemia-reperfusion model had a protective effect by preventing elevated cell death. Similarly, Nec-1 treatment reduced infarction size in a myocardial ischemia-reperfusion mouse model *in vivo*, were Nec-1 was injected 5 minutes prior to reperfusion [13]. The protective effect of Nec-1 has also been tested in isolated guinea pig hearts in 2014 [22]. In this study 10 µM Nec-1 was given 5 minutes before ischemia, and during the following 30 minutes of reperfusion [22]. Here, infarction size was significantly reduced in Nec-1 treated hearts, without having any significant effect on heart function [22]. In pigs, subjected to 75 minutes surgical ischemia, followed by 24 hours of reperfusion, Nec-1 treatment, given 10 minutes prior to reperfusion, significantly reduced infarction size and improved heart function [85]. Conflicting with these observations, we were not able to find any protective effect of Nec-1 treatment in *ex vivo* Langendorff perfused mouse hearts. Although Nec-1 had been given prior to reperfusion in most of the studies that have shown a protective effect [13, 22, 84, 85], we wanted to make the drug delivery applicable to acute and clinical injuries. We therefore administrated the

inhibitors at the beginning of reperfusion. With this treatment, Nec-1 failed to protect the hearts from ischemia-reperfusion injury. It is possible that timing of drug delivery is a deciding factor and that to obtain a protective effect Nec-1 must be delivered to the heart before reperfusion. This makes Nec-1 a poor candidate for treating MI in patients.

In contrast to Nec-1, Nec-1S, given at reperfusion, improved post-ischemic heart function of *ex vivo* perfused mouse hearts. 1 µM Nec-1S showed significant decrease in LVEDP, 5 minutes into reperfusion. Left ventricular function is the most important predictor of recovery after a MI [98]. LVEDP reflects ventricular performance and increased diastolic pressure is an indication of diastolic dysfunction, and used as a measurement to identify post ischemic risk of developing heart failure [99, 100]. Even though the only significant difference was after 5 minutes, it is a clear trend of decreased LVEDP for all time points in Nec-1S treated hearts compared to the control group. Our results show that Nec-1S protect from enhanced LVEDP, and thereby improves the prognosis of the hearts.

Nec-1S did not on the other hand, affect infarction size. Infarction size and heart function do not always correlate [99]. It is possible that Nec-1S only succeeded in protecting the hearts early in reperfusion, but without sustained effect, and that the rate of cell death increased later in the reperfusion period. This could explain the result, which shows no difference in infarction size. Another possible explanation could be that inhibition of necroptosis led to activation of other cell death pathways, thereby resulting in the same infarction size.

Our group has previously shown that mitochondrial DNA is released into circulation after MI [101] and that mitochondrial debris increases cardiomyocyte cell death (Torp et al unpublished). As a pilot, we tested the effect of Nec-1 on primary adult mouse cardiomyocytes. Even though the results were not significantly different, Nec-1 tended to protect the cells from rapid death caused by mitochondrial debris exposure. These findings indicate a potential protective effect of Nec-1, although we were not able to show this in our ischemia-reperfusion model.

Taken together, our observations and other reports clearly show that necrostatins have a very strong dose- and cell-dependent effect that needs to be considered when using necrostatins in future studies. It appears that the protective effect of necrostatins in ischemia-reperfusion also depends on time of drug delivery.

4.1.1 Reduced p38 phosphorylation in Nec-1S treated hearts

Phosphorylation of p38 was reduced in the perfused hearts treated with Nec-1S. In general, p38 is known to be involved in a variety of different molecular events, including inflammation and cell death. In the myocardium, p38 is present and is activated during ischemia in response to pressure overload, but only to a limited extent [102-105]. The increase in p38 phosphorylation is a transient response, which occurs during the first 10 minutes of reperfusion [102, 103]. Inhibition of p38 phosphorylation has been shown to reduce cardiomyocyte apoptosis, post-ischemic necrotic injury and improve cardiac function [102, 104]. Phosphorylation of p38 has been shown to influence the contractile properties of cardiomyocytes [105, 106]. When phosphorylation of p38 is inhibited, cardiomyocyte contractility is preserved [106]. Another known consequence of p38 inhibition is a decreased production of the pro-inflammatory cytokine TNF-α [103].

In this study we found that Nec-1S reduced p38 phosphorylation. We also saw significantly improved post-ischemic cardiac function after 5 minutes of reperfusion, which matches previous observations regarding the time of the major p38 phosphorylation. Our findings support other studies that have indicated a close correlation between p38 activation and reduced heart function after ischemia-reperfusion. Based on these findings, the necrostatins could improve post-ischemic heart function by reducing phosphorylation of p38.

4.1.2 Hearts treated with necrostatins show increased IL-1β mRNA

Our results show an upregulated mRNA expression of IL-1β in the hearts that were treated with necrostatins. IL-1β is a cytokine involved in acute and chronic inflammation, primarily produced and secreted from macrophages [107]. Macrophages are abundant in the heart [108], and could be a source of IL-1β. In cardiac tissue it has also been shown that fibroblasts can be major producers of IL-1β [109]. These findings can be linked to the small pilot performed with NF-kB luciferase reporter mice. NF-κB has been shown to play an important role in transcriptional regulation of IL-1β [110]. We found that NF-κB activity was highly increased in primary mouse cardiac fibroblasts exposed to Nec-1. Even though only a few animals were included in this pilot, the results indicate that blocking of RIPK1 in cardiac fibroblasts activates the NF-κB signaling pathway. When apoptosis was also blocked, even higher NF-κB activity was measured. This underlines the importance of RIPK1 role in determining cell fate, and indicates that if the necroptotic-dependent activity of RIPK1 is inhibited, other pathways can be activated. Our results show that Nec-1 can influence NF-κB signaling activity in cardiac fibroblasts and potentially increase IL-1β mRNA expression.

Another known source of IL-1β secretion is pyroptotic cell death, which is a specific type of regulated necrosis. Pyroptosis highly depends on caspase-1, which is often described as an inflammatory caspase [111]. Activation of caspase-1 is regulated by the inflammasome [111]. If necroptosis is blocked by the necrostatins, it is possible that cell death happens through the pyroptotic pathway. Increased mRNA expression is not enough evidence to confirm this, and investigation of caspase-1 activation or other involved proteins will be necessary to confirm this hypothesis.

4.1.3 Increased Bax levels indicate activated apoptosis

Bcl-2 family members are known to be involved in apoptotic cell death. Among these, Bax and Bak mediate mitochondrial outer membrane permeabilization, resulting in cytochrome c release and caspase activation [73]. We found elevated levels of Bax in the Langendorff-perfused mouse hearts treated with necrostatins. Based on the knowledge of the shared molecular pathways in apoptosis and necroptosis, it is possible that blockade of one signaling pathway leads to cell death through another mechanism.

Recently, studies have suggested that there could also be important roles for Bax/Bak in necrotic cell death. Bax/Bax may serve as functional components of MPTP formation, leading towards mitochondrial swelling and eventually organelle rupture [73]. Bax/Bak have also been shown to be important in necroptosis, as Bax/Bak were required for execution of necroptosis in mouse embryonic fibroblasts (MEFs) [62].

Increased Bax levels could indicate apoptotic cell death, as well as necrotic or necroptotic cell death. Since infarction size did not differ between the groups, it is possible that blocking necroptotic cell death could lead to activation of apoptosis.

4.2 The widely used model for mechanistic studies of necroptosis is not applicable to cardiac cells

The best studied necroptotic pathway, and most commonly used model, is initiated by TNF-α at the same time as blockers are used to prohibit apoptotic activation. Therefore we decided to expose cardiac cells to the well-known death inducer, but to our surprise TNF-α did not affect viability of the cells. TNF-α has previously been shown to induce cell death through the apoptotic pathway in neonatal cardiomyocytes and HL-1 cells [112, 113]. Due to time limitations, some of the experiments that involved TNF-α were performed at the same time as the dose-response. In retrospect, the blocking studies therefore do not add in. After consulting with one of the leading groups in the field of necroptosis (Professor Peter Vandenabeele, personal communication), the doses were kept at the same concentrations, but the exposure time of TNF-α was reduced from overnight to 4 hours. However, this did not affect the outcome of the treatment and we could not observe a sufficient amount of cell death initiated by TNF-a. CCCP treatment, a model often used to mimic mitochondrial uncoupling in ischemia-reperfusion [114], was also utilized in attempt to initiate cell death in HL-1 cells, also without success. To allow further investigation of details in the necroptotic pathway a study model suitable for cardiac cells must be identified.

4.2.1 Indirect evidence for necroptotic activation

During this project many attempts were made trying to find molecular evidence of necroptosis in cardiac tissue. Even though we found improved cardiac function in the Langendorff-perfused mouse hearts treated with Nec-1S, which indirectly showed involvement of necroptosis in ischemia-reperfusion injury, we did not see any significant difference in p-MLKL or in mRNA expression of RIPK1, RIPK3 or MLKL in cardiac cells or Langendorff-perfused hearts treated with necrostatins.

From what is known about the mechanisms in necroptosis, phosphorylation of MLKL is a crucial step in the machinery. Since the necrostatins are blocking the signaling pathway prior to phosphorylation of MLKL, differences would be expected to be found between groups.

4.3 Concluding remarks

Little was known about necroptosis in the heart when we started this project. We showed, for the first time, that Nec-1S improves cardiac function in Langendorff-perfused mouse hearts and that Nec-1 tends to protect primary mouse cardiomyocytes from cell death caused by mitochondrial debris exposure. Our goal was to study the molecular mechanisms of necroptosis in cardiac cells, but we were unable to establish a good model that could be used to identify molecular details in the machinery. Nevertheless, we did find that necrostatins reduce p38 phosphorylation, which may be of importance for the understanding of the necroptotic pathway and the effect of necrostatins.

Based on the knowledge of similarities and shared molecular signaling pathways of apoptosis and necroptosis, we also hypothesized that by inhibiting necroptosis, the apoptotic pathway may be activated, leading to reduced sterile inflammation. Our finding of increased Bax levels indicates that if necroptosis is blocked, execution of cell death could happen through the apoptotic machinery and thereby reduce sterile inflammation.

4.3.1 Future prospects

Despite our troubles elucidating the molecular mechanisms of necroptosis, further work should be considered, since necroptosis could be a contributor to the pathogenesis of a variety of health problems and diseases affecting humans. The understanding of necroptotic mechanisms is unfolding at great speed, and more phospho-specific antibodies, inhibitors and transgenic animal models are becoming available, holding great promise to unlock more of the mechanisms of necroptosis. The prominent role of RIPK3 is of great interest in the future as a potential therapeutic target to inhibit necroptosis.

To confirm the results obtained in this project, follow up studies should be performed. The protective effect of Nec-1S should be investigated further. Studies should also be performed on the involvement of p38 in necroptosis. Our findings of increased Bax levels indicate increased levels of apoptosis in hearts subjected to necrostatins. The possibility of redirecting the necroptotic pathway to the apoptotic pathway has potential for research and therapy and should be a priority in the future.

5 References

[1] Gersh BJ, Sliwa K, Mayosi BM, Yusuf S. Novel therapeutic concepts: the epidemic of cardiovascular disease in the developing world: global implications. European heart journal. 2010;31:642-8.
[2] Frangogiannis NG. The immune system and cardiac repair. Pharmacological research. 2008;58:88-111.
[3] Yellon DM, Hausenloy DJ. Myocardial reperfusion injury. The New England journal of medicine. 2007;357:1121-35.
[4] Pellman J, Zhang J, Sheikh F. Myocyte-fibroblast communication in cardiac fibrosis and arrhythmias: Mechanisms and model systems. Journal of molecular and cellular cardiology. 2016;94:22-31.
[5] Woodcock EA, Matkovich SJ. Cardiomyocytes structure, function and associated pathologies. The international journal of biochemistry & cell biology. 2005;37:1746-51.
[6] Camelliti P, Borg TK, Kohl P. Structural and functional characterisation of cardiac fibroblasts. Cardiovasc Res. 2005;65:40-51.
[7] Ahuja P, Sdek P, MacLellan WR. Cardiac myocyte cell cycle control in development, disease, and regeneration. Physiological reviews. 2007;87:521-44.
[8] Orogo AM, Gustafsson AB. Cell death in the myocardium: my heart won't go on. IUBMB life. 2013;65:651-6.
[9] Hashmi S, Al-Salam S. Acute myocardial infarction and myocardial ischemia-reperfusion injury: a comparison. International journal of clinical and experimental pathology. 2015;8:8786-96.
[10] Frangogiannis NG. The inflammatory response in myocardial injury, repair, and remodelling. Nature reviews Cardiology. 2014;11:255-65.
[11] Shinde AV, Frangogiannis NG. Fibroblasts in myocardial infarction: a role in inflammation and repair. Journal of molecular and cellular cardiology. 2014;70:74-82.
[12] Frangogiannis NG, Smith CW, Entman ML. The inflammatory response in myocardial infarction. Cardiovasc Res. 2002;53:31-47.
[13] Oerlemans MI, Liu J, Arslan F, den Ouden K, van Middelaar BJ, Doevendans PA, et al. Inhibition of RIP1-dependent necrosis prevents adverse cardiac remodeling after myocardial ischemia-reperfusion in vivo. Basic research in cardiology. 2012;107:270.
[14] Richardson WJ, Clarke SA, Quinn TA, Holmes JW. Physiological Implications of Myocardial Scar Structure. Comprehensive Physiology. 2015;5:1877-909.
[15] Epelman S, Liu PP, Mann DL. Role of innate and adaptive immune mechanisms in cardiac injury and repair. Nature reviews Immunology. 2015;15:117-29.
[16] Chen GY, Nunez G. Sterile inflammation: sensing and reacting to damage. Nature reviews Immunology. 2010;10:826-37.
[17] Rock KL, Kono H. The inflammatory response to cell death. Annual review of pathology. 2008;3:99-126.
[18] Baum J, Duffy HS. Fibroblasts and myofibroblasts: what are we talking about? Journal of cardiovascular pharmacology. 2011;57:376-9.
[19] Hausenloy DJ, Yellon DM. Reperfusion injury salvage kinase signalling: taking a RISK for cardioprotection. Heart failure reviews. 2007;12:217-34.
[20] Hardie DG. AMP-activated protein kinase: the guardian of cardiac energy status. The Journal of clinical investigation. 2004;114:465-8.
[21] Hausenloy DJ, Yellon DM. Survival kinases in ischemic preconditioning and postconditioning. Cardiovasc Res. 2006;70:240-53.

[22] Koshinuma S, Miyamae M, Kaneda K, Kotani J, Figueredo VM. Combination of necroptosis and apoptosis inhibition enhances cardioprotection against myocardial ischemia-reperfusion injury. J Anesth. 2014;28:235-41.
[23] Takemura G, Kanoh M, Minatoguchi S, Fujiwara H. Cardiomyocyte apoptosis in the failing heart--a critical review from definition and classification of cell death. International journal of cardiology. 2013;167:2373-86.
[24] Chiong M, Wang ZV, Pedrozo Z, Cao DJ, Troncoso R, Ibacache M, et al. Cardiomyocyte death: mechanisms and translational implications. Cell Death Dis. 2011;2:e244.
[25] Festjens N, Vanden Berghe T, Vandenabeele P. Necrosis, a well-orchestrated form of cell demise: signalling cascades, important mediators and concomitant immune response. Biochim Biophys Acta. 2006;1757:1371-87.
[26] Brookes PS, Yoon Y, Robotham JL, Anders MW, Sheu SS. Calcium, ATP, and ROS: a mitochondrial love-hate triangle. American journal of physiology Cell physiology. 2004;287:C817-33.
[27] Halestrap AP, Pasdois P. The role of the mitochondrial permeability transition pore in heart disease. Biochim Biophys Acta. 2009;1787:1402-15.
[28] Zheng Y, Gardner SE, Clarke MC. Cell death, damage-associated molecular patterns, and sterile inflammation in cardiovascular disease. Arteriosclerosis, thrombosis, and vascular biology. 2011;31:2781-6.
[29] Anders HJ, Schaefer L. Beyond tissue injury-damage-associated molecular patterns, toll-like receptors, and inflammasomes also drive regeneration and fibrosis. Journal of the American Society of Nephrology : JASN. 2014;25:1387-400.
[30] Tak PP, Firestein GS. NF-kappaB: a key role in inflammatory diseases. The Journal of clinical investigation. 2001;107:7-11.
[31] Strasser A, O'Connor L, Dixit VM. Apoptosis signaling. Annual review of biochemistry. 2000;69:217-45.
[32] Degterev A, Yuan J. Expansion and evolution of cell death programmes. Nature reviews Molecular cell biology. 2008;9:378-90.
[33] Kerr JF, Harmon B, Searle J. An electron-microscope study of cell deletion in the anuran tadpole tail during spontaneous metamorphosis with special reference to apoptosis of striated muscle fibers. Journal of cell science. 1974;14:571-85.
[34] Kroemer G, Galluzzi L, Vandenabeele P, Abrams J, Alnemri ES, Baehrecke EH, et al. Classification of cell death: recommendations of the Nomenclature Committee on Cell Death 2009. Cell death and differentiation. 2009;16:3-11.
[35] Martin SJ, Henry CM. Distinguishing between apoptosis, necrosis, necroptosis and other cell death modalities. Methods. 2013;61:87-9.
[36] Pasparakis M, Vandenabeele P. Necroptosis and its role in inflammation. Nature. 2015;517:311-20.
[37] Linkermann A, Green DR. Necroptosis. The New England journal of medicine. 2014;370:455-65.
[38] Vanden Berghe T, Vanlangenakker N, Parthoens E, Deckers W, Devos M, Festjens N, et al. Necroptosis, necrosis and secondary necrosis converge on similar cellular disintegration features. Cell death and differentiation. 2010;17:922-30.
[39] Vanden Berghe T, Kaiser WJ, Bertrand MJ, Vandenabeele P. Molecular crosstalk between apoptosis, necroptosis, and survival signaling. Molecular & cellular oncology. 2015;2:e975093.
[40] Giampietri C, Starace D, Petrungaro S, Filippini A, Ziparo E. Necroptosis: molecular signalling and translational implications. International journal of cell biology. 2014;2014:490275.

[41] Christofferson DE, Yuan J. Necroptosis as an alternative form of programmed cell death. Current opinion in cell biology. 2010;22:263-8.
[42] Zheng L, Bidere N, Staudt D, Cubre A, Orenstein J, Chan FK, et al. Competitive control of independent programs of tumor necrosis factor receptor-induced cell death by TRADD and RIP1. Mol Cell Biol. 2006;26:3505-13.
[43] Chan FK, Shisler J, Bixby JG, Felices M, Zheng L, Appel M, et al. A role for tumor necrosis factor receptor-2 and receptor-interacting protein in programmed necrosis and antiviral responses. The Journal of biological chemistry. 2003;278:51613-21.
[44] de Almagro MC, Vucic D. Necroptosis: Pathway diversity and characteristics. Seminars in cell & developmental biology. 2015;39:56-62.
[45] Orozco S, Yatim N, Werner MR, Tran H, Gunja SY, Tait SW, et al. RIPK1 both positively and negatively regulates RIPK3 oligomerization and necroptosis. Cell death and differentiation. 2014;21:1511-21.
[46] Vandenabeele P, Melino G. The flick of a switch: which death program to choose? Cell death and differentiation. 2012;19:1093-5.
[47] Festjens N, Vanden Berghe T, Cornelis S, Vandenabeele P. RIP1, a kinase on the crossroads of a cell's decision to live or die. Cell death and differentiation. 2007;14:400-10.
[48] Luedde M, Lutz M, Carter N, Sosna J, Jacoby C, Vucur M, et al. RIP3, a kinase promoting necroptotic cell death, mediates adverse remodelling after myocardial infarction. Cardiovasc Res. 2014;103:206-16.
[49] Han J, Zhong CQ, Zhang DW. Programmed necrosis: backup to and competitor with apoptosis in the immune system. Nature immunology. 2011;12:1143-9.
[50] Sun L, Wang X. A new kind of cell suicide: mechanisms and functions of programmed necrosis. Trends in biochemical sciences. 2014;39:587-93.
[51] Chan FK, Luz NF, Moriwaki K. Programmed necrosis in the cross talk of cell death and inflammation. Annual review of immunology. 2015;33:79-106.
[52] Rose BA, Force T, Wang Y. Mitogen-activated protein kinase signaling in the heart: angels versus demons in a heart-breaking tale. Physiological reviews. 2010;90:1507-46.
[53] Cargnello M, Roux PP. Activation and function of the MAPKs and their substrates, the MAPK-activated protein kinases. Microbiology and molecular biology reviews : MMBR. 2011;75:50-83.
[54] Steenbergen C. The role of p38 mitogen-activated protein kinase in myocardial ischemia/reperfusion injury; relationship to ischemic preconditioning. Basic research in cardiology. 2002;97:276-85.
[55] Murphy JM, Czabotar PE, Hildebrand JM, Lucet IS, Zhang JG, Alvarez-Diaz S, et al. The pseudokinase MLKL mediates necroptosis via a molecular switch mechanism. Immunity. 2013;39:443-53.
[56] Wu J, Huang Z, Ren J, Zhang Z, He P, Li Y, et al. Mlkl knockout mice demonstrate the indispensable role of Mlkl in necroptosis. Cell research. 2013;23:994-1006.
[57] Xia B, Fang S, Chen X, Hu H, Chen P, Wang H, et al. MLKL forms cation channels. Cell research. 2016.
[58] Dondelinger Y, Declercq W, Montessuit S, Roelandt R, Goncalves A, Bruggeman I, et al. MLKL compromises plasma membrane integrity by binding to phosphatidylinositol phosphates. Cell Rep. 2014;7:971-81.
[59] Wang H, Sun L, Su L, Rizo J, Liu L, Wang LF, et al. Mixed lineage kinase domain-like protein MLKL causes necrotic membrane disruption upon phosphorylation by RIP3. Molecular cell. 2014;54:133-46.
[60] Zhang J, Yang Y, He W, Sun L. Necrosome core machinery: MLKL. Cellular and molecular life sciences : CMLS. 2016.

[61] Baines CP. Role of the mitochondrion in programmed necrosis. Frontiers in physiology. 2010;1:156.
[62] Irrinki KM, Mallilankaraman K, Thapa RJ, Chandramoorthy HC, Smith FJ, Jog NR, et al. Requirement of FADD, NEMO, and BAX/BAK for aberrant mitochondrial function in tumor necrosis factor alpha-induced necrosis. Mol Cell Biol. 2011;31:3745-58.
[63] Tait SW, Oberst A, Quarato G, Milasta S, Haller M, Wang R, et al. Widespread mitochondrial depletion via mitophagy does not compromise necroptosis. Cell Rep. 2013;5:878-85.
[64] Conrad M, Angeli JP, Vandenabeele P, Stockwell BR. Regulated necrosis: disease relevance and therapeutic opportunities. Nat Rev Drug Discovovery. 2016;15:345-66.
[65] Zhang T, Zhang Y, Cui M, Jin L, Wang Y, Lv F, et al. CaMKII is a RIP3 substrate mediating ischemia- and oxidative stress–induced myocardial necroptosis. Nature. 2016.
[66] Yin B, Xu Y, Wei RL, He F, Luo BY, Wang JY. Inhibition of receptor-interacting protein 3 upregulation and nuclear translocation involved in Necrostatin-1 protection against hippocampal neuronal programmed necrosis induced by ischemia/reperfusion injury. Brain research. 2015;1609:63-71.
[67] Kaczmarek A, Vandenabeele P, Krysko DV. Necroptosis: the release of damage-associated molecular patterns and its physiological relevance. Immunity. 2013;38:209-23.
[68] Cai Z, Zhang A, Choksi S, Li W, Li T, Zhang XM, et al. Activation of cell-surface proteases promotes necroptosis, inflammation and cell migration. Cell research. 2016;26:886-900.
[69] Vandenabeele P, Galluzzi L, Vanden Berghe T, Kroemer G. Molecular mechanisms of necroptosis: an ordered cellular explosion. Nature reviews Molecular cell biology. 2010;11:700-14.
[70] Vercammen D, Beyaert R, Denecker G, Goossens V, Van Loo G, Declercq W, et al. Inhibition of caspases increases the sensitivity of L929 cells to necrosis mediated by tumor necrosis factor. J Exp Med. 1998;187:1477-85.
[71] Oberst A, Dillon CP, Weinlich R, McCormick LL, Fitzgerald P, Pop C, et al. Catalytic activity of the caspase-8-FLIP(L) complex inhibits RIPK3-dependent necrosis. Nature. 2011;471:363-7.
[72] Kinnally KW, Peixoto PM, Ryu SY, Dejean LM. Is mPTP the gatekeeper for necrosis, apoptosis, or both? Biochim Biophys Acta. 2011;1813:616-22.
[73] Karch J, Kwong JQ, Burr AR, Sargent MA, Elrod JW, Peixoto PM, et al. Bax and Bak function as the outer membrane component of the mitochondrial permeability pore in regulating necrotic cell death in mice. eLife. 2013;2:e00772.
[74] Wree A, Broderick L, Canbay A, Hoffman HM, Feldstein AE. From NAFLD to NASH to cirrhosis-new insights into disease mechanisms. Nature reviews Gastroenterology & hepatology. 2013;10:627-36.
[75] Vandenabeele P, Grootjans S, Callewaert N, Takahashi N. Necrostatin-1 blocks both RIPK1 and IDO: consequences for the study of cell death in experimental disease models. Cell death and differentiation. 2013;20:185-7.
[76] Degterev A, Huang Z, Boyce M, Li Y, Jagtap P, Mizushima N, et al. Chemical inhibitor of nonapoptotic cell death with therapeutic potential for ischemic brain injury. Nature chemical biology. 2005;1:112-9.
[77] Degterev A, Hitomi J, Germscheid M, Ch'en IL, Korkina O, Teng X, et al. Identification of RIP1 kinase as a specific cellular target of necrostatins. Nature chemical biology. 2008;4:313-21.
[78] Kung G, Konstantinidis K, Kitsis RN. Programmed necrosis, not apoptosis, in the heart. Circulation research. 2011;108:1017-36.

[79] Biton S, Ashkenazi A. NEMO and RIP1 control cell fate in response to extensive DNA damage via TNF-alpha feedforward signaling. Cell. 2011;145:92-103.
[80] Takahashi N, Duprez L, Grootjans S, Cauwels A, Nerinckx W, DuHadaway JB, et al. Necrostatin-1 analogues: critical issues on the specificity, activity and in vivo use in experimental disease models. Cell Death Dis. 2012;3:e437.
[81] Degterev A, Maki JL, Yuan J. Activity and specificity of necrostatin-1, small-molecule inhibitor of RIP1 kinase. Cell death and differentiation. 2013;20:366.
[82] Linkermann A, Hackl MJ, Kunzendorf U, Walczak H, Krautwald S, Jevnikar AM. Necroptosis in immunity and ischemia-reperfusion injury. American journal of transplantation. 2013;13:2797-804.
[83] Linkermann A, Brasen JH, Himmerkus N, Liu S, Huber TB, Kunzendorf U, et al. Rip1 (receptor-interacting protein kinase 1) mediates necroptosis and contributes to renal ischemia/reperfusion injury. Kidney international. 2012;81:751-61.
[84] Smith CC, Davidson SM, Lim SY, Simpkin JC, Hothersall JS, Yellon DM. Necrostatin: a potentially novel cardioprotective agent? Cardiovascular drugs and therapy / sponsored by the International Society of Cardiovascular Pharmacotherapy. 2007;21:227-33.
[85] Koudstaal S, Oerlemans MI, Van der Spoel TI, Janssen AW, Hoefer IE, Doevendans PA, et al. Necrostatin-1 alleviates reperfusion injury following acute myocardial infarction in pigs. European journal of clinical investigation. 2015;45:150-9.
[86] Dhein S. The Langendorff Heart Springer; 2005.
[87] O'Connell TD, Rodrigo MC, Simpson PC. Isolation and culture of adult mouse cardiac myocytes. Journal of pharmacological and toxicological methods. 2007;357:271-96.
[88] Claycomb WC, Lanson NA, Jr., Stallworth BS, Egeland DB, Delcarpio JB, Bahinski A, et al. HL-1 cells: a cardiac muscle cell line that contracts and retains phenotypic characteristics of the adult cardiomyocyte. Proc Natl Acad Sci U S A. 1998;95:2979-84.
[89] Carlsen H, Moskaug JO, Fromm SH, Blomhoff R. In vivo imaging of NF-kappa B activity. Journal of immunology (Baltimore, Md : 1950). 2002;168:1441-6.
[90] Miao B, Degterev A. Methods to analyze cellular necroptosis. Methods in molecular biology (Clifton, NJ). 2009;559.
[91] Melo-Lima S, Celeste Lopes M, Mollinedo F. Necroptosis is associated with low procaspase-8 and active RIPK1 and -3 in human glioma cells. Oncoscience. 2014;1:649-64.
[92] Teng X, Degterev A, Jagtap P, Xing X, Choi S, Denu R, et al. Structure-activity relationship study of novel necroptosis inhibitors. Bioorganic & medicinal chemistry letters. 2005;15:5039-44.
[93] Wu JR, Wang J, Zhou SK, Yang L, Yin JL, Cao JP, et al. Necrostatin-1 protection of dopaminergic neurons. Neural regeneration research. 2015;10:1120-4.
[94] Cho Y, McQuade T, Zhang H, Zhang J, Chan FK. RIP1-dependent and independent effects of necrostatin-1 in necrosis and T cell activation. PloS one. 2011;6:e23209.
[95] Friedmann Angeli JP, Schneider M, Proneth B, Tyurina YY, Tyurin VA, Hammond VJ, et al. Inactivation of the ferroptosis regulator Gpx4 triggers acute renal failure in mice. Nature cell biology. 2014;16:1180-91.
[96] Degterev A, Linkermann A. Generation of small molecules to interfere with regulated necrosis. Cellular and molecular life sciences : CMLS. 2016;73:2251-67.
[97] LaRocca TJ, Sosunov SA, Shakerley NL, Ten VS, Ratner AJ. Hyperglycemic Conditions Prime Cells for RIP1-dependent Necroptosis. The Journal of biological chemistry. 2016;291:13753-61.
[98] White HD, Norris RM, Brown MA, Brandt PW, Whitlock RM, Wild CJ. Left ventricular end-systolic volume as the major determinant of survival after recovery from myocardial infarction. Circulation. 1987;76:44-51.

[99] Mielniczuk LM, Lamas GA, Flaker GC, Mitchell G, Smith SC, Gersh BJ, et al. Left ventricular end-diastolic pressure and risk of subsequent heart failure in patients following an acute myocardial infarction. Congestive heart failure (Greenwich, Conn). 2007;13:209-14.
[100] Mandinov L, Eberli FR, Seiler C, Hess OM. Diastolic heart failure. Cardiovasc Res. 2000;45:813-25.
[101] Bliksoen M, Mariero LH, Ohm IK, Haugen F, Yndestad A, Solheim S, et al. Increased circulating mitochondrial DNA after myocardial infarction. International journal of cardiology. 2012;158:132-4.
[102] Ma XL, Kumar S, Gao F, Louden CS, Lopez BL, Christopher TA, et al. Inhibition of p38 mitogen-activated protein kinase decreases cardiomyocyte apoptosis and improves cardiac function after myocardial ischemia and reperfusion. Circulation. 1999;99:1685-91.
[103] Cain BS, Meldrum DR, Meng X, Dinarello CA, Shames BD, Banerjee A, et al. p38 MAPK inhibition decreases TNF-alpha production and enhances postischemic human myocardial function. The Journal of surgical research. 1999;83:7-12.
[104] Wang Y, Huang S, Sah VP, Ross J, Jr., Brown JH, Han J, et al. Cardiac muscle cell hypertrophy and apoptosis induced by distinct members of the p38 mitogen-activated protein kinase family. The Journal of biological chemistry. 1998;273:2161-8.
[105] Liao P, Georgakopoulos D, Kovacs A, Zheng M, Lerner D, Pu H, et al. The in vivo role of p38 MAP kinases in cardiac remodeling and restrictive cardiomyopathy. Proc Natl Acad Sci U S A. 2001;98:12283-8.
[106] Liao P, Wang SQ, Wang S, Zheng M, Zheng M, Zhang SJ, et al. p38 Mitogen-activated protein kinase mediates a negative inotropic effect in cardiac myocytes. Circulation research. 2002;90:190-6.
[107] Delaleu N, Bickel M. Interleukin-1 beta and interleukin-18: regulation and activity in local inflammation. Periodontology 2000. 2004;35:42-52.
[108] Frangogiannis NG. Inflammation in cardiac injury, repair and regeneration. Current opinion in cardiology. 2015;30:240-5.
[109] Grimstad O, Sandanger O, Ryan L, Otterdal K, Damaas JK, Pukstad B, et al. Cellular sources and inducers of cytokines present in acute wound fluid. Wound repair and regeneration : official publication of the Wound Healing Society [and] the European Tissue Repair Society. 2011;19:337-47.
[110] Cogswell JP, Godlevski MM, Wisely GB, Clay WC, Leesnitzer LM, Ways JP, et al. NF-kappa B regulates IL-1 beta transcription through a consensus NF-kappa B binding site and a nonconsensus CRE-like site. Journal of immunology (Baltimore, Md : 1950). 1994;153:712-23.
[111] Miao EA, Rajan JV, Aderem A. Caspase-1-induced pyroptotic cell death. Immunological reviews. 2011;243:206-14.
[112] Bajaj G, Sharma RK. TNF-alpha-mediated cardiomyocyte apoptosis involves caspase-12 and calpain. Biochemical and biophysical research communications. 2006;345:1558-64.
[113] Song W, Lu X, Feng Q. Tumor necrosis factor-alpha induces apoptosis via inducible nitric oxide synthase in neonatal mouse cardiomyocytes. Cardiovasc Res. 2000;45:595-602.
[114] Ganote CE, Armstrong SC. Effects of CCCP-induced mitochondrial uncoupling and cyclosporin A on cell volume, cell injury and preconditioning protection of isolated rabbit cardiomyocytes. Journal of molecular and cellular cardiology. 2003;35:749-59.

6 Appendix

6.1.1 Reagents

Table 2: List of reagents in alphabetical order

Reagent:	Manufacturer:	Catalog number from manufacturer:
1X Halt Protease and Phosphatase Inhibitor Cocktail (Thermo Scientific	Thermo Scientific	78441
β-mercaptoethanol	Sigma-Aldrich	M6250
Akt Antibody	Cell signaling technology	9272
AMPKα Antibody	Cell signaling technology	2532
Annexin V-FITC	BioVision	1001-200
Annexin V Binding Buffer	BioVision	1006-100
Anti-MLKL antibody-N-terminal	Abcam	ab194699
Anti-MLKL (phospho S345) antibody	Abcam	ab196436
Bax Antibody (N-20)	Santa Cruz Biotechnology	sc-493
Bcl-2 Antibody (N-19)	Santa Cruz Biotechnology	sc-492
BDM	Sigma-Aldrich	B0753-25G
Bromophenol blue	Sigma-Aldrich	B0126-25G
BSA	Sigma-Aldrich	A2153-100G
CaCl2	Merck-Millipore	F1221583 346
CaCl2- 2H2O	Sigma-Aldrich	C7902-500G
CCCP	Sigma-Aldrich	C2759-100MG
Claycomb Medium	Sigma-Aldrich	51800C-500mL
Collagenase 2	Worthington Biochemical	LS004194
D-Luciferin	Biotherma	BT11-100
DMSO	Sigma-Aldrich	41640
Dulbecco`s PBS	Sigma-Aldrich	D8537
EDTA	CalBioChem	324503
Fetal bovine serum	Sigma-Aldrich	F2442

Fetal calf serum (HyClone)	Thermo-Scientific	SH30073.03
Fibronectin	Sigma-Aldrich	F1141
Gelatin	Sigma-Aldrich	G9391
Glucose-1H2O	Merck-Millipore	K34340042 512
Glycine	Sigma-Aldrich	G7126-1KG
Glycerol	Merck-Millipore	ZC766895 612
Goat Anti Mouse	Southern Biotech	1030-05
Goat Anti Rabbit	Southern Biotech	4050-05
Heparin	Leo Pharma A/S	585679
Hoecst	Invitrogen	33528
KCl	Merck-Millipore	K34333136 516
KH2PO4	Merck-Millipore	A436873 348
L-Ascorbic acid, sodium salt	Sigma-Aldrich	A7631
L-Glutamine	Sigma-Aldrich	G7513
Laminin	Life Sciences	354232
Micro BCA Protein Assay Kit	Thermo-Scientific	PIER23235
Minimum essential medium eagle w/ Hanks salt	Sigma-Aldrich	M5775
MgSO4-7H20	Merck-Millipore	A436186 329
NaCl	Merck-Millipore	K46559204 531
NaHCO3	Merck-Millipore	K41415829 041
Na-Hepes	Sigma-Aldrich	H4034-500G
Na2HPO4-2 H2O	Merck-Millipore	K36794180 704
Necrostatin-1	Sigma-Aldrich	N9037
Necrostatin-1S	BioVision	2263-1, 5
Non-fat dry milk	BioRad	170-6404
Norepinephrine ((±)-Arterenol)	Sigma-Aldrich	A0937
Mitrotracker® Deep Red	Invitrogen	M22426
p38 MAPK Antibody	Cell signaling technology	9212
p44/42 MAPK (Erk1/2) Antibody	Cell signaling technology	9102
Paraformaldehyde	Merck-Millipore	K36530805 644

Penicillin-Streptomycin	Sigma-Aldrich	P4333
Pentobarbital	Ås Produksjonslab AS	306498
Phospho-Akt (Ser473) Antibody	Cell signaling technology	9271
Phospho-AMPKα (Thr172) (40H9) Rabbit mAb	Cell signaling technology	2535
Phospho-p38 MAPK (Thr180/Tyr182) Antibody	Cell signaling technology	9211
Phospho-p44/42 MAPK (Erk1/2) (Thr202/Tyr204) Antibody	Cell signaling technology	9101
Phospho-SAPK/JNK (Thr183/Tyr185) Antibody	Cell signaling technology	9251
Ponceau	Merck-Millipore	1142750010
Power SYBR Green PCR Master Mix	Applied Biosystems	4367659
Precision Plus Protein - Dual color standards	BioRad	161-0374
Propidium Iodide	Sigma-Aldrich	P4864-10ml
Propidium Iodide	BioVision	1056-1
RIPA lysis buffer	Merck-Millipore	20-188
RNeasy Mini KIT	Qiagen	74104
Rnase-Free DNase Set	Qiagen	79254
SAPK/JNK Antibody	Cell signaling technology	9252
Sodium dodecyl sulfate (SDS)	BioRad	161-0302
Sucrose	Sigma-Aldrich	S1888-500G
Taurine	Sigma-Aldrich	T0625-100G
TNF-a	RD Systems	CS1314111
Tris-base	Sigma-Aldrich	T1503-1KG
Trypsin-EDTA, 1x	Sigma-Aldrich	T3924
Trypsin inhibitor, soybean	Sigma-Aldrich	T6522
TTC	Sigma-Aldrich	T8877-100G
TWEEN	Sigma-Aldrich	9005-64-5
qScript cDNA Synthesis Kit	Quanta Biosciences	733-1176
Z-VAD-FMK	BioVision	1010-100

6.1.2 Recipes for buffers

Krebs-Henseleit buffer:	**mM/L**	**g/5L**
NaCl	118.5	34.63
$NaHCO_3$	25	10.50
KCl	4.7	1.75
KH_2PO_4	1.2	0.82
$MgSO_4$-$7H_20$	1.2	1.48
Glucose-$1H_2O$	11.1	11.0
$CaCl_2$	2.4	1.33
$CaCl_2$- $2H_2O$	2.4	1.76

Perfusion buffer: (0.5L)	**Conc. (mM)**	**mL**	**g**
NaCl	120.4	24.08	
KCl	14.7	7.35	
KH_2PO_4	0.6	0.3	
Na_2HPO_4-2 H_2O	0.6	1.2	
$MgSO_4$-7 H_2O	1.2	0.6	
Na-Hepes liquid	10.0	5.0	
Glucose-H_20	5.5	0.1375	
$NaHCO_3$	4.6		0.193
Taurine	30.0		1.877
BDM	10.0		0.506

Digestion buffer:	**Conc. (mg/ml)**
Perfusion buffer	
Collagenase 2	1.3 mg

Plating medium: (50mL)	**Conc.**	**Volume (mL)**
MEM w Hanks BSS		42.5
Fetal calf serum	10 %	5
BDM (500mM)	10mM	1
Penicillin	100U/mL	0.5
Glutamine	2mM	0.5

Short term medium: (50mL)	**Conc.**	**Volume (mL)**
MEM w Hanks BSS		48.5
BSA Fa-free (10 %)	0.10 %	0.5
Penicillin	100U/mL	0.5
Glutamine	2mM	0.5
BDM (500mM)	1mM	0.1

Fibroblast medium: (50mL)	**Conc.**	**Volume (mL)**
MEM w Hanks BSS		42.5
Calf serum	10 %	5
Penicillin	100 U/mL	0.5
Glutamine	2mM	0.5

Mounting medium;

Gelatin	7 g
H_2O	42 mL
Glycerol	50 mL

HL-1 cells:

Supplemented Claycomb Medium:	**Conc.**	**Volume (mL)**
Claycomb Medium		87
Fetal bovine serum	10 %	10
Penicillin/Streptomycin	100 U/mL: 100µg/mL	1
Norepinephrine (10mM stock)	0.1 mM	1
L-Glutamine (200 mM stock)	2 mM	1

Wash Medium:	**Conc.**	**Volume (mL)**
Claycomb Medium		94
Fetal bovine serum	5 %	5
Penicillin/Streptomycin	100 U/mL	1

Norepinephrine (10mM stock):

Norepinephrine	80 mg
Ascorbic acid (30 mM)	25 mL

Soybean Trypsin Inhibitor:

Soybean Trypsin Inhibitor	25 mg
PBS	100 mL

Gelatin/Fibronectin:

Gelatin (0.02 %)	199 mL
Fibronectin	1 mL

Freezing medium:

Fetal bovine serum	95 %
DMSO	5 %

Western blotting:

4X Laemmli Sample Buffer: (10mL)	mL	g
Sucrose		5
SDS 10 %	7.5	
Tris-HCl 0.5M (pH 6.8)	1.25	
EDTA 0.2M (pH 7.5)	100µL	
β-mercaptoethanol 14.7M	0.4	
Bromophenol blue 1 %	0.2	
H_2O		

10X Running buffer: (1L)

Tris-base	30.3g
Glycine	144g
SDS	10g
H_2O	

1X Running buffer: (1L)	Volume (ml)
10X Running buffer	100
H_2O	900

10x Transfer buffer: (1L)

Tris-base	30.3g
Glycine	144g
H_2O	

1X Transfer buffer: (1L)	Volume (mL)
10X Transfer buffer	100
Methanol	200
H_2O	700

10X TBS: (1L)

Tris-base	24.23g
NaCl	80.06
H_2O	

1X TBSt: (1L)	**Volume (mL)**
10X TBS	100
TWEEN	5
H_2O	895

5 % NFDM:

1X TBSt	100mL
NFDM	5g

5 % BSA:

1X TBSt	100mL
BSA	5g

6.1.3 List of machines in alphabetical order

Machines:	Manufacturer:
7900HT Fast Real-Time PCR system, SDS2.3	Applied Biosystems, Thermo Fisher Scientific, Massachusetts, US
BD FACSCanto™ II flow cytometer	BD Biosciences, California, US
ChemiDoc Touch Imaging System	BioRad, Hercules, CA
Countess automated cell counter	Thermo Scientific, Rockford, US
Emax Precision Microplate Reader	Molecular Devices, California, US
Fast Prep™ FP120	Thermo Savant, Thermo Fisher scientific, Rockford, US
Heraus fresco 21	Thermo Fisher scientific, Rockford, US
Heraeus Megafuge 16 centrifuge	Thermo Scientific, Massachusetts, US
IVIS Spectrum camera	PerkinElmer, Massachusetts, US
Olympus ScanR imaging station	Olympus life science, Olympus Corporation, Tokyo, Japan
Nano Drop 1000 Spectrophometer	Thermo Fisher Scientific, Rockland, US
T3 Thermocycler	Biometra, Gottingen, Germany
T8-knife homogenizer	IKA-Works, Breisgau, Germany
V700 Photo scanner	EPSON, Suwa, Japan

6.1.4 List of software in alphabetical order

Software:	Manufacturer:
EndNote X7	Thomson Reuters, New York, US
GraphPad Prism 6	GraphPad Software, California, US
Image Lab Software	BioRad, Hercules, CA
Lab Chart 7	ADInstruments, Sydney, Australia
Primer3	http://bioinfo.ut.ee/primer3-0.4.0/
RQ manager 1.2.1	Applied Biosystems, Thermo Fisher Scientific, Massachusetts, US

6.1.5 Supplemental figures

Figure S1

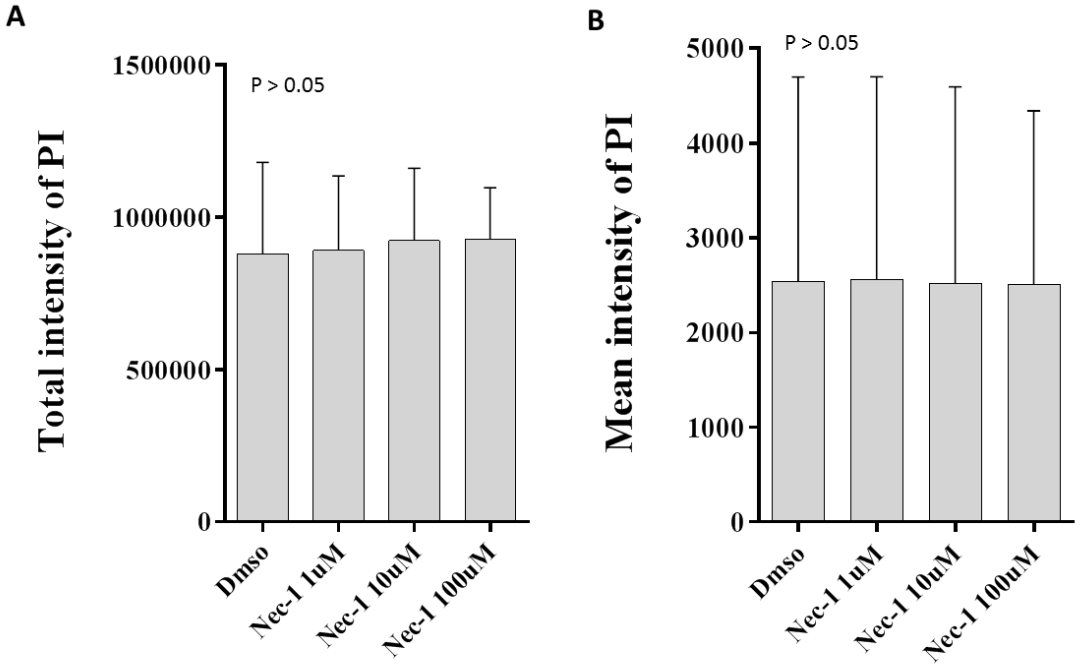

Figure S128: Effect of Nec-1 on adult mouse primary cardiomyocytes: Cardiomyocytes were isolated from WT mice (N=6) and treated with different concentrations of Nec-1 (dissolved in DMSO). Quantification and visualization of the cells was done on an Olympus Scan^R imaging station. **A)** Total intensity of PI. **B)** Mean intensity of PI. Values are presented as mean ± SD. Effect of treatment was evaluated with one-way ANOVA, followed by Dunnett`s multiple comparison test.

Figure S2

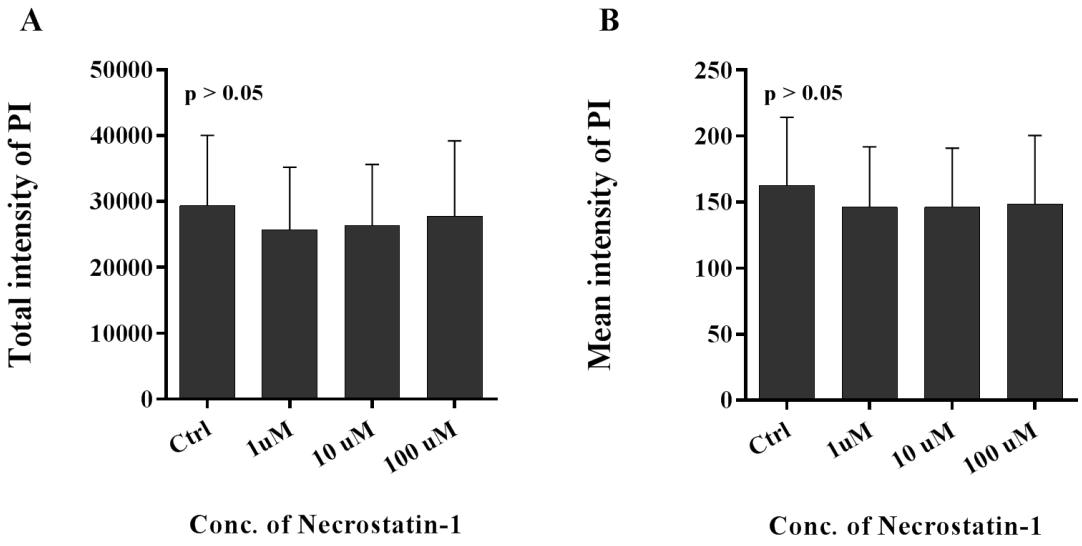

Figure S2: The effect of Nec-1 on primary adult mouse cardiac fibroblasts: Cardiac fibroblasts were isolated from WT mice (N=6) and treated with different concentrations of Nec-1 (dissolved in DMSO). Quantification and visualization of the cells was done on an Olympus Scan^R imaging station. **A)** Total Intensity of PI. **B)** Mean Intensity of PI. Values are presented as mean ± SD. Effects of treatment were evaluated with one-way ANOVA.

Figure S3

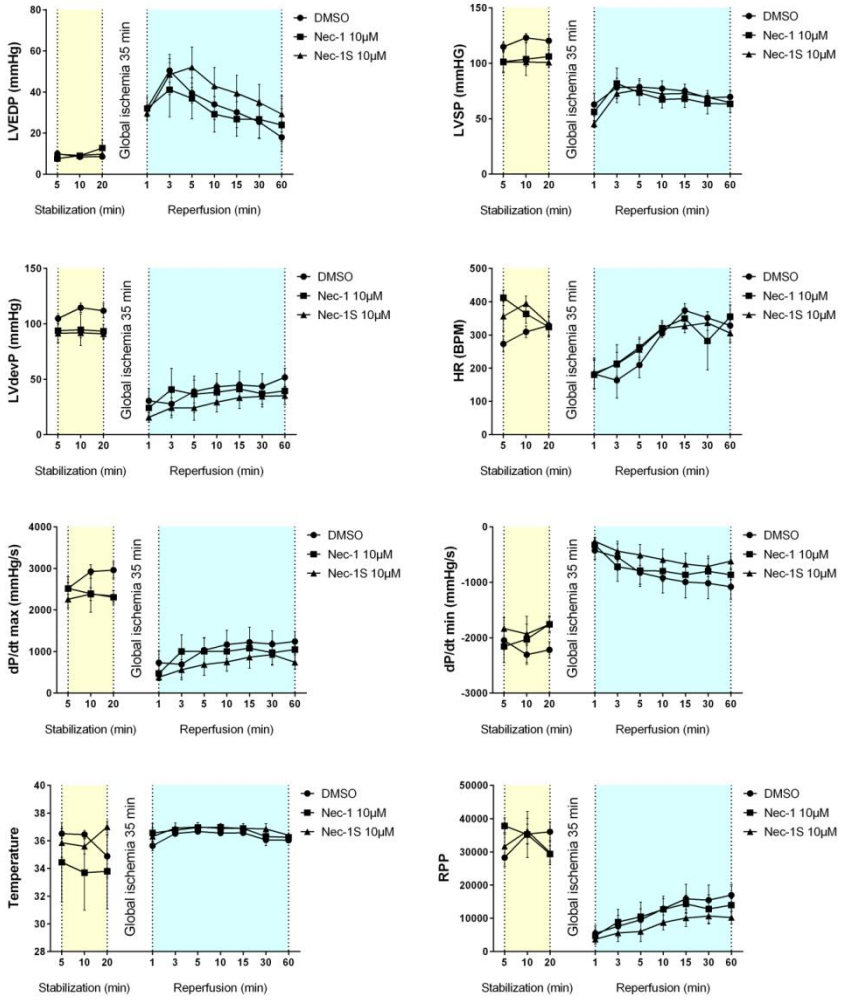

Figure S3: Effect of necrostatins on heart function in Langendorff-perfused mouse hearts, series 1: Functional data from the Langendorff- perfused mouse hearts in Series 1 (DMSO (Ctrl, circles N=5), 10 µM Nec-1 (squares N=4) and 10 µM Nec-1S (triangles N=5), the blockers were delivered to the hearts during the first minutes of the reperfusion period. **LVEDP =** left ventricular end-diastolic pressure (mm/Hg). **LVSP =** left ventricular systolic pressure (mm/Hg). **LVdevP =** left ventricular developed pressure (mm/Hg). **HR =** heart rate (beats per minute (BPM)). **dP/dt max** = maximal left ventricular global contractility (mm/Hg/s). **dP/dt min** = minimal left ventricular global contractility (mm/Hg/s). **Temperature** = temperature (°C). **RPP** = Rate pressure product (HR*LVSP). Values are presented as mean ± SEM. Effect of treatment was evaluated with a two-way ANOVA, followed by a Dunnett`s multiple comparison test.

Figure S4

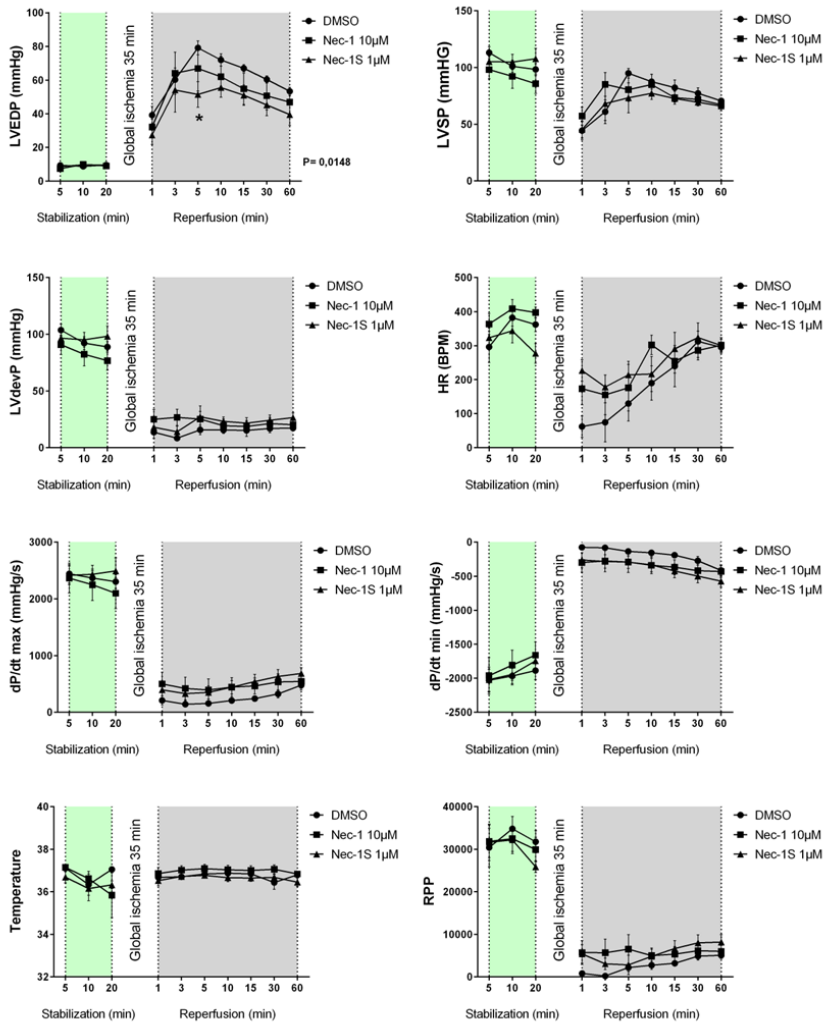

Figure S4: Effect of necrostatins on heart function in Langendorff-perfused mouse hearts, series 2: Functional data from the Langendorff- perfused mouse hearts in Series 2 DMSO (Ctrl, circles N=7), 10 µM Nec-1 (squares N=7), and 1 µM Nec-1S (triangles N=6), the blockers were delivered to the hearts from the first second of the reperfusion period. **LVEDP =** left ventricular end-diastolic pressure (mm/Hg). **LVSP =** left ventricular systolic pressure (mm/Hg). **LVdevP =** left ventricular developed pressure (mm/Hg). **HR =** heart rate (beats per minute (BPM)). **dP/dt max** = maximal left ventricular global contractility (mm/Hg/s). **dP/dt min** = minimal left ventricular global contractility (mm/Hg/s). **Temperature** = temperature (°C). **RPP** = Rate pressure product (HR*LVSP). Values are presented as mean ± SEM. Effect of treatment was evaluated with a two-way ANOVA, followed by a Dunnett`s multiple comparison test.

Figure S5

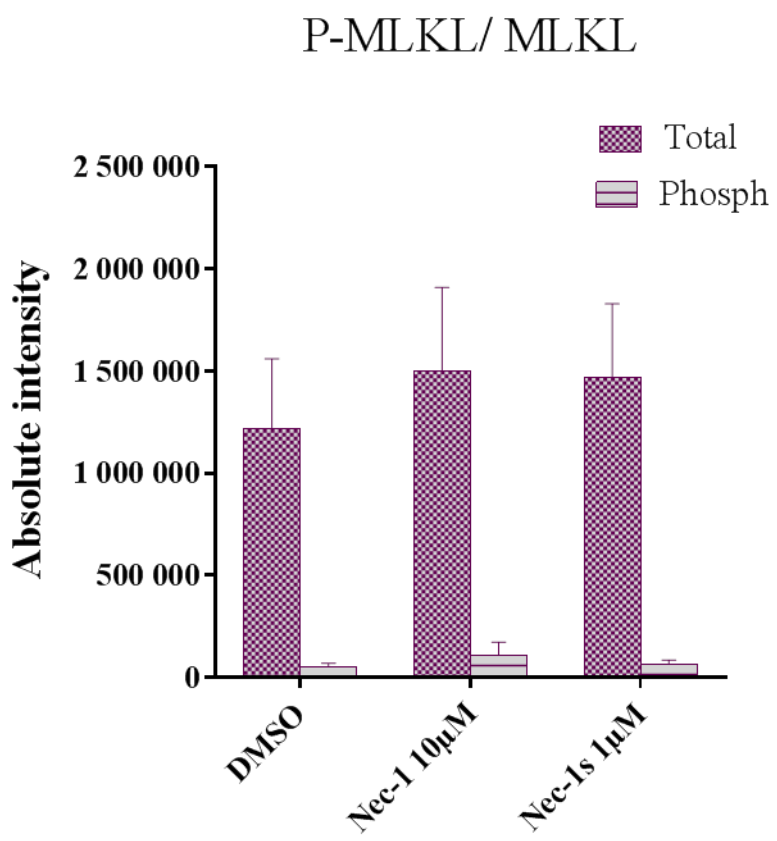

Figure S5: Western Blotting results of P-MLKL/MLKL: Total-MLKL and phosphorylated-MLKL in the different exposure groups from the Langendorff-perfused hearts, series 2, (Ctrl (N=6), 10 µM Nec-1 (N=6), 1 µM Nec-1S (N=5)). A representation of absolute intensity calculated from the two bands from all groups. All values are presented as mean ± SD.

Figure S6

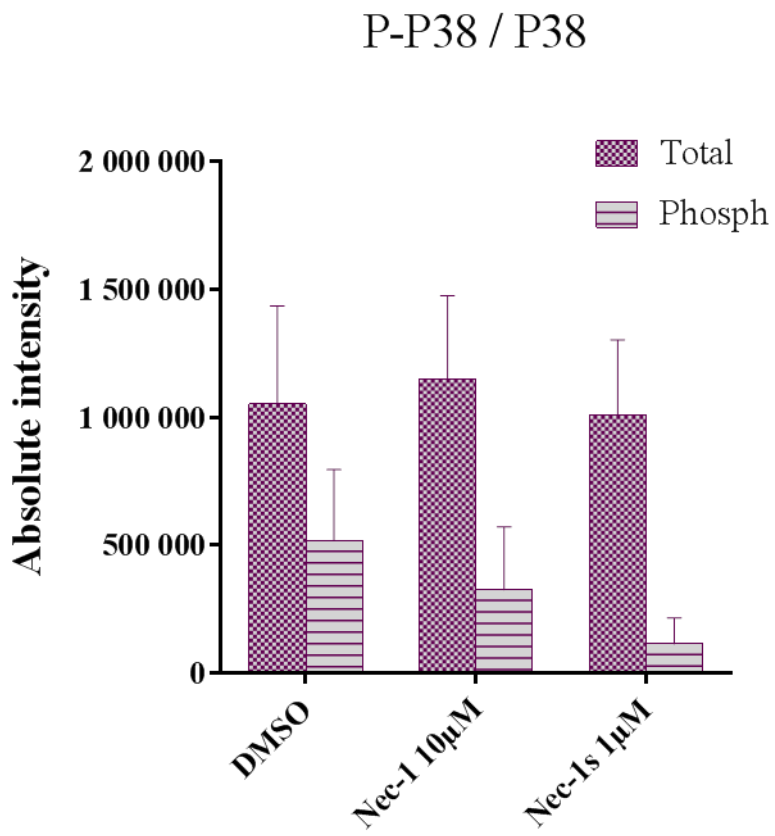

Figure S6: Western Blotting results of p38: Total-p38 and phosphorylated-p38 in the different exposure groups from the Langendorff-perfused hearts, series 2, (Ctrl (N=6), 10 µM Nec-1 (N=6), 1 µM Nec-1S (N=5)). A representation of absolute intensity calculated from the two bands from all groups. All values are presented as mean ± SD.

Figure S7:

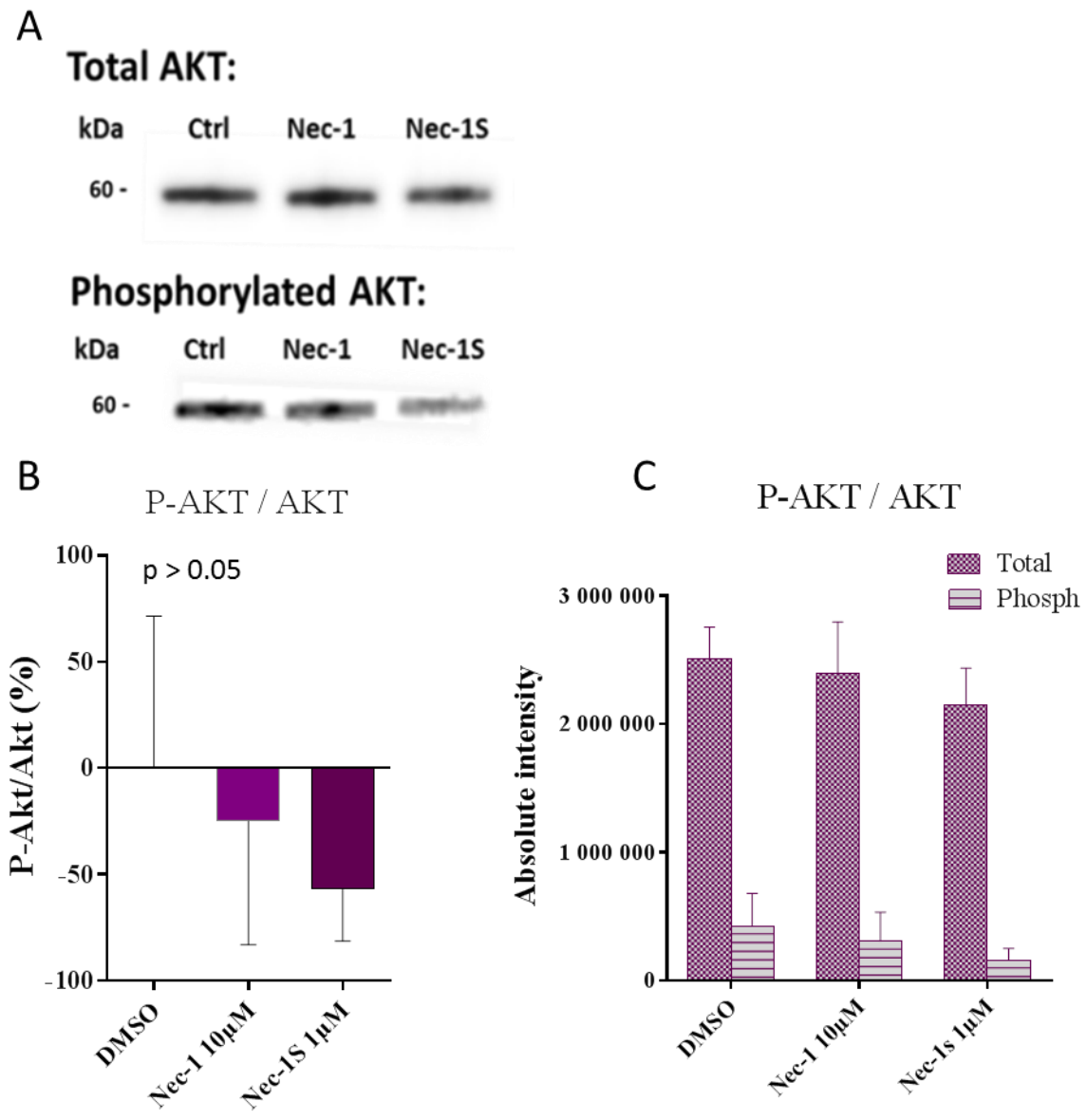

Figure S7: Western Blotting results of total-AKT and phosphorylated-AKT: Western blots were done with both phosphospecific- and total protein of AKT in the different groups from the Langendorff-perfused hearts, series 2, (Ctrl (N=6), 10 µM Nec-1 (N=6), 1 µM Nec-1S (N=5)). **A)** A representation of the 60 kDa band. **B)** Changes are expressed as a ratio between phospho/total. Results are normalized to control group. Effect of treatment was evaluated with non-parametric ANOVA (Kruskal Wallis). **C)** A representation of absolute intensity calculated from the two bands from all groups. All values are presented as mean ± SD.

Figure S8

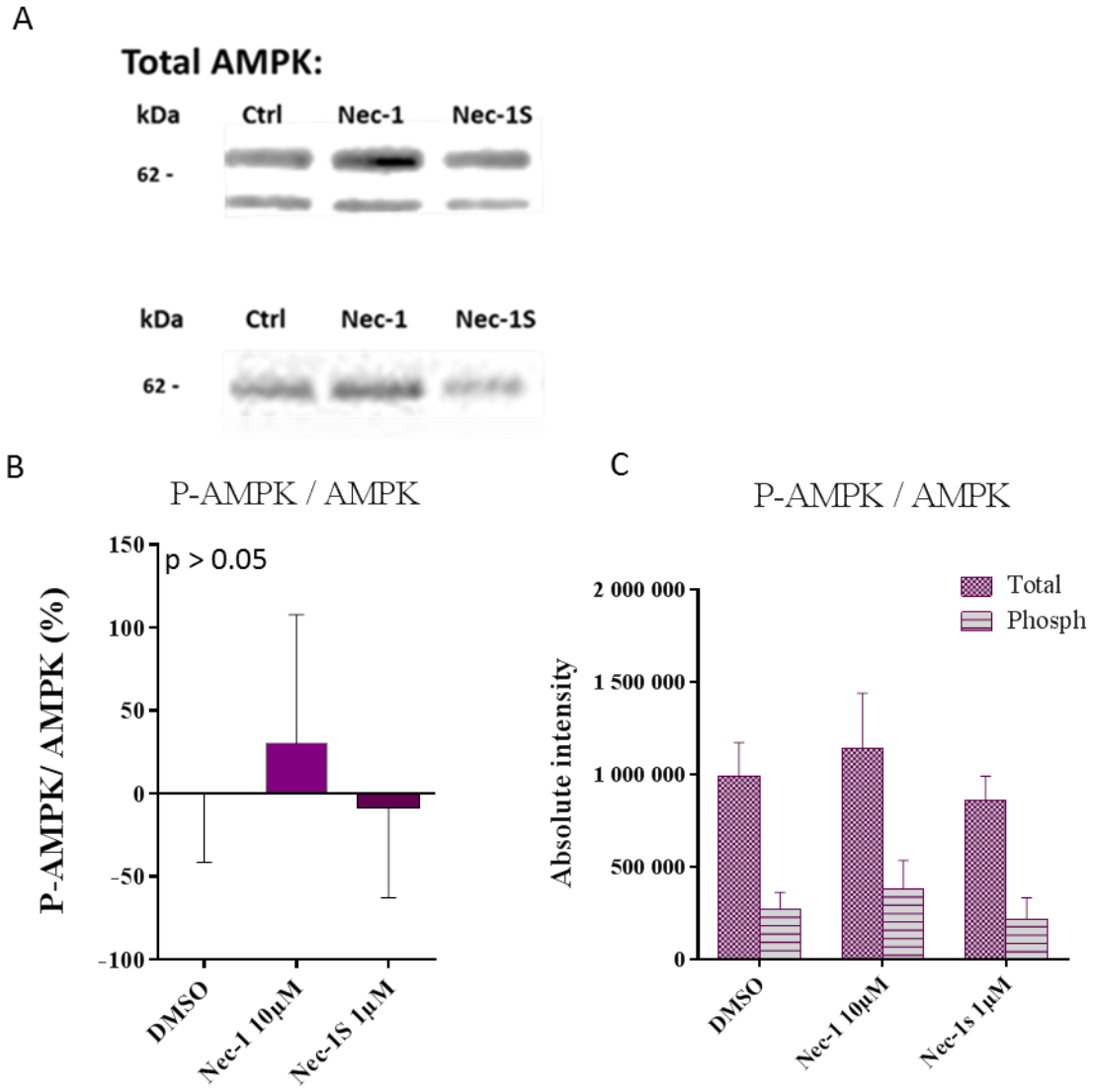

Figure S8: Western Blotting results of total-AMPK and phosphorylated-AMPK: Western blots were done with both phosphospecific- and total protein of AMPK in the different groups from the Langendorff-perfused hearts, series 2, (Ctrl (N=6), 10 µM Nec-1 (N=6), 1 µM Nec-1S (N=5)). **A)** A representation of the 62 kDa band. **B)** Changes are expressed as a ratio between phospho/total. Results are normalized to control group. Effect of treatment was evaluated with non-parametric ANOVA (Kruskal Wallis). **C)** A representation of absolute intensity calculated from the two bands from all groups. All values are presented as mean ± SD.

Figure S9:

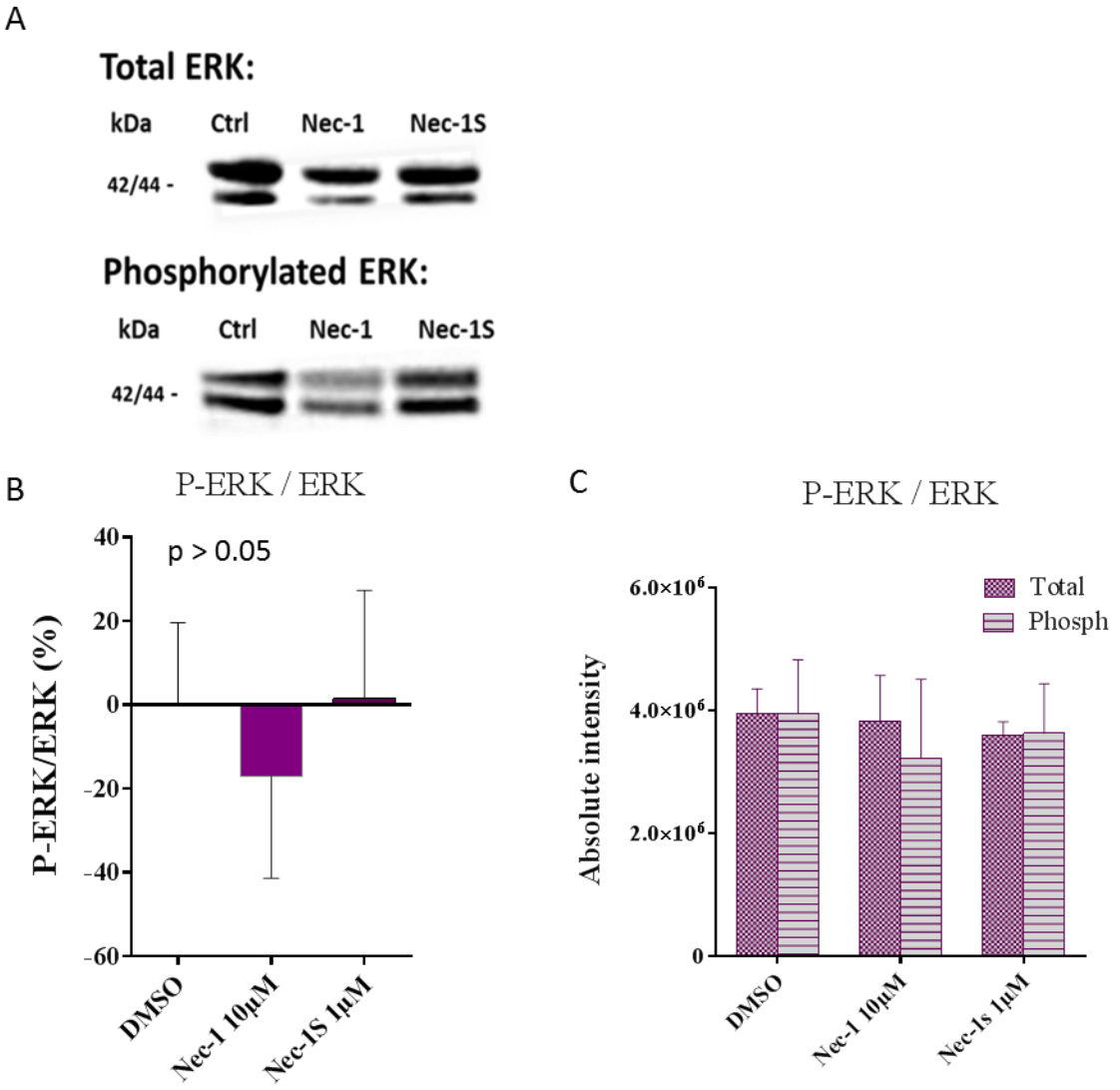

Figure S9: Western Blotting results of total-ERK and phosphorylated-ERK: Western blots were done with both phosphospecific- and total protein of ERK in the different groups from the Langendorff-perfused hearts, series 2, (Ctrl (N=6), 10 µM Nec-1 (N=6), 1 µM Nec-1S (N=5)). **A)** A representation of the two bands. **B)** Changes are expressed as a ratio between phospho/total. Results are normalized to control group. Effect of treatment was evaluated with non-parametric ANOVA (Kruskal Wallis). **C)** A representation of absolute intensity calculated from the two bands from all groups. All values are presented as mean ± SD.

Figure S10:

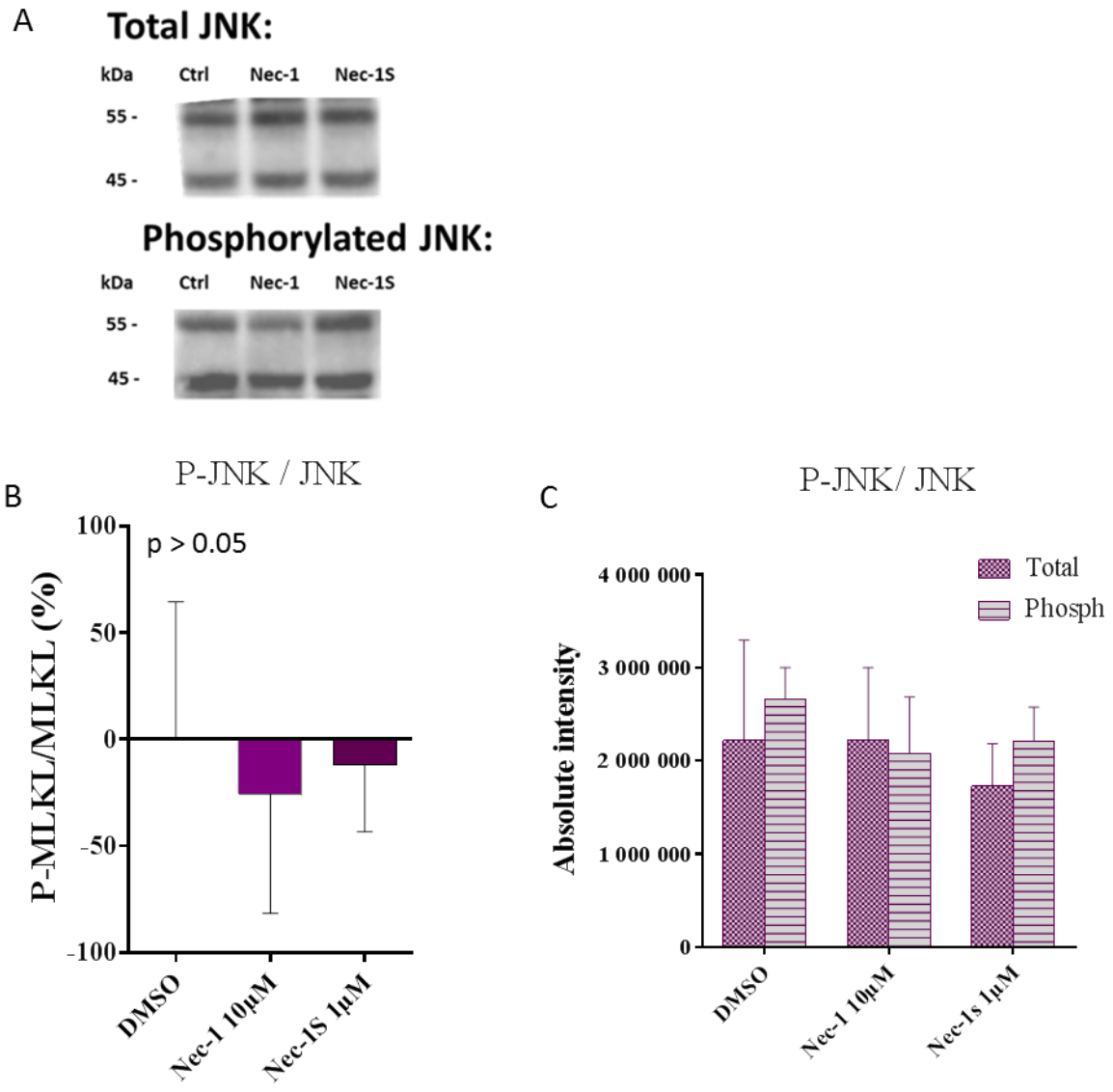

Figure S10: Western Blotting results of total-JNK and phosphorylated-JNK: Western blots were done with both phosphospecific- and total protein of JNK in the different groups from the Langendorff-perfused hearts, series 2, (Ctrl (N=6), 10 µM Nec-1 (N=6), 1 µM Nec-1S (N=5)). **A)** A representation of the two bands. **B)** Changes are expressed as a ratio between phospho/total. Results are normalized to control group. Effect of treatment was evaluated with non-parametric ANOVA (Kruskal Wallis). **C)** A representation of absolute intensity calculated from the two bands from all groups. All values are presented as mean ± SD.

Figure S11:

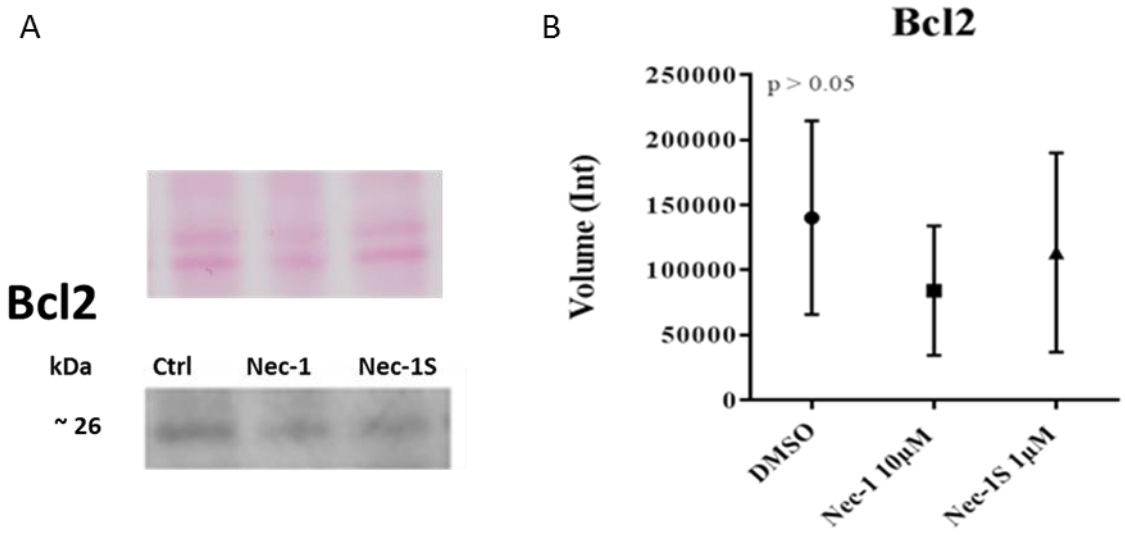

Figure S11: Western blot results of Bcl-2: Western blots were done on the different groups of the Langendorff-perfused hearts, series 2, (Ctrl (N=6), 10 µM Nec-1 (N=6), 1 µM Nec-1S (N=5)).**A)** Above; Ponceau staining confirming equal loading, below; abundance of the 26 kDa protein in the different exposure groups. **B)** The results of the effect of the different treatments presented as mean ± SD. Effect of treatment was evaluated with non-parametric ANOVA (Kruskal Wallis).

Figure S12:

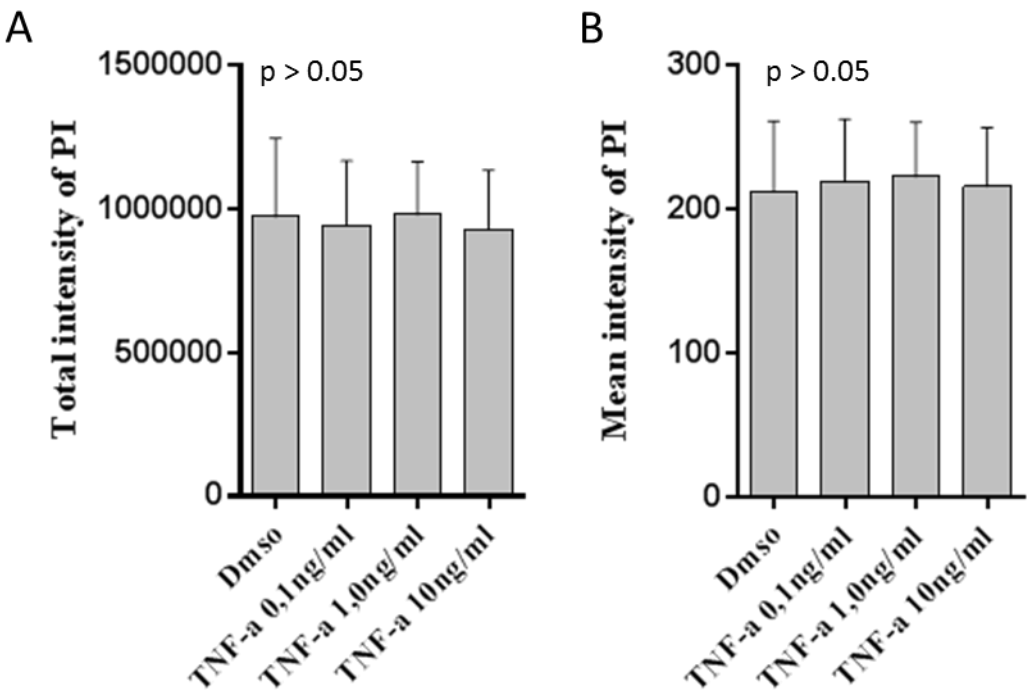

Figure S12: Effect TNF-α on adult mouse primary cardiomyocytes. Adult cardiomyocytes were isolated from WT mice (N=6) and treated with different concentrations of Nec-1 (dissolved in DMSO). Quantification and visualization of the cells was done on an Olympus Scan^R imaging station. **A)** Total Intensity of PI. **B)** Mean Intensity of PI. All values are presented as mean ± SD. Effects of treatment were evaluated with one-way ANOVA followed by Dunnett`s multiple comparison test.

Figure S13:

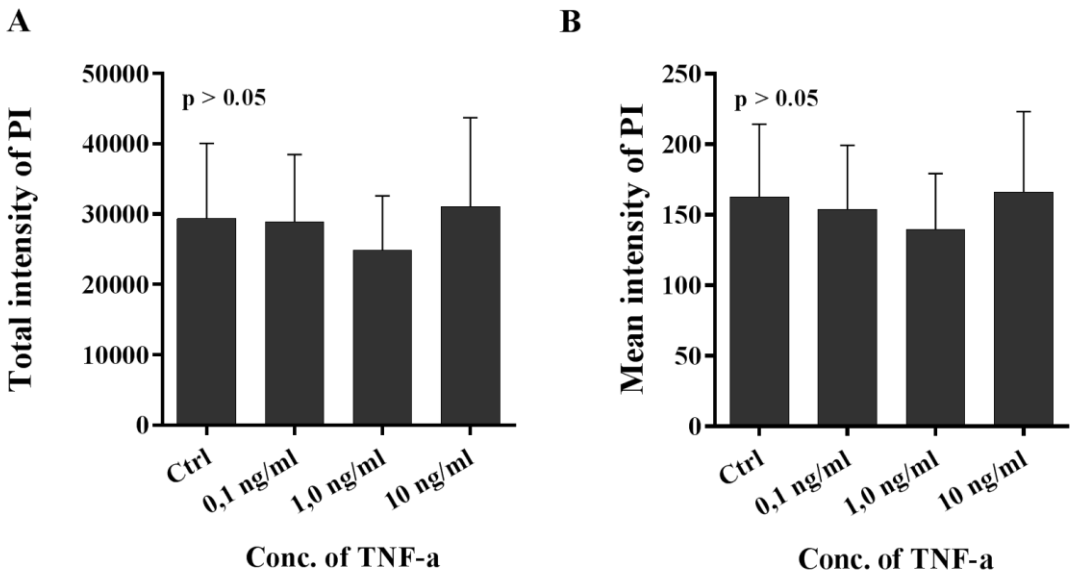

Figure S13: Effect of TNF-α on adult primary mouse cardiac fibroblasts: Cardiac fibroblasts were isolated from WT mice (N=6) and treated with different concentrations of TNF-α. Quantification and visualization of the cells was done on an Olympus Scan^R imaging station. **A)** Total Intensity of PI. **B)** Mean Intensity of PI. All values are presented as mean ± SD. Effects of treatment were evaluated with one-way ANOVA, followed by Dunnett`s multiple comparison test.